TRANSDERMAL MICRONEEDLES FOR INSULIN DELIVERY

CRISTIANE PATRICIA PISSINATO PERE

A thesis submitted in partial fulfilment of the requirements of the University of Kent and the University of Greenwich for the Degree of Doctor of Philosophy.

MAY 2019

DECLARATION

" I certify that this work has not been accepted in substance for any degree and is not concurrently being submitted for any degree other than that of Doctor of Philosophy being studied at the Universities of Kent and Greenwich. I also declare that this work is the result of my own investigations except where otherwise identified by references and that I have not plagiarised the work of others ".

Signed _____ (Student)

Mrs Cristiane Patricia Pissinato Pere

Signed _____ (Supervisor)

Professor Dionysios Douroumis

Signed _____ (Second supervisor)

Dr. Gurprit Lall

Date: _____

ACKNOWLEDGEMENTS

First of all, I would like to thank God for this amazing experience called life and for every single soul that inspired and helped me along the way. I would like to thank my family for the unconditional support, patience and motivation during all these years, especially my husband Marcelo, my daughter Helena, my Mom Rosa my sister Juliane, my brother Fernando and my father Amauri.

I would like to thank my first supervisor Professor Dionysios Douroumis for trusting me and giving me this opportunity since before applying for this project. His guidance, patience and support helped throughout my PhD and I am grateful for having him as my supervisor.

In addition, I would like to thank my second supervisor Dr Gurprit Lall for all the support and insightful discussions. I also would like to thank Professor Iain Cumming for the opportunity and the support during the time he was my supervisor.

My sincere thanks and appreciation also go to Dr Bruce Alexander that happily collaborated with our project and helped me a lot with many techniques, discussions and support.

I would like to thank Devyani Amin and Andy Hurt for all the help with the instruments, different techniques and shared knowledge. I am also really grateful to Dr Jasim Uddin for the collaboration with the animal studies and discussions.

My sincere thanks to Lynn Gallagher and Joanna Mowbray who were always kind and helped me a lot with many things.

A special thank for my close and dear friend Sophia Economidou who helped and supported me a lot along my journey.

A special thank for my dearest friend Voula Kasapidou who has been supporting me since the beginning.

Finally, but not less important, I would like to thank all my friends and fellow PhD students for the friendship, especially my dear friends Ouafa Benlaouer, Mervat Shafik, Rachel Sully, Viktorija Kuziene, Clémentine Giraud, Jaya Chakraborty, Samuel Owusu-Ware, Roxanne Khalaj, Forough Hafezi, Uttom Nandi, Tumpa Dey, Steven Ross, Suha Dadou, Svetlana Sakhnevych, Atabak Ghanizadeh, Karifa Sanfo, Sadeque Mithu, Will Mason, Stratos Sitsanidis and Danny Da`Val.

ABSTRACT

Diabetes is a chronic metabolic disease that occurs when there is a deficiency in the production of insulin by the pancreas or when the body cannot effectively use the insulin it produces. Therefore, the treatment of diabetes aims to control the levels of glucose in the blood, which involves many different approaches, including insulin therapy many times.

To date, even though many strategies have been proposed as alternative administration routes for insulin, subcutaneous injections still the most common administration route. To overcome the disadvantages imposed by the daily subcutaneous injections of insulin and to increase patient compliance, this thesis aimed to develop stable coated microneedles for rapid transdermal delivery of insulin. For that, polymeric microneedles made of a biocompatible resin class I were developed using 3D printing technology and studied along with a commercial metallic microneedle. The penetration studies showed that the 3D printed MNs presented superior penetration capacity compared to the metallic microneedles.

To apply specific doses of insulin on the microneedles, an Inkjet printing technology was used. The SEM revealed the formation of fine layers on the microneedles without loss of insulin during the coating process. Moreover, Micro-CT showed that the films stayed onto the MNs surfaces during the piercing.

In order to address the challenges with insulin instability, different polymers and sugars were used as drug carriers to preserve insulin integrity during the coating process as well as to form uniform coating layers and facilitate rapid release rates. Circular dichroism and Raman spectroscopy demonstrated that most of the carriers maintained the secondary structure of insulin in its native form in the films. Moreover, X-ray diffraction analysis revealed that the insulin-carriers tended to originate amorphous films. The release studies using Franz cell diffusion showed that insulin is quickly released from the coated microneedles within 30 min. Furthermore, the animal studies showed that the coated 3D printed microneedles promoted a similar initial profile release to the SC injections, followed by a more sustained release pattern for all tested insulins (bovine, aspart and glargine).

TABLE OF CONTENTS

LIST OF FIGURES

LIST OF TABLES

LIST OF ABBREVIATIONS

µ-CT	X-ray computed microtomography
µ-M	Micromolar
2PP	Two-Photon polymerisation
AAC	Area under the curve
AAC	Area above the curve
CD	Circular Dichroism
CE	Coating efficiency
C_{max}	Maximum plasma insulin concentration
C_{min}	Minimum glucose level
DL	Detection limit
DLP	Digital Light Processing
FDM	Fused Deposition Modelling
Gel	Gelatin
HPLC	High Performance Liquid Chromatography
HU	Hounsfield units
Ins	Insulin
IU	International Units
Man	Mannitol
MNs	Microneedles
PBS 7.4	Saline phosphate buffer pH 7.4
QL	Quantification limit
RBA	Relative bioavailability
RPA	Relative Pharmacology
SC	Subcutaneous
SEM	Scanning Electron Microscopy
SLA	Stereolithography
Sol	Soluplus
T0	Time zero
T30	Time 30 days
TDDS	Transdermal Drug Delivery Systems
TFA	Trifluoroacetic acid
T_{max}	Time point of maximum plasma insulin concentration
T_{min}	Time point of minimum glucose level
Treh	Trehalose
Tyr	Tyrosine
WHO	World Health Organization
XRD	X-ray diffraction
Xy	Xylitol

1 CHAPTER

INTRODUCTION

Diabetes mellitus is a chronic metabolic disorder characterised by high blood glucose levels that occurs when the insulin produced is not enough and/or when the body cannot use it effectively. When the diabetes is uncontrolled, the risk of infection, blindness, lower limbs gangrene and sometimes amputation thereof increase. In this direction, it is extremely important a safe and effective treatment for disease control, since there is no cure yet. The treatment involves a healthy diet, regular physical exercise, oral medications and in many cases daily injection of insulin (WHO, 1999, 2018).

Like many drugs, insulin undergoes enzymatic degradation in the gastrointestinal tract and presents difficulties to permeate it. Although other routes of administration were proposed (Jose *et al.* 2012; Veuillez *et al.* 2001; Hollander 2007; Yaturu 2013; Chaudhury and Das 2011; Viswanathan, Muralidaran and Ragavan 2017), the daily subcutaneous injection is the most common alternative. However, these hypodermic needles present some disadvantages such as local pain, allergy, lipodystrophy, hyperinsulinemia, fear of needles, anxiety and difficulties application for senile people (Kinesh *et al.* 2010; Ramaiya *et al.* 2018).

Due to those issues caused by daily insulin subcutaneous injections of two or three times a day, several efforts have been made to improve insulin therapy and patient compliance (Khafagy *et al.* 2007; Brunton 2008).

Transdermal administration is an excellent route for the administration of drugs that are degraded in the gastrointestinal tract. However, the barriers imposed by the skin, especially the stratum corneum and epidermis, limit the passage of substances through it. Thus, only lipophilic molecules and low molecular weight can cross these barriers and be absorbed into the bloodstream (Bariya *et al.* 2012).

Though many different strategies have been studied to enhance skin permeability and create pathways big enough for molecules pass through it, the safe delivery of hydrophilic molecules and macromolecules still be a challenge (Benson 2005; Paudel *et al.* 2010; Wu *et al.* 2019; Szunerits and Boukherroub 2018).

Recently, many studies have been reported great results using microneedles as an alternative transdermal delivery system to deliver a wide range of materials through the skin including insulin (Chen *et al.* 2016; Mahato 2017; Chen *et al.* 2015; Ross *et al.* 2015; Uddin *et al.* 2015). Microneedles are minimally invasive systems composed by micrometric needles included in the same array capable of creating superficial pathways across the skin to allow the drug bypass the stratum corneum layer of the epidermis and then be absorbed systemically without however stimulating nerves (Kim, Park and Prausnitz 2012).

1.1 Diabetes

Diabetes is a worldwide chronical disease that according to its cause, it be classified by diabetes type 1 or diabetes type 2. Type 1 diabetes (formerly called insulin-dependent or childhood-onset) is characterised by irreversible destruction of pancreatic beta cells, which are responsible for the production of insulin. Because of the deficient insulin production, the body requires daily administration of insulin. On the other hand, type 2 diabetes (well known as non-insulin-dependent or adult-onset) comprises 90% of people with diabetes around the world and usually is characterised by the body's ineffective use of insulin. This type of diabetes is largely related to the excess of body weight and physical inactivity (WHO, 1999; 2013).

The imbalance between insulin sensitivity and insulin secretion presented in type 2 diabetes leads to an increase of the insulin secretion in the early stage of the disease as a tentative to metabolise a given amount of glucose. However, the insulin production is slowly decreased with the progressive destruction of the β-cells (Niswender 2011). Unfortunately, as a result, it is estimated that about 50% of the patients with diabetes type 2 will require insulin therapy within 6 years follow-up (Wright *et al.* 2002).

In both cases, hyperglycemia is a common effect of uncontrolled diabetes that over the time can lead to serious damage to many of the body's systems, especially to the heart, blood vessels, eyes, kidneys, and nerves, affecting the patients' quality of life (WHO, 1999; 2018). Then, optimal glycemic control in patients with diabetes can be achieved by a healthy diet, regular physical exercise, oral

medications and in many cases, daily injection of insulin which will altogether delay or even prevent those complications (American Diabetes Association 2010).

Studies have shown that diabetes is one of the fastest growing diseases in recent years, affecting millions of people worldwide. According to the International Diabetes Federation (IDF) in its eighth edition of the IDF Diabetes Atlas (2017), it is estimated that 425 million of people are suffering from diabetes with ages ranging from 20 to 79 years. From those, 30.2 million are in the United States, 12.5 million in Brazil and 2.7 million in the UK.

1.2 Skin structure

The skin represents 10% of the total body mass in adults, with an average total surface area of 2 m^2 and it is one of the most important organs of the body responsible for several essential functions including the maintenance of the body hydration, thermoregulation, hormonal synthesis, sensory perception and barrier protection against exogenous substances (Barry 2007; Waugh, Anne; Grant 2014).

The human skin is formed by three main layers which one with specific characteristics and some appendages such as hair follicles, sebaceous glands and sweat glands which offer aqueous channels into the skin (Figure 1.1). The exposed layer is the epidermis, followed by the dermis and finally the innermost layer, the hypodermis (HAE Benson, 2012).

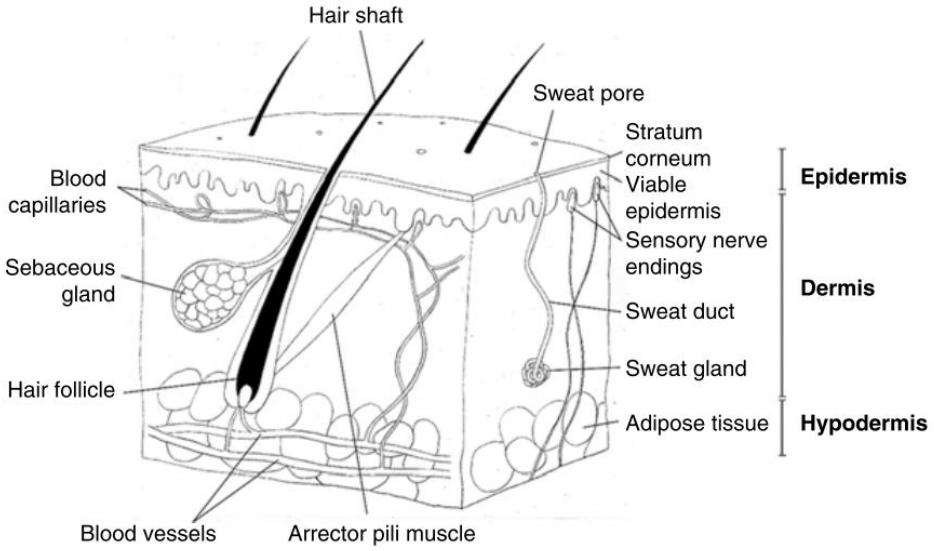

Figure 1.1. Diagrammatic representation of the different layers of human skin (Ng and Lau 2015).

Epidermis

The epidermis is 150 –200 μm thick formed by a stratified squamous epithelium arranged in five distinct layers, the stratum corneum and four others viable layers: the stratum lucidum, stratum granulosum, stratum spinosum and stratum basale or germinativum at the bottom. Besides all these layers, the epidermis does not have a vascular network, so it obtains all its nutritional needs by passive diffusion through the interstitial fluid (Bruno, Miller and Lim 2013).

Keratinocytes, Langerhans cells and melanocytes are the most common cells presents in the epidermis. The first ones are the main cells of the epidermis and reproduce themselves by mitosis at the stratum germinativum where they are attached to hemidesmosomes. The new cells produced slowly migrate towards the surface of the epidermis while their morphology gradually changes according to the maturation process through the layers. As they approach the surface, the cytoplasm is replaced by the fibrous protein keratin forming the stratum corneum (Alkilani, McCrudden and Donnelly 2015).

Melanocytes synthesise the pigment melanin in the deep germinative layer which is absorbed by the surrounding epithelial cells (keratinocytes) and provides protection against UV radiation. The colour of the skin is related to the concentration of melanin present in the skin whereas the amount produced depends on the genetics factors of each person and the environmental stimulation. The more the skin is exposed to sunlight more melanin is produced to protect that skin (Waugh, Anne; Grant 2014).

Finally, in a small proportion, Langerhans cells are antigens present in the stratum basale which can easily migrate to the epidermis or the dermis when it is needed and generate an immune response very easily (Benson 2012).

Stratum corneum

The stratum corneum is the main responsible for the efficient physical barrier of the skin. It consists of 10-30 layers (10-20μm) of maturated keratinocyte known as corneocytes which are mainly composed of keratin and lipid in a small proportion within a cornified cell envelope surrounded by a lipid extracellular matrix (Marwah *et al.* 2017).

Despite this efficient physical barrier, the skin has been explored for drug administration. The active molecules can be placed on the skin surface into an epidermal formulation such as cosmetics and insect repellents. They can also be delivered into deeper regions of the skin when it is in a topical formulation, or they can be absorbed systemically when designed for transdermal delivery which is an excellent route for administration of drugs that are degraded in the gastrointestinal tract (Bariya *et al.* 2012; Benson 2012).

Dermis

The dermis is a fibrous network of tissue that provides structure and resilience to the skin. It is approximately 3-5mm thick, consists of a matrix of connective tissue mainly composed of fibrous proteins such as collagen, elastin and reticulin which are surrounded by mucopolysaccharide (Barry 2007).

The dermis also contains many specialised cells and structures. The main cells present are fibroblasts, macrophages and mast cells whereas the main structures are sweat glands, sebaceous glands, hairs, sensory nerve endings and a rich capillary system (Waugh, Anne; Grant 2014).

1.3 Skin as a site of drug delivery

Once in contact with the skin surface, molecules have three potential pathways across the epidermis: through sweat ducts, via appendageal route (hair follicles and sebaceous glands) or across the stratum corneum (Figure 1.2). For most compounds, the skin permeation is a combination of those pathways, although the predominant permeation route is across the continuous stratum corneum. Furthermore, the appendage fractional area available for absorption is only 0.1%.

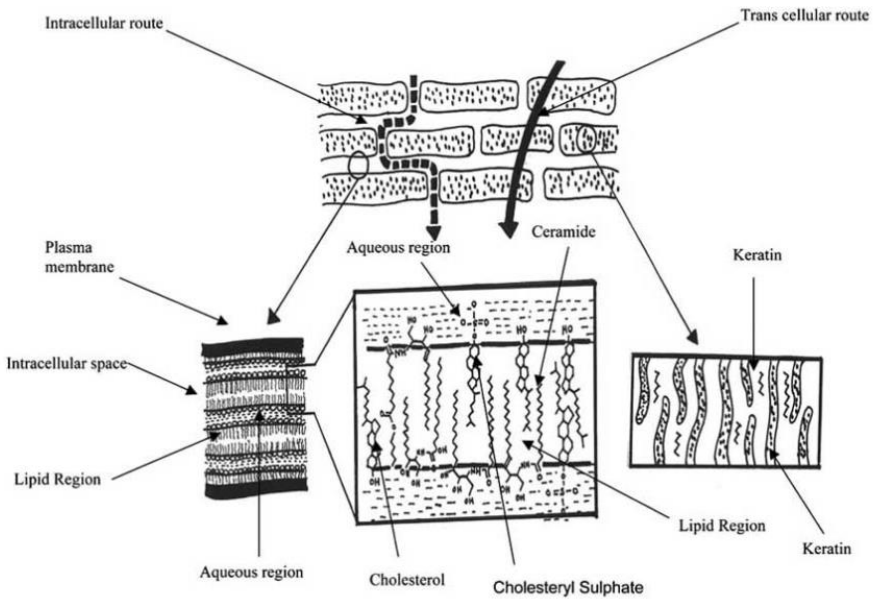

Figure 1.2. Diagrammatic representation of the route of penetration of drug molecules via the stratum corneum (Benson, 2005).

The stratum corneum permeation is due to passive absorption (diffusion) through the cells via transcellular route or into the cells via intercellular route (Benson 2012).

In a transcellular diffusion, the molecules need to pass through the corneocytes and interleaving lipids. Therefore, the molecules need to be eighter hydrophilic due to the high amount of keratin inside of the corneocytes and hydrophobic due to the intercellular lipid matrix. Whereas the diffusion via intercellular route, the molecules need to show hydrophobic properties to diffuse and partition through the intercellular lipid matrix (Benson 2012). Then only lipophilic molecules and low molecular weight can cross these barriers and be absorbed into the bloodstream (Bariya *et al.* 2012).

1.4 Insulin

Insulin is an anabolic hormone secreted by the pancreatic β-cells that is responsible for the uptake of glucose, free fatty acids and amino acids into adipose tissue, muscle, and the liver. Therefore, this hormone influences the storage of all macronutrients, being essential for life (Niswender 2011).

Insulin is a small globular protein with 5800 Daltons and made up of two peptide chains A and B linked together by two disulfide bonds. The A chain has 21 amino acids residues, it is fairly compact and consists of 2 sections of α-helix. The B-chain wrap around the A chain, and it has 30 amino acids residues and consists of a larger section of alpha-helix (Sluzky and Langer 1992; Ortiz *et al.* 2004).

In the first 50 years after being discovered, insulin was extracted and purified from bovine and porcine pancreas. Only in the 1980s with the recombinant DNA techniques that human insulin became commercially available for therapy (Bethel and Feinglos 2005). The difference among the human, porcine and bovine insulin takes place in their first structure (in their backbone) (Figure 1.3). While porcine insulin differs by only one amino acid at B30 residue, bovine insulin differs by three amino acids at A8, A10 and B30 (Ortiz *et al.* 2004).

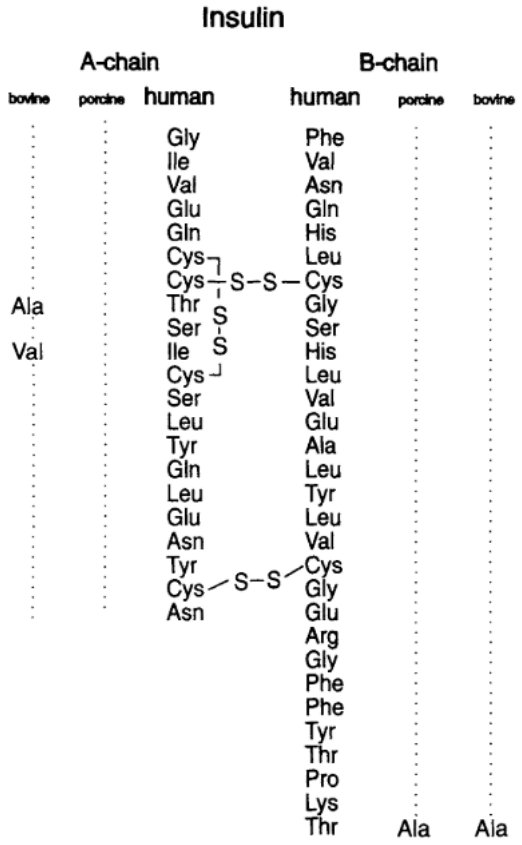

Figure 1.3. Structure of human, bovine and porcine insulin molecules (Testa and Meyer 1996).

Since the obtention of human insulin by recombinant DNA, many approaches have been studied to improve insulin therapy to approximate it to the physiological insulin profile (Melo *et al.* 2019). In healthy individuals, insulin is secreted in two phases 1) At a basal rate which is continuously released at low levels in response

to the endogenous glucose production from the liver and 2) In bolus, where insulin concentration quickly increases in response to food ingestion (Niswender 2011).

Once the purpose of the treatment of diabetes with insulin is to regulate an adequate blood glucose level by mimicking the physiologic pattern of insulin secretion, many insulin analogs were proposed for both basal and bolus phases (Bethel and Feinglos 2005). Therefore, insulin preparations are available as short-acting insulin to be used for bolus therapy (regular, lispro and aspart) and Intermediate (NPH) and Long-acting insulins (glargine and detemir) to replace the basal insulin secretion (Waller and Sampson 2018).

1.5 Insulin administration routes

Once insulin is a protein that is degraded in the gastrointestinal tract, hypodermic needles, insulin infusion pumps, jet injectors and pens are the most common methods for daily administration. The problem lies on the main disadvantages such as local pain, allergy, lipodystrophy, hyperinsulinemia, fear of needles, anxiety and difficulties application for senile people (Kinesh, Neelam, Punit, Bhavesh, & Pragna, 2010).

To overcome those issues, several non-invasive approaches for insulin delivery are being pursued. Nanoparticles, microparticles, micelles and other systems have been studied for oral administration of proteins (Jose *et al.* 2012; Chaudhury and Das 2011; Pan *et al.* 2002; Luo *et al.* 2016; Anselmo, Gokarn and Mitragotri 2018; Ibsen *et al.* 2018; Yaturu 2013). However, the low bioavailability still is the major challenge once insulin is degraded by the low pH in the stomach and by different digestive enzymes in the stomach and small intestine.

The oral mucosa is also an alternative route for the administration of insulin. Although, only a few studies have evaluated the buccal route in humans (Veuillez *et al.* 2001; Senel *et al.* 2001; Heinemann and Jacques 2009). The main barrier here is the multi-layered structure of the oral epithelium combined with the continuous but highly variable flow of saliva which difficult the absorption of insulin. (Owens and Zinman 2003).

The pulmonary route for insulin delivery is an interesting route due to the large surface area and high permeability for drug absorption. The drugs can be formulated as dried powder or solutions and used like asthma inhalers. However, more studies need to be done to guarantee the safety of the lungs (Hollander 2007; Yaturu 2013; Sibum *et al.* 2018; Huang and Wang 2006).

1.6 Transdermal Delivery Systems

Transdermal drug delivery systems (TDDS) are an attractive alternative route for drugs that undergo enzymatic degradation in the gastrointestinal tract or presents difficulties to permeate it, such as large and hydrophilic proteins. Those systems are designed to overcome the stratum corneum barrier and release the drug into the viable epidermis or dermis to be systemically absorbed without stimulating nerves or damaging the deeper tissues (Alexander *et al.* 2012).

The key factors that determine the success of a TDDS are related to the physical-chemical characteristics of the drug into the formulation (partition coefficient, molecular size and solubility) the characteristics of the skin (if it is intact, skin age and site, degree of hydration and skin temperature) and finally, the area of application, if there is any pre-treatment of the skin and the contact time of the formulation with the skin (Alexander *et al.* 2012).

In order to enhance skin permeability and create pathways big enough for molecules pass through it a number of different strategies ranging from chemical to physical methods have been studied (Benson 2005; Paudel *et al.* 2010; Chen *et al.* 2009; Bolhassani 2019; Patel, Cholkar and Mitra 2014) and according to their approach and physical-chemical properties Prausnitz and Langer (2008) have classified the TDDS into 3 different generations:

First generation TDDS

The first generation of TDDS is represented by transdermal patches which are basically an adhesive to be placed on the skin where the drug can be stored into the adhesive layer or in a reservoir which is usually made by a special membrane to control the drug release through the skin. Along with those patches, metered liquid sprays, gels and other topical formulations were developed to be applied on

the skin. Furthermore, mostly small lipophilic and potent drugs can be delivered in the therapeutic range by passive diffusion alone through these systems.

Even though the first-generation approach to transdermal delivery is limited primarily by the barrier posed by stratum corneum, many products used for clinical applications are in the market now such as patches of nitroglycerin, scopolamine, lidocaine, testosterone, estradiol, nicotine and many others (Al-Hanbali *et al.* 2019).

Overall, the first-generation approach is used to deliver mostly small lipophilic and potent drugs once it is driven by passive diffusion alone.

Second generation TDDS

The second generation of TDDS includes conventional chemical enhancers, iontophoresis and non-cavitational ultrasound. Basically, all methods developed in this generation are guided by the necessity to increase skin permeability and application of an external driven force for transport the drug into the skin.

Solvents and surfactants are the most common chemical enhancers used for transdermal delivery along with liposomes, dendrimers, microemulsions and prodrugs. Among the physical methods, iontophoresis is a technique used to enhance the transdermal delivery of charged compounds through the skin using a continuous low voltage current whereas non-cavitational ultrasound uses an oscillating pressure wave to disrupt stratum corneum lipid structure and thereby increase drug permeability.

Third generation TDDS

The third generation of TDDS aims a stronger disruption of the stratum corneum and employs techniques like chemical enhancers combined, biochemical enhancers, electroporation, microporation (thermal ablation, laser ablation and microneedles), cavitational ultrasound and microdermabrasion (sandpaper and pressurized particles) (Prausnitz and Langer 2008; Paudel *et al.* 2010).

Combinations of chemical enhancers

Chemical enhancers are substances that facilitate transdermal drug delivery by altering the lipid structure of the stratum corneum and thus increasing its

permeability for molecules pass through it. Although there are several different categories of components, the delivery of high-molecular-weight compounds still a challenge and the irritation of the skin a major problem. To overcome those issues, different combinations of chemical enhancers at a low concentration and specific ratios can exhibit high potent penetration with a relative lack of irritation (Karande, Jain, & Mitragotri, 2004).

Biochemical enhancers

Biochemical enhancers are used to improve skin permeability using peptides which interact with the skin by different mechanisms increasing the amount of drug that can pass through the stratum corneum (Y. Chen et al., 2006; Kim, Ludovice, & Prausnitz, 2007; Li et al., 2008; Rothbard et al., 2000). A study shows that in some cases they can be much more effective when combined with a chemical enhancer (Kim et al., 2007).

Cavitational ultrasound

When applied to the skin, ultrasound can produce cavitation bubbles at low frequencies which can disrupt the stratum corneum structure and increase skin permeability. One knows that low-frequency ultrasound is capable of generating microbubbles in the water and tissue that after being collapsed generates water channels within the lipid bilayers (Baris E. Polat1, Douglas Hart2, Robert Langer1, 2011; Smith, 2007).

Electroporation

In electroporation, high-voltage electrical pulses are applied in the skin for a few milliseconds to create transient disruptions in the structure of the stratum corneum which facilitate the transport of small and large molecules otherwise unable to permeate at all (Denet, Vanbever and Gale 2004; Ita 2016).

Microdermabrasion

Microdermabrasion uses pressurised particles, such as alumina or sodium chloride, to remove the stratum corneum and increases skin permeability. A similar effect can be achieved by using sandpaper. Though it was developed in the 1980s

for cosmetics procedures in order to reduce superficial scars, tattoos, wrinkles and fine lines, several studies have shown that microdermabrasion can be used effectively to increase transdermal delivery of low molecular weight compounds (Fujimoto, Shirakami and Tojo 2005; Andrews *et al.* 2011).

Microporation

Microporation involves the creation of microchannels in the skin in order to transport of water-soluble molecules and macromolecules through it. Thermal or radiofrequency ablation and laser ablation can create microchannels in the skin by exposure it to short, high-temperature pulses which can cause structural disruption and removal of stratum corneum without significantly heating or damaging the deeper tissues. Whereas microneedles create those channels by cutting a pathway in the skin (Banga, 2009).

1.7 Microneedles

Microneedles are considered as a hybrid technique between hypodermic needles and transdermal patches and are composed of micrometric needles included in the same array (Figure 1.4), which depending on their size, they can pierce the stratum corneum and the epidermis without, however, stimulating nerves (Donnelly, Raj Singh and Woolfson 2010; Tuan-Mahmood *et al.* 2013).

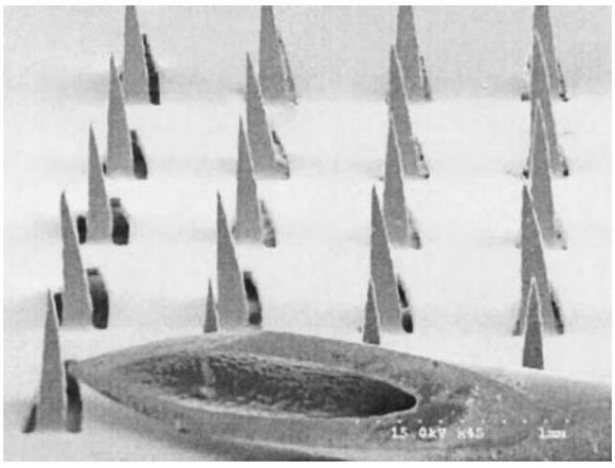

Figure 1.4. Comparison between hypodermic needle and microneedles (Martanto et al. 2004).

Such systems are a promising strategy to deliver drugs independent of their size or lipophilicity and can be obtained from a variety of materials (metals,

polymers, silicon, ceramic) (Figure 1.5) and techniques (infrared laser, lithography, micromolds, electroplating, etching) (Mcallister et al., 2003, Tuan-Mahmood et al., 2013; van der Maaden, Jiskoot, & Bouwstra, 2012).

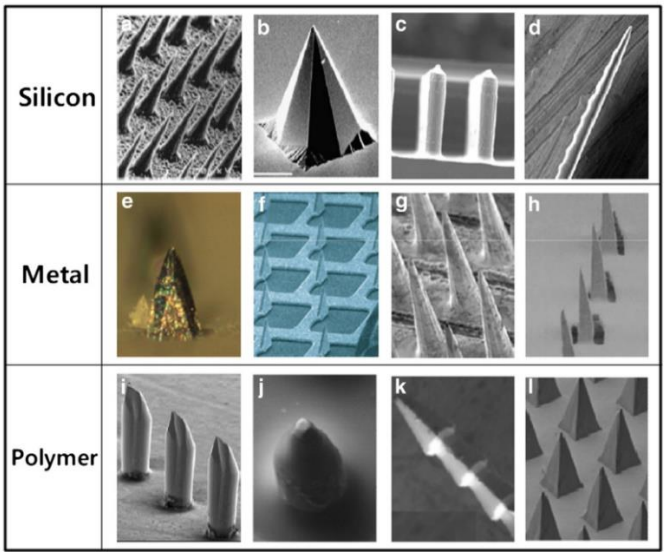

Figure 1.5. Solid microneedles made of silicon, metal and polymer (Kim, Park, and Prausnitz 2012).

Usually, MN can be classified into 5 different types - poke-and-patch, coat-and-poke, poke-and-release, poke-and-flow and hydrogel-forming MN as Figure 1.6 shows.

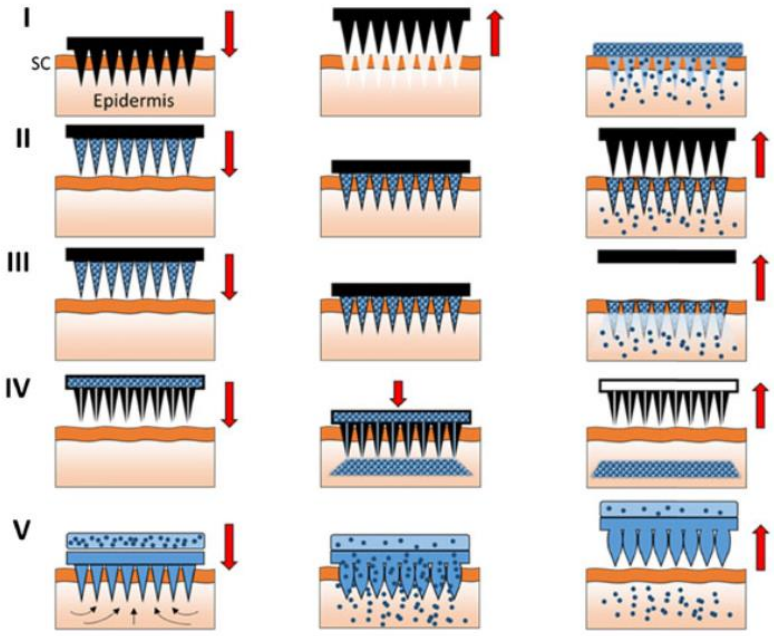

Figure 1.6. Schematic representation of Microneedles classification.I) poke-and-patch, II) coat-and-poke, III) poke-and-release, IV) poke-and-flow and V) hydrogel-forming MN (Larrañeta *et al.* 2016).

Poke-and-patch

In the poke and patch approach, solid microneedles arrays are used as a pre-treatment to pierce the skin and create microchannels upon which a transdermal patch or a conventional drug formulation is subsequently applied, and the molecules move passively through these microchannels. However, the major disadvantage of these solid microneedles is the requirement of a two-step application process (Tuan-Mahmood et al., 2013).

Coat-and-poke

Coat and poke approach consists of solid microneedles coated with a drug/vaccine formulation that after being inserted into the skin the formulation is dissolved and the drug released. The major advantage is the avoidance of heating process (Vrdoljak *et al.* 2012; Harvinder S Gill and Prausnitz 2007). Such coated MNs have been used to deliver vaccines, proteins, peptides and DNA into the skin. (Larrañeta *et al.* 2016; Qiu *et al.* 2012).

Poke-and-release

Poke and Release are related to dissolvable microneedles which are made of soluble/biodegradable substances such as sugars, carbohydrates or synthetic polymers. Studies have been shown that those MN can be utilised to deliver a range of different substances including insulin (Ito *et al.* 2012; Liu *et al.* 2012; M.-H. Ling and Chen 2013) and vaccines (Matsuo et al., 2012; Wu, 2013). They also have been used with iontophoresis (Garland *et al.* 2012).

Poke-and-flow

Poke and flow are related to hollow MN of different materials such as silicon, metal, hollow glass, polymers and ceramic. As the name suggests, there is a hollow inside of each microneedle through which the molecules can be transported to the interior of the epidermis. The microneedles have a conical geometry with an internal cavity which is also conical and through which a convective flux of drug is delivered into deeper skin layers (Xie, Li and Yu 2015; Lhernould, Deleers and Delchambre 2015).

Hydrogel-forming MN

Finally, hydrogel-forming MN arrays consist of MN made of polymers such as hyaluronic acid, agarose, chitosan, polyvinyl alcohol and many others compounds which exhibit the ability to swell in water and keep a significant amount of water within the structures. Attached to the baseplate of the array there is a patch containing the drug which rapidly diffuses through the swollen microprojections (Donnelly *et al.* 2012; Hong *et al.* 2014). They can also be made in a wide range of patch sizes and geometries and be easily sterilised. Furthermore, they can be employed to deliver high-molecular-weight compounds (Donnelly *et al.* 2012; Donnelly *et al.* 2014; Banga 2009; McCrudden, Alkilani, Courtenay, *et al.* 2014).

Even though many different MNs approaches have been developed, the best piercing properties are usually offered by solid MNs, mostly due to the inherent characteristics of the applied materials, yet, for most of them, the fabrication process is usually time-consuming and involve a complex multi-step process which can limit a scaling up production. In this sense, 3D printed microneedles can be an interesting strategy for the rapid fabrication of solid MNs with good mechanical properties.

1.8 3D Printed Microneedles

3D printing is a family of different techniques that apply a computer model design to create physical three-dimensional objects. The main technologies that have or are expected to present the most promising contribution in the field of transdermal drug delivery, more specifically with microneedles are a) Fused Deposition Modelling and b) Photopolymerization-based technologies.

1.9 Fused Deposition Modelling (FDM)

FDM is one of the most commonly 3D printing techniques and it is based on the melt-extrusion process where thermoplastic polymers in the form of filaments are heated and the semi-melted material is deposited in thin strands in a layer-by-layer manner (Park *et al.* 2018).

Although this technology has been demonstrating successful pharmaceutical applications in drug delivery (Goyanes, Chang, *et al.* 2015; Sadia *et al.* 2016; Alhijjaj,

Belton and Qi 2016), the resolution of elaborate structures in the microscale still a challenge and cannot be yet successfully applied for MNs fabrication (Economidou, Lamprou and Douroumis 2018; Low *et al.* 2017).

1.10 Photopolymerization-based technologies

Photopolymerization-based technologies use photopolymer resin that is hardened or cured through a selective polymerisation upon laser stimulation. The most promising technologies in this group for microneedles applications are a) Two-Photon Polymerisation (2PP), b) Stereolithography (SLA) and c) Digital Light Processing (DLP).

Two-Photon polymerisation (2PP)

The two-photon polymerisation (2PP) also uses photo-sensitive polymers with, however, a near-infrared laser with ultrashort pulses. In this case, the laser beam focus on local points volumes which is solidified by two-photon absorption. The main advantage of this technology is the capability of production of elaborate and complex structures in the micro and nanoscale (Gittard *et al.* 2010; Lee *et al.* 2008; Zhou, Hou and Lin 2015). Although 2PP allows the manufacture of structures with small details, the technology still very expensive and the large industrial production of MNs could be a challenge.

Stereolithography and Digital Light Processing

SLA was the first commercially available solid freeform fabrication technique developed in the 1980s. This additive manufacturing process solidifies the liquid resin contained in a reservoir through an UV-laser beam process in a layer-by-layer manner while DLP is an evolution of SLA technology but instead of a laser beam, it uses a projector laser which makes it much faster than SLA once it prints the whole layer at once (Figure 1.7) (Economidou, Lamprou and Douroumis 2018).

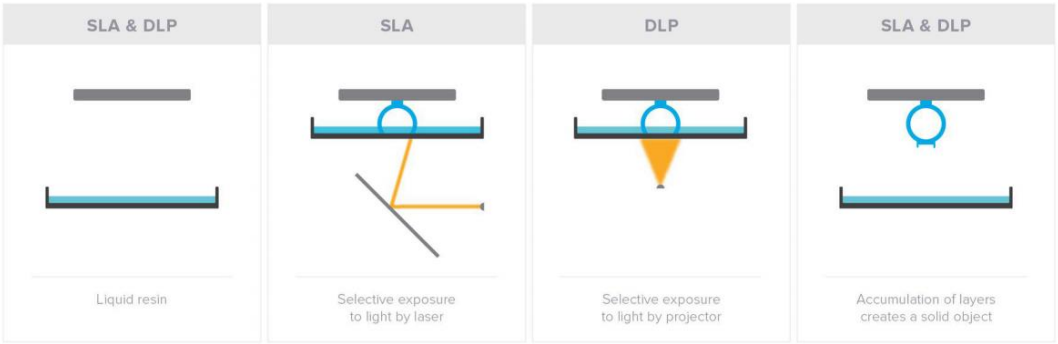

Figure 1.7. SLA and DLP photopolymerization laser mechanisms (Formlabs 2017).

Although they follow the same principle, in the SLA technique, the laser beam solidifies the resin drawing rounded lines as it goes along, while in the DLP approach, a digital projector screen flashes a single image of each layer across the entire cross-section of the object.

Even though DLP has the advantage of achieving faster print times, its resolution is dependent of the projector and it is limited by its fixed number of pixels, what makes it challenging to print small and detailed objects. In this sense, once SLA printers do not depend on the resolution of the projector, they are capable of printing small structure with a high resolution, making them a good option for transdermal delivery applications and microneedles fabrication.

Among all the available materials for 3D printing, only a few biocompatible resins are available for stereolithography. Dental SG resin is an FDA approved Class I biocompatible resin (EN-ISO 10993-1:2009/AC:2010, USP Class VI) used for dental applications with excellent mechanical strength that can be successfully applied for fabrication of microneedles (Pere *et al.* 2018).

Overall, 3D printing is a promising approach for MNs fabrication that overcomes many limitations and drawbacks imposed by other techniques such as costly equipment, multiple complex step-processes, time-consuming and difficult to scale up.

1.11 Coated Microneedles

Many studies have been reported great results using microneedles to deliver a wide range of drugs (Martanto *et al.* 2004; Davis *et al.* 2005; Wu *et al.* 2010; Qin *et al.* 2012), however, the difficulty of dose control imposed by the two-step

administration process of solid MNs, the blocking channels with hollow MNs and the harsh processing conditions for manufacture dissolvable MNs are the most limiting factors for a successful therapy.

On the other hand, coated microneedles is an appealing approach of transdermal delivery that involves only one-step administration process and can be used for rapid delivery of drugs (Kim *et al.* 2010; Ng, Fernando and Kendall 2012; Tas *et al.* 2012). It is made by solid microneedles coated with a drug formulation that after being inserted into the skin; the formulation is dissolved and the drug is released (Tuan-Mahmood *et al.* 2013).

Among the great variety of coating methods already developed, the most popular used to coat microneedles are dip coating and spray coating.

Dip coating

In the dip coating method, the microneedles are coated by dipping the MN array into a drug solution and then allowed it to dry to form a solid film coating. Many studies with successful results have been reported using this technique (Harvinder S. Gill and Prausnitz 2007; Ameri *et al.* 2014). However, the major challenges related with this process are (1) the difficulty to obtain an uniform coating related with the surface tension and (2) the imprecision of the dose desired due the slow drying process during which the solution layer can move and be relocated off the MN surface and consequently reduce or vary the dose desired (Haj-Ahmad *et al.* 2015).

Spray coating

Spray coating process is a reproducible and scalable process very common for coating tablets in the pharmaceutical industry that has been explored to film-coat microneedle arrays. Spray coating process undergoes three steps (1) atomisation, generation of fine droplets from the formulation, (2) the deposition and adherence of droplets onto the surface of MNs and the substrate and finally (3) the coalescence of droplets on the substrate forming an intact film coating (Vrdoljak *et al.* 2012; Perfetti *et al.* 2011; Haj-Ahmad *et al.* 2015). The major issue related to this technique is the great loss of the coating material on the substrate as well as the difficulty to control a specific dose.

1.12 Inkjet Printing

Inkjet printing is a liquid deposition technique that can build two and three-dimensional patterns and has been recently applied for coating solid MNs (Ross *et al.* 2015; Pere *et al.* 2018; Boehm *et al.* 2011; Uddin *et al.* 2015). Inkjet printing is a general term to describe both Continuous Inkjet (CIJ) and Drop on Demand (DoD) printings. Although they are guided for different physical process, they place tiny liquid drops which are digitally controlled (Daly *et al.* 2015).

The inkjet printing used in this work is based on a drop on demand and it is basically formed by (1) a piezodriven dispenser, a pipette formed by a piezoelectric ceramic that is deformed upon voltage appliance, thus ejecting a droplet from the nozzle, (2) Oscilloscope which controls the operation process and (3) Stroboscope which catches images before and after samples dispensing, analysing the pipette performance (see Figure 1.8) (Uddin *et al.* 2015).

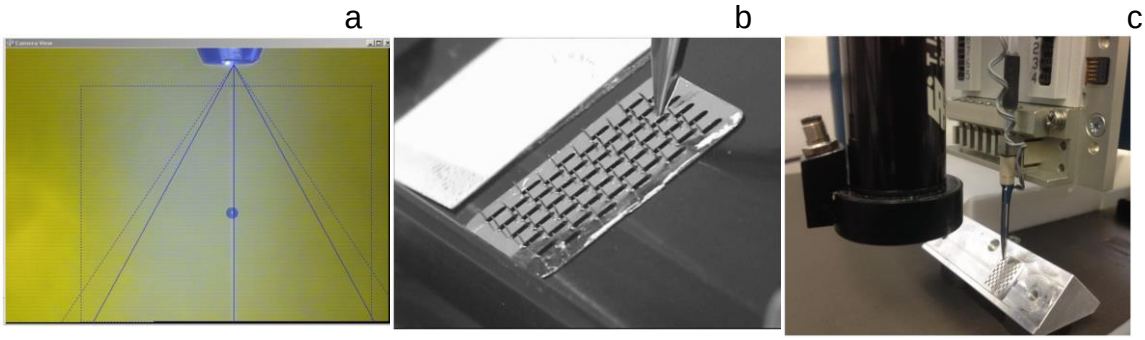

Figure 1.8. Inkjet coating of metallic microneedles array. (a) Drop diameter measured by a stroboscope. (b) MN positioned on a holder at an angle of 45°. (c) the overall image of the coating process (Modified from Uddin et al. 2015).

The process involves the ejection of a fixed volume of the formulation (solution or dispersion of the drug) to a substrate which then dries through solvent evaporation. The drop volume range from picoliters to microliters depending on the nozzle dimensions (Boehm *et al.* 2013).

1.13 Microneedles for insulin delivery

Recently, several polymeric and coated microneedles have been used to deliver a wide range of drugs into the skin in one step application process (Katsumi *et al.* 2012; McCrudden, Alkilani, Cian M McCrudden, *et al.* 2014; McGrath *et al.* 2014; Lahiji, Dangol and Jung 2015) but only a few studies involving insulin have

been done (Ito et al. 2006; Ito et al. 2012; Liu et al. 2012; Ling and Chen 2013; Lahiji, Dangol, and Jung 2015).

A study found that the amount of insulin loaded into the dissolvable microneedle can easily control the extent of the hypoglycaemic response. In this research, Liu et al. (2012) developed an insulin-loaded microneedles array using no heating step or organic solvents during its fabrication. They found that the microneedles made by hyaluronic acid using micromolding technique totally dissolved and released the insulin from microneedles within one hour.

Another biodegradable microneedle patch made of 3-aminophenyl boronic acid-modified alginate and hyaluronate, made by micromolding technique, was developed for quick release of insulin in the interstitial fluid of skin. However, to reach the minimum blood glucose level, the MNs needed twice the time for the same dose of SC injection (2hs) (Yu, Jiang, Zhang, *et al.* 2017).

Ling and Chen (2013) developed dissolvable MNs composed of starch and gelatin for rapid insulin release. In addition to the improvement of the insulin stability, the study showed that those polymeric microneedles can release the encapsulated insulin into the skin within 2 hours and exhibit an approximately 90% of the relative bioavailability (M.-H. Ling and Chen 2013).

In 2015, Lahiji et al. introduced a patchless dissolving microneedle called Microlancer. They proposed a carboxymethyl cellulose microneedle loaded with insulin whose needles are inserted into the skin through a device. They also compared the results of the insulin release profile and the *in vivo* delivery with the respective microneedles patch and the SC injection. They noted that the Microlancer insulin release was much more effective than its respective microneedle patch, reaching the minimum blood glucose level in 3 hours.

Even though those studies have been shown considerable results, most of the polymeric materials used for dissolvable MNs are suitable for sustained delivery of drugs but not convenient for rapid transdermal delivery due to its slow-degrading properties (Liu *et al.* 2012; Xie, Li and Yu 2015).

Moreover, the fabrication processes for the manufacture of dissolvable MNs is timing consuming and usually involves high temperatures and organic solvents which can limit the types of molecules that can be kept stable into the MN system.

Besides that, the incorporation of the drug inside the system can also compromise the mechanical strength of the MNs and therefore its performance. (Lee *et al.* 2015; Migalska *et al.* 2011).

Since the inkjet printing was successfully applied to coat different active agents onto MNs (Uddin *et al.* 2015; Boehm *et al.* 2013; Boehm *et al.* 2014; Boehm *et al.* 2011), in 2015, Ross et al. achieved uniform and reproducible polymeric-insulin coatings on metallic microneedle arrays whose release studies revealed rapid insulin release profiles.

To date, many interesting strategies have been proposed as alternatives to subcutaneous injection of insulin; however, only a limited number of studies has focused on the delivery of insulin through a transdermal route using microneedles.

1.14 Insulin stabilisers

Among many materials that have been used for transdermal drug delivery, sugars and polymers are an interesting strategy to protect insulin molecules against degradation. Depending on their characteristics, they can also be used for rapid release of macromolecules such as insulin. In this sense, below are the selected materials used in this research.

Gelatin

Gelatin is a biopolymer obtained by controlled denaturation of collagen isolated from bovine and pigskin, cartilages and bones. Depending on the procedures of the pre-treatment of the collagen and the conditions of its denaturation, basically two types of gelatin can be obtained, type-A and type-B gelatin. Type-A gelatin is obtained under acid treatment conditions and has an isoelectric point at pH≈ 8-9 whereas Type-B gelatin is obtained under alkaline conditions and has an isoelectric point at pH ≈ 4-5 (Gomez-Guillen *et al.* 2011).

Gelatins have been widely used in pharmaceutical applications as stabilisers of macromolecules due to its biodegradability, biocompatibility, non-immunogenicity and film-forming ability (Thyagarajapuram, Olsen and Middaugh 2007; Chen, Shyu and Chen 2018; Lee *et al.* 2017; Nair and Laurencin 2007). Furthermore, previous

studies have been shown that gelatin enhanced insulin absorption through transmucosal membranes (Seki *et al.* 2005).

Soluplus

Soluplus ® is a new polymer composed by 57% vinyl caprolactam, 30% vinyl acetate (hydrophobic groups) and 13% PEG 6000 (hydrophilic groups) whose molecular weight ranges from 90,000 to 140,000 Daltons. This polymer is soluble in water, acetone (up to 50%), methanol (up to 45%), ethanol (up to 25%) and dimethylformamide (up to 50%) (BASF 2010).

Soluplus is a copolymer with amphiphilic properties that is widely used to stabilize molecules, enhance the solubility of poorly soluble drugs and promote fast drug release (Ross *et al.* 2015; Agrawal *et al.* 2016; Cavallari *et al.* 2016; Altamimi and Neau 2017; Homayouni *et al.* 2014; Paaver *et al.* 2014).

Trehalose

Trehalose is a water-soluble disaccharide with low chemical reactivity and a non-reducing nature. The anhydrous form ($C_{12}H_{22}O_{11}$) has 342.31g/mol while the dehydrated form ($C_{12}H_{22}O_{11}.2H_20$) has 378.33 g/mol (Rowe *et al.* 2012b). Previous studies found that trehalose were capable of inhibiting or reduce aggregates of denaturated protein molecules (Singer and Lindquist 1998) and because its unique properties, trehalose has also been used to stabilize proteins and vaccines during dehydration processes (Haque *et al.* 2015; Chang *et al.* 2005; Allison *et al.* 1999; Yong *et al.* 2009; Faghihi *et al.* 2016).

Recently, trehalose was also successfully applied for molecule stabilisation of dissolvable (Lee *et al.* 2011; Dillon *et al.* 2017) and coated microneedles (Ross *et al.* 2015; Pere *et al.* 2018; Tas *et al.* 2012; Kim *et al.* 2010; Choi *et al.* 2013). Those results are very promising and appealing for stabilisation of macromolecules for transdermal delivery through microneedles.

Xylitol

Xylitol is a natural sugar that occurs in many fruits. Industrially, it is commonly derived from various types of hemicellulose obtained from wood, corn cobs, cane

pulp, seed hulls and shells. This polyol ($C_5H_{12}O_5$) has a molecular weight of 152.15 g/mol and is highly soluble in water (Rowe *et al.* 2012c).

Xylitol is largely used in the food industry and due to its extremely low relative glycemic response, it can also be safely consumed as a diabetic sweetener (Olinger and Pepper 2001). Besides that, xylitol is also widely used in the odontological and pharmaceutical industry (Dasgupta *et al.* 2017; Yu 2001; Ur-Rehman *et al.* 2013); Furthermore, previous studies showed that xylitol can be used to improve the stability of proteins and enzymes (Martin *et al.* 2012; Usha *et al.* 2006; Gekko and Mirikawa 1981) and also promote the rapid release of drugs (Pere *et al.* 2018; Arafa *et al.* 2016; Sjökvist and Nyström 1991).

Mannitol

Mannitol also occurs as a natural alcohol sugar ($C_6H_{14}O_6$) that is largely used in the food, odontological and pharmaceutical industry (Olinger and Pepper 2001). Differently from its isomer sorbitol, mannitol is an inert non-hygroscopic powder (Rowe *et al.* 2012a).

In the drug delivery field, several studies have been reported the good stabilisation properties of mannitol on proteins (Kim, Sioutas and Shing 2009), and enzymes (Izutsu, Ken-ichi; Yoshioka, Sumie; Terao 1994; Kim, Akers and Nail 1998). Mannitol has also shown excellent properties to protect protein molecules during the dehydration process (Ohtake, Kita and Arakawa 2011) which makes it a good candidate for stabilising proteins of coated MNs.

1.15 Key objectives of the research

The purpose of this research was to develop coated microneedles for rapid transdermal delivery of insulin by 1) Finding stable aqueous polymeric and sugary insulin formulations ratios for coating microneedles through inkjet printing, 2) Developing 3D printed microneedles using stereolithography technique, 3) Optimizing the coating formulations onto metallic and 3D printed MNs according to the required dose, 4) Evaluating the *in vitro* release of insulin by the MNs and 5) Evaluating the *in vivo* release of the best coated MNs system.

1.16 References

Agrawal, A., Dudhedia, M., Deng, W., Shepard, K., Zhong, L., Povilaitis, E. and Zimny, E. (2016). Development of Tablet Formulation of Amorphous Solid Dispersions Prepared by Hot Melt Extrusion Using Quality by Design Approach. *AAPS PharmSciTech*, 17(1), 214–232.

Al-Hanbali, O.A., Khan, H.M.S., Sarfraz, M., Arafat, M., Ljaz, S. and Hammed, A. (2019). Transdermal patches: Design and current approaches to painless drug delivery. *Acta Pharmaceutica*, 69.

Alexander, A., Dwivedi, S., Ajazuddin, Giri, T.K., Saraf, Swarnlata, Saraf, Shailendra and Tripathi, D.K. (2012). Approaches for breaking the barriers of drug permeation through transdermal drug delivery. *Journal of Controlled Release*, 164(1), 26–40.

Alhijjaj, M., Belton, P. and Qi, S. (2016). An investigation into the use of polymer blends to improve the printability of and regulate drug release from pharmaceutical solid dispersions prepared via fused deposition modeling (FDM) 3D printing. *European Journal of Pharmaceutics and Biopharmaceutics*, 108, 111–125.

Alkilani, A.Z., McCrudden, M.T.C. and Donnelly, R.F. (2015). Transdermal drug delivery: Innovative pharmaceutical developments based on disruption of the barrier properties of the stratum corneum. *Pharmaceutics*, 7(4), 438–470.

Allison, S.D., Chang, B., Randolph, T.W. and Carpenter, J.F. (1999). Hydrogen Bonding between Sugar and Protein Is Responsible for Inhibition of Dehydration-Induced Protein Unfolding. *Archives of Biochemistry and Biophysics*, 365(2), 289–298.

Altamimi, M.A. and Neau, S.H. (2017). Investigation of the in vitro performance difference of drug-Soluplus® and drug-PEG 6000 dispersions when prepared using spray drying or lyophilization. *Saudi Pharmaceutical Journal*, 25(3), 419–439.

Ameri, M., Kadkhodayan, M., Nguyen, J., Bravo, J.A., Su, R., Chan, K., Samiee, A. and Daddona, P.E. (2014). Human growth hormone delivery with a microneedle transdermal system: Preclinical formulation, stability, delivery and PK of therapeutically relevant doses. *Pharmaceutics*, 6(2), 220–234.

American Diabetes Association (2010). Diagnosis and Classification of Diabetes Mellitus. *Diabetes Care*. 33(Suppl 1), pp. S62–S69.

Andrews, S.N., Zarnitsyn, V., Bondy, B. and Prausnitz, M.R. (2011). Optimization of microdermabrasion for controlled removal of stratum corneum*. International Journal of Pharmaceutics*, 407(1–2), 95–104.

Anselmo, A.C., Gokarn, Y. and Mitragotri, S. (2018). Non-invasive delivery strategies for biologics. *Nature Reviews Drug Discovery*, 18(1), 19–40.

Arafa, M.F., El-Gizawy, S.A., Osman, M.A. and El Maghraby, G.M. (2016). Xylitol as a potential co-crystal co-former for enhancing dissolution rate of felodipine: preparation and evaluation of sublingual tablets. *Pharmaceutical Development and Technology*, 23(5), 454–463.

Banga, A.K. (2009). Microporation applications for enhancing drug delivery. *Expert opinion on drug delivery*, 6(4), 343–354.

Bariya, S.H., Gohel, M.C., Mehta, T.A. and Sharma, O.P. (2012). Microneedles: an emerging transdermal drug delivery system. *Journal of Pharmacy and Pharmacology*, 64(1), 11–29.

Barry, B. (2007). Transdermal Drug Delivery In: M. E. Aulton, ed. Aulton's *Pharmaceutics the design and manufacture of medicines*. Elsevier Ltd, pp.565–597.

BASF (n.d.). Soluplus®. [Online]. Available from: https://industries.basf.com/bin/bws/documentDownload.en.8805242743253 [Accessed 3 March 2019]

Benson, H. (2012). Skin Structure, Function, and Permeation In: A. C. Benson, H. A. E; Watkinson, ed. *Transdermal and Topical Drug Delivery: Principles and Practice*, pp.448.

Benson, H. (2005). Transdermal Drug Delivery: Penetration Enhancement Techniques. *Current Drug Delivery*, 2(1), 23–33.

Bethel, M.A. and Feinglos, M.N. (2005). Basal insulin therapy in type 2 diabetes. *The Journal of the American Board of Family Practice*, 18(3), 199–204.

Boehm, R.D., Miller, P.R., Daniels, J., Stafslien, S. and Narayan, R.J. (2014). Inkjet printing for pharmaceutical applications. *Biochemical Pharmacology*, 17(5), 247–252.

Boehm, R.D., Miller, P.R., Hayes, S.L., Monteiro-Riviere, N.A. and Narayan, R.J. (2011). Modification of microneedles using inkjet printing. *AIP Advances*, 1(2),1–13.

Boehm, R.D., Miller, P.R., Schell, W.A., Perfect, J.R. and Narayan, R.J. (2013). Inkjet printing of amphotericin B onto biodegradable microneedles using piezoelectric inkjet printing. *Jom*, 65(4), 525–533.

Bolhassani, A. (2019). Improvements in chemical carriers of proteins and peptides. *Cell Biology International*, 43, 437-452.

Bruno, B.J., Miller, G.D. and Lim, C.S. (2013). Basics and recent advances in peptide and protein drug delivery. *Therapeutic Delivery*, 4(11), 1443–1467.

Brunton, S. (2008). Insulin delivery systems: reducing barriers to insulin therapy and advancing diabetes mellitus treatment. *The American journal of medicine*. 121(6 Suppl), S35-41.

Cavallari, C., Ternullo, S., Tarterini, F. and Fini, A. (2016). Release Problems for Nifedipine in the Presence of Soluplus. *Journal of Pharmacy and Pharmaceutics*. 3(2), 70–82.

Chang, L., Shepherd, D., Sun, J., Ouellette, D., Grant, K.L., Tang, X. and Pikal, M.J. (2005). Mechanism of protein stabilization by sugars during freeze-drying and storage: Native structure preservation, specific interaction, and/or immobilization in a glassy matrix. *Journal of Pharmaceutical Sciences*, 94(7), 1427–1444.

Chaudhury, A. and Das, S. (2011). Recent Advancement of Chitosan-Based Nanoparticles for Oral Controlled Delivery of Insulin and Other Therapeutic Agents. *AAPS PharmSciTech*, 12(1), 10–20.

Chen, C.H., Shyu, V.B.H. and Chen, C.T. (2018). Dissolving microneedle patches for transdermal insulin delivery in diabetic mice: Potential for clinical applications. *Materials*, 11(9), 1-10.

Chen, H., Zhu, H., Zheng, J., Mou, D., Wan, J., Zhang, J., Shi, T., Zhao, Y., Xu, H. and Yang, X. (2009). Iontophoresis-driven penetration of nanovesicles through microneedle-induced skin microchannels for enhancing transdermal delivery of insulin. *Journal of Controlled Release*, 139(1), 63–72.

Chen, J., Qiu, Y., Zhang, S., Yang, G. and Gao, Y. (2015). Controllable coating of microneedles for transdermal drug delivery. *Drug development and industrial pharmacy*, 3(41), 415–422.

Chen, W., Li, H., Shi, D., Liu, Z. and Yuan, W. (2016). Microneedles As a Delivery System for Gene Therapy*. Fronties in Pharmacolocy*, 7, 137.

Choi, H.J., Bondy, B.J., Yoo, D.G., Compans, R.W., Kang, S.M. and Prausnitz, M.R. (2013). Stability of whole inactivated influenza virus vaccine during coating onto metal microneedles. *Journal of Controlled Release*, 166(2), 159–171.

Daly, R., Harrington, T.S., Martin, G.D. and Hutchings, I.M. (2015). Inkjet printing for pharmaceutics – A review of research and manufacturing. *International Journal of Pharmaceutics*, 494(2), 554-567.

Dasgupta, Q., Movva, S., Chatterjee, K. and Madras, G. (2017). Controlled release from aspirin based linear biodegradable poly(anhydride esters) for anti-inflammatory activity. *International Journal of Pharmaceutics*, 528(1–2), 732–740.

Davis, S.P., Martanto, W., Allen, M.G., Member, S. and Prausnitz, M.R. (2005). Hollow Metal Microneedles for Insulin Delivery to Diabetic Rats. *IEEE Transactions on Biomedical Engineering*, 52(5), 909–915.

Denet, A., Vanbever, R. and Gale, D.P. (2004). Skin electroporation for transdermal and topical delivery. *Advanced Drug Delivery Reviews*, 56, 659–674.

Dillon, C., Hughes, H., O'Reilly, N.J. and McLoughlin, P. (2017). Formulation and characterisation of dissolving microneedles for the transdermal delivery of therapeutic peptides. *International Journal of Pharmaceutics*, 526(1–2), 125–136.

Donnelly, R.F., McCrudden, M.T.C., Alkilani, A.Z., Larrañeta, E., McAlister, E., Courtenay, A.J., Kearney, M.C., Raj Singh, T.R., McCarthy, H.O., Kett, V.L.,

Caffarel-Salvador, E., Al-Zahrani, S. and Woolfson, A.D. (2014). Hydrogel-forming microneedles prepared from ‘super swelling’ polymers combined with lyophilised wafers for transdermal drug delivery, *PLOS One*, 9(10), 1-10.

Donnelly, R.F., Raj Singh, T.R. and Woolfson, A. D. (2010). Microneedle-based drug delivery systems: microfabrication, drug delivery, and safety. *Drug delivery*, 17(4), 187–207.

Donnelly, R.F., Singh, T.R.R., Garland, M.J., Migalska, K., Majithiya, R., McCrudden, C.M., Kole, P.L., Mahmood, T.M.T., McCarthy, H.O. and Woolfson, A.D. (2012). Hydrogel-forming microneedle arrays for enhanced transdermal drug delivery. *Advanced Functional Materials*, 22(23), 4879–4890.

Economidou, S.N., Lamprou, D.A. and Douroumis, D. (2018). 3D printing applications for transdermal drug delivery. *International Journal of Pharmaceutics*, 544(2), 415–424.

Faghihi, H., Merrikhihaghi, S., Ruholamini Najafabadi, A., Ramezani, V., Sardari, S. and Vatanara, A. (2016). A Comparative Study to Evaluate the Effect of Different Carbohydrates on the Stability of Immunoglobulin G during Lyophilization and Following Storage. *Pharmaceutical Sciences*, 22(4), 251–259.

Formlabs (n.d.). A 3D Printing Technology Comparison. [Online]. Available from: https://formlabs.com/blog/3d-printing-technology-comparison-sla-dlp [Accessed 17 February 2019].

Fujimoto, T., Shirakami, K. and Tojo, K. (2005). Effect of microdermabrasion on barrier capacity of stratum corneum. *Chemical & Pharmaceutical Bulletin*, 53(8), 1014–1016.

Garland, M.J., Caffarel-Salvador, E., Migalska, K., Woolfson, A.D. and Donnelly, R.F. (2012). Dissolving polymeric microneedle arrays for electrically assisted transdermal drug delivery. *Journal of Controlled Release*, 159(1), 52–59.

Gekko, K. and Mirikawa, T. (1981). Preferential hydration of bovine serum albumin in polyhydric alcohol-water mixtures. *Journal of Biochemistry*, 90(1), 39–50.

Gill, Harvinder S and Prausnitz, M.R. (2007). Coated microneedles for transdermal delivery. *Journal of controlled release*, 117(2), 227–37.

Gill, Harvinder S. and Prausnitz, M.R. (2007). Coating formulations for microneedles. *Pharmaceutical research*, 24(7), 1369–80.

Gittard, S.D., Ovsianikov, A., Chichkov, B.N., Doraiswamy, A. and Narayan, R.J. (2010). Two Photon Polymerization of Microneedles for Transdermal Drug Delivery. *Expert Opinion on Drug Delivery*, 7(4), 513–533.

Gomez-Guillen, M.C., Gimenez, B., Lopez-Caballero, M.E. and Montero, M.P. (2011). Functional and bioactive properties of collagen and gelatin from alternative sources: A review. *Food Hydrocolloids*, 25(8), 1813–1827.

Goyanes, A., Chang, H., Sedough, D., Hatton, G.B., Wang, J., Buanz, A., Gaisford, S. and Basit, A.W. (2015). Fabrication of controlled-release budesonide tablets via desktop (FDM) 3D printing. *International Journal of Pharmaceutics*, 496(2), 414–420.

Haj-Ahmad, R., Khan, H., Arshad, M.S., Rasekh, M., Hussain, A., Walsh, S., Li, X., Chang, M.W. and Ahmad, Z. (2015). Microneedle coating techniques for transdermal drug delivery. *Pharmaceutics*, 7(4), 486–502.

Haque, M.A., Chen, J., Aldred, P. and Adhikari, B. (2015). Drying and denaturation characteristics of whey protein isolate in the presence of lactose and trehalose. *Food Chemistry*, 177, 8–16.

Heinemann, L. and Jacques, Y. (2009). Oral insulin and buccal insulin: A critical reappraisal. *Journal of Diabetes Science and Technology*, 3(3), 568–584.

Hollander, P.A. (2007). Evolution of a pulmonary insulin delivery (Exubera) for patients with diabetes. *Medscape General Medicine*, 9(1), 45.

Homayouni, A., Sadeghi, F., Varshosaz, J., Afrasiabi Garekani, H. and Nokhodchi, A. (2014). Promising dissolution enhancement effect of soluplus on crystallized celecoxib obtained through antisolvent precipitation and high pressure homogenization techniques. *Colloids and Surfaces B: Biointerfaces*, 122, 591–600.

Hong, X., Wu, Z., Chen, L., Wu, F., Wei, L. and Yuan, W. (2014). Hydrogel Microneedle Arrays for Transdermal Drug Delivery. *Nano-Micro Letters*, 6(3),191–199.

Huang, Y.Y. and Wang, C.H. (2006). Pulmonary delivery of insulin by liposomal carriers. *Journal of Controlled Release*, 113(1), 9–14.

Ibsen, K., Chen, R., Brown, T., Banerjee, A., Agatemor, C. and Mitragotri, S. (2018). Ionic liquids for oral insulin delivery. *Proceedings of the National Academy of Sciences*, 115(28), 7296–7301.

Ita, K. (2016). Perspectives on Transdermal Electroporation. *Pharmaceutics*, 8(9), 1–14.

Ito, Y., Hagiwara, E., Saeki, A., Sugioka, N. and Takada, K. (2006). Feasibility of microneedles for percutaneous absorption of insulin. *European Journal of Pharmaceutical Sciences*, 29(1), 82–88.

Ito, Y., Hirono, M., Fukushima, K., Sugioka, N. and Takada, K. (2012). Two-layered dissolving microneedles formulated with intermediate-acting insulin. *International Journal of Pharmaceutics*, 436(1–2), 387–393.

Izutsu, K., Yoshioka, S., Terao, T. (1994). Effect of Mannitol Crystallinity on the Stabilization of Enzymes during Freeze-Drying. *Chemical and Pharmaceutical Bulletin*, 42(1), 5–8.

Jose, S., Fangueiro, J.F., Smitha, J., Cinu, T.A., Chacko, A.J., Premaletha, K. and Souto, E.B. (2012). Cross-linked chitosan microspheres for oral delivery of insulin: Taguchi design and in vivo testing. *Colloids and Surfaces B: Biointerfaces*, 92, 175–179.

Katsumi, H., Liu, S., Tanaka, Y., Hitomi, K., Hayashi, R., Hirai, Y., Kusamori, K., Quan, Y.-S., Kamiyama, F., Sakane, T. and Yamamoto, A. (2012). Development of a Novel Self-Dissolving Microneedle Array of Alendronate, a Nitrogen-Containing Bisphosphonate: Evaluation of Transdermal Absorption, Safety, and Pharmacological Effects After Application in Rats. *Journal of pharmaceutical sciences*, 101(9), 3230–3238.

Khafagy, E.S., Morishita, M., Onuki, Y. and Takayama, K. (2007). Current challenges in non-invasive insulin delivery systems: A comparative review. *Advanced Drug Delivery Reviews*, 59(15), 1521–1546.

Kim, A.I., Akers, M.J. and Nail, S.L. (1998). The physical state of mannitol after freeze-drying: Effects of mannitol concentration, freezing rate, and a noncrystallizing cosolute. *Journal of Pharmaceutical Sciences*, 87(8), 931–935.

Kim, Y.-C., Park, J.-H. and Prausnitz, M.R. (2012). Microneedles for drug and vaccine delivery. *Advanced drug delivery reviews*, 64(14), 1547–68.

Kim, Y.C., Quan, F.S., Compans, R.W., Kang, S.M. and Prausnitz, M.R. (2010). Formulation and coating of microneedles with inactivated influenza virus to improve vaccine stability and immunogenicity. *Journal of Controlled Release*, 142(2), 187–195.

Kim, Y.H., Sioutas, C. and Shing, K.S. (2009). Influence of stabilizers on the physicochemical characteristics of inhaled insulin powders produced by supercritical antisolvent process. *Pharmaceutical Research*, 26(1), 61–71.

Kinesh, V.P., Neelam, D.P., Punit, B.P., Bhavesh, S.B. and Pragna, K.S. (2010). Novel Approaches for Oral Delivery of Insulin and Current Status of Oral Insulin Products. *International Journal of Pharmaceutical Sciences and Nanotechnology*, 3(3), 1057–1064.

Lahiji, S.F., Dangol, M. and Jung, H. (2015). A patchless dissolving microneedle delivery system enabling rapid and efficient transdermal drug delivery. *Scientific Reports*, 5, 1–7.

Larrañeta, E., McCrudden, M.T.C., Courtenay, A.J. and Donnelly, R.F. (2016). Microneedles: A New Frontier in Nanomedicine Delivery. *Pharmaceutical Research*, 33(5), 1055–1073.

Lee, I.C., He, J.S., Tsai, M.T. and Lin, K.C. (2015). Fabrication of a novel partial dissolving polymer microneedle patch for transdermal drug delivery. *Journal of Materials Chemistry B*, 3(2), 276–285.

Lee, I.C., Wu, Y.C., Tsai, S.W., Chen, C.H. and Wu, M.H. (2017). Fabrication of two-layer dissolving polyvinylpyrrolidone microneedles with different molecular weights for: In vivo insulin transdermal delivery. *RSC Advances*, 7(9), 5067–5075.

Lee, J.W., Choi, S.O., Felner, E.I. and Prausnitz, M.R. (2011). Dissolving microneedle patch for transdermal delivery of human growth hormone. *Small*, 7(4), 531–539.

Lee, K.S., Kim, R.H., Yang, D.Y. and Park, S.H. (2008). Advances in 3D nano/microfabrication using two-photon initiated polymerization. *Progress in Polymer Science*, 33(6), 631–681.

Lhernould, M.S. ausse, Deleers, M. and Delchambre, A. (2015). Hollow polymer microneedles array resistance and insertion tests. *International journal of pharmaceutics*, 480(1–2),152–157.

Ling, M.-H. and Chen, M.-C. (2013). Dissolving polymer microneedle patches for rapid and efficient transdermal delivery of insulin to diabetic rats. *Acta biomaterialia*. 9(11), 8952–61.

Liu, S., Jin, M., Quan, Y., Kamiyama, F., Katsumi, H., Sakane, T. and Yamamoto, A. (2012). The development and characteristics of novel microneedle arrays fabricated from hyaluronic acid, and their application in the transdermal delivery of insulin. *Journal of controlled release*, 161(3), 933–41.

Low, Z.X., Chua, Y.T., Ray, B.M., Mattia, D., Metcalfe, I.S. and Patterson, D.A. (2017). Perspective on 3D printing of separation membranes and comparison to related unconventional fabrication techniques. *Journal of Membrane Science*. 523, 596–613.

Luo, Y.Y., Xiong, X.Y., Tian, Y., Li, Z.L., Gong, Y.C. and Li, Y.P. (2016). A review of biodegradable polymeric systems for oral insulin delivery. *Drug Delivery*, 23(6), 1882–1891.

Maaden, K.V., Jiskoot, W. and Bouwstra, J. (2012). Microneedle technologies for (trans)dermal drug and vaccine delivery. *Journal of controlled release*, 161(2), 645–55.

Mahato, R. (2017). Microneedles in Drug Delivery. In: Mitra, A.K et al. ed. *Emerging nanotechnologies for diagnostics, drug delivery and medical devices*. Amsterdam: Elsevier pp. 331-353.

Martanto, W., Davis, S.P., Holiday, N.R., Wang, J., Gill, H.S. and Prausnitz, M.R. (2004). Transdermal delivery of insulin using microneedles *in vivo*. *Pharmaceutical Research*, 21(6), 947–952.

Martin, C.J., Allender, C.J., Brain, K.R., Morrissey, A. and Birchall, J.C. (2012). Low temperature fabrication of biodegradable sugar glass microneedles for transdermal drug delivery applications. *Journal of Controlled Release*,158(1), 93–101.

Marwah, H., Garg, T., Goyal, A.K., Rath, G., Marwah, H., Garg, T., Goyal, A.K. and Rath, G. (2017). Permeation enhancer strategies in transdermal drug delivery. *Drug Delivery*, 23(2), 564-578.

Mcallister, D. V, Wang, P.M., Davis, S.P., Park, J., Canatella, P.J., Allen, M.G. and Prausnitz, M.R. (2003). Microfabricated needles for transdermal delivery of macromolecules and nanoparticles: Fabrication methods and transport studies. *Proceedings of the National Academy of Sciences of the United States of America.* 100(24), 13755–13760.

McCrudden, M.T.C., Alkilani, A.Z., Courtenay, A.J., McCrudden, C.M., McCloskey, B., Walker, C., Alshraiedeh, N., Lutton, R.E.M., Gilmore, B.F., Woolfson, A.D. and Donnelly, R.F. (2014). Considerations in the sterile manufacture of polymeric microneedle arrays. *Drug Delivery and Translational Research*, 5(1), 3–14.

McCrudden, M.T.C., Alkilani, A.Z., McCrudden, C.M., McAlister, E., McCarthy, H.O., Woolfson, A. D. and Donnelly, R.F. (2014). Design and physicochemical characterisation of novel dissolving polymeric microneedle arrays for transdermal delivery of high dose, low molecular weight drugs. *Journal of controlled release*, 180, 71–80.

McGrath, M.G., Vucen, S., Vrdoljak, A., Kelly, A., O'Mahony, C., Crean, A.M. and Moore, A. (2014). Production of dissolvable microneedles using an atomised spray

process: Effect of microneedle composition on skin penetration. *European Journal of Pharmaceutics and Biopharmaceutics*, 86(2), 200–211.

Melo, K.F.S., Bahia, L.R., Pasinato, B., Porfirio, G.J.M., Martimbianco, A.L., Riera, R., Calliari, L.E.P., Minicucci, W.J., Turatti, L.A.A., Pedrosa, H.C. and Schaan, B.D. (2019). Short-acting insulin analogues versus regular human insulin on postprandial glucose and hypoglycemia in type 1 diabetes mellitus: a systematic review and meta-analysis. *Diabetology and Metabolic Syndrome*, 11(1), 1–13.

Migalska, K., Morrow, D.I.J., Garland, M.J., Thakur, R., Woolfson, A.D. and Donnelly, R.F. (2011). Laser-engineered dissolving microneedle arrays for transdermal macromolecular drug delivery. *Pharmaceutical Research*, 28(8), 1919–1930.

Nair, L.S. and Laurencin, C.T. (2007). Biodegradable polymers as biomaterials. *Progress in Polymer Science*. 32(8–9), 762–798.

Ng, H.I., Fernando, G.J.P. and Kendall, M.F. (2012). Induction of potent CD8+ T cell responses through the delivery of subunit protein vaccines to skin antigen-presenting cells using densely packed microprojection arrays. J*ournal of Controlled Release*, 162(3), 477–484.

Ng, K.W. and Lau, W.M. (2015). Skin Deep: The Basics of Human Skin Structure and Drug Penetration In: N. Dragicevic and H. I. Maibach, eds. *Percutaneous Penetration Enhancers Chemical Methods in Penetration Enhancement*. Berlin, Heidelberg: Springer Berlin Heidelberg, pp.3–11.

Niswender, K.D. (2011). Basal Insulin: Physiology, Pharmacology, and Clinical Implications. *Postgraduate Medicine*, 123(4), 17–26.

Ohtake, S., Kita, Y. and Arakawa, T. (2011). Interactions of formulation excipients with proteins in solution and in the dried state. *Advanced Drug Delivery Reviews*. 63(13), 1053–1073.

Olinger, P.M. and Pepper, T. (2001). Xylitol. In: Nabors, L. O. *ed. Alternative Sweeteners.* 3rd ed., pp.335-353.

Ortiz, C., Zhang, D., Xie, Y., Davisson, V.J. and Ben-Amotz, D. (2004). Identification of insulin variants using Raman spectroscopy. *Analytical Biochemistry*, 332(2), 245–252.

Owens, D.R. and Zinman, B. (2003). Alternative routes of insulin delivery. *Diabetic Medicine*, 20(11), 886–898.

Paaver, U., Tamm, I., Laidmäe, I., Lust, A., Kirsimäe, K., Veski, P., Kogermann, K. and Heinämäki, J. (2014). Soluplus graft copolymer: Potential novel carrier polymer in electrospinning of nanofibrous drug delivery systems for wound therapy. *BioMed Research International*,1–7.

Pan, Y., Li, Y., Zhao, H., Zheng, J., Xu, H., Wei, G., Hao, J. and Cui, F. (2002). Bioadhesive polysaccharide in protein delivery system: chitosan nanoparticles improve the intestinal absorption of insulin in vivo. *International Journal of Pharmaceutics*, 249(1–2), 139–147.

Park, B.J., Choi, H.J., Moon, S.J., Kim, S.J., Bajracharya, R., Min, J.Y. and Han, H.-K. (2018). Pharmaceutical applications of 3D printing technology: current understanding and future perspectives. *Journal of Pharmaceutical Investigation*, 1-11.

Patel, A., Cholkar, K. and Mitra, A.K. (2014). Recent developments in protein and peptide parenteral delivery approaches. *Therapeutic Delivery*, 5(3), 337–365.

Paudel, K.S., Milewski, M., Swadley, C.L., Brogden, N.K., Ghosh, P. and Stinchcomb, A.L. (2010). Challenges and opportunities in dermal/transdermal delivery. *Therapeutic Delivery*, 1(1), 109–131.

Pere, C.P.P., Economidou, S.N., Lall, G., Ziraud, C., Boateng, J.S., Alexander, B.D., Lamprou, D.A. and Douroumis, D. (2018). 3D printed microneedles for insulin skin delivery. *International Journal of Pharmaceutics*, 544(2), 425–432.

Perfetti, G., Alphazan, T., Van Hee, P., Wildeboer, W.J. and Meesters, G.M.H. (2011). Relation between surface roughness of free films and process parameters in spray coating. *European Journal of Pharmaceutical Sciences*, 42(3), 262–272.

Prausnitz, M.R. and Langer, R. (2008). Transdermal drug delivery. *Nature biotechnology*, 26(11), 1261–8.

Qin, G., Gao, Y., Wu, Y., Zhang, S., Qiu, Y., Li, F. and Xu, B. (2012). Simultaneous basal-bolus delivery of fast-acting insulin and its significance in diabetes management. *Nanomedicine: Nanotechnology, Biology, and Medicine*. 8(2), 221–227.

Qiu, Y., Qin, G., Zhang, S., Wu, Y., Xu, B. and Gao, Y. (2012). Novel lyophilized hydrogel patches for convenient and effective administration of microneedle-mediated insulin delivery. *International Journal of Pharmaceutics*, 437(1–2), 51–56.

Ramaiya, K., Bajaj, S., Claudine, K., Andrew, S.B., Fredrick, O., Kalra, S., Silver, B., Makhoba, A. and Charlotte, B.M. (2018). EADSG Guidelines: Insulin Therapy in Diabetes. *Diabetes Therapy*. 9(2), 449–492.

Ross, S., Scoutaris, N., Lamprou, D., Mallinson, D. and Douroumis, D. (2015). Inkjet printing of insulin microneedles for transdermal delivery. *Drug Delivery and Translational Research*, 5(4), 451–461.

Rowe, R.C., Sheskey, P.J., Cook, W.G. and Fenton, M.E. eds. (2012a). Mannitol In: *Handbook of Pharmaceutical Excipients*., 479–482.

Rowe, R.C., Sheskey, P.J., Cook, W.G. and Fenton, M.E. eds. (2012b). Trehalose In: *Handbook of Pharmaceutical Excipients*., pp.756–747.

Rowe, R.C., Sheskey, P.J., Cook, W.G. and Fenton, M.E. eds. (2012c). Xylitol In: *Handbook of Pharmaceutical Excipients*., p.786-789.

Sadia, M., Sośnicka, A., Arafat, B., Isreb, A., Ahmed, W., Kelarakis, A. and Alhnan, M.A. (2016). Adaptation of pharmaceutical excipients to FDM 3D printing for the fabrication of patient-tailored immediate release tablets. *International Journal of Pharmaceutics*, 513(1–2), 659–668.

Seki, T., Kanbayashi, H., Nagao, T., Chono, S., Tomita, M., Hayashi, M., Tabata, Y. and Morimoto, K. (2005). Effect of Aminated Gelatin on the Nasal Absorption of Insulin in Rats. *Biological & Pharmaceutical Bulletin*, 28(3), 510–514.

Senel, S., Kremer, M., Nagy, K. and Squier, C. (2001). Delivery of bioactive peptides and proteins across oral (buccal) mucosa. *Current pharmaceutical biotechnology*, 2(2), 175–86.

Sibum, I., Hagedoorn, P., de Boer, A.H., Frijlink, H.W. and Grasmeijer, F. (2018). Challenges for pulmonary delivery of high powder doses. *International Journal of Pharmaceutics*, 548(1), 325–336.

Singer, M.A. and Lindquist, S. (1998). Multiple effects of trehalose on protein folding invitro and *in vivo*. *Molecular cell*, 1(5), 639–48.

Sjökvist, E. and Nyström, C. (1991). Physicochemical aspects of drug release. XI. Tableting properties of solid dispersions, using xylitol as carrier material. *International Journal of Pharmaceutics*, 67(2), 139–153.

Szunerits, S. and Boukherroub, R. (2018). Heat: A Highly Efficient Skin Enhancer for Transdermal Drug Delivery. *Frontiers in Bioengineering and Biotechnology*, 6, 1–13.

Tas, C., Mansoor, S., Kalluri, H., Zarnitsyn, V.G., Choi, S.O., Banga, A.K. and Prausnitz, M.R. (2012). Delivery of salmon calcitonin using a microneedle patch. *International Journal of Pharmaceutics*. 423(2), 257–263.

Testa, B. and Meyer, U.A. (eds.). (1996). Therapeutic Use of Insulin In: *Advances in Drug Research*. [Online]. pp.49–76. Available from: https://linkinghub.elsevier.com/retrieve/pii/S0065249096800396.

Thyagarajapuram, N., Olsen, D. and Middaugh, R. (2007). Stabilization of Proteins by Recombinant Human Gelatins. *Journal of Pharmaceutical Sciences*, 96(12), 3304–3315.

Tuan-Mahmood, T.M., McCrudden, M.T.C., Torrisi, B.M., McAlister, E., Garland, M.J., Singh, T.R.R. and Donnelly, R.F. (2013). Microneedles for intradermal and transdermal drug delivery. *European journal of pharmaceutical sciences*, 50(5), 623–37.

Uddin, M.J., Scoutaris, N., Klepetsanis, P., Chowdhry, B., Prausnitz, M.R. and Douroumis, D. (2015). Inkjet printing of transdermal microneedles for the delivery of anticancer agents. *International Journal of Pharmaceutics*, 494(2), 593–602.

Ur-Rehman, S., Mushtaq, Z., Zahoor, T., Jamil, A. and Murtaza, M.A. (2013). Xylitol: A Review on Bioproduction, Application, Health Benefits, and Related Safety Issues. *Critical Reviews in Food Science and Nutrition*, 55(11)1514–1528.

Usha, R., Raman, S.S., Subramanian, V. and Ramasami, T. (2006). Role of polyols (erythritol, xylitol and sorbitol) on the structural stabilization of collagen. *Chemical Physics Letters*, 430(4–6), 391–396.

Veuillez, F., Kalia, Y.N., Jacques, Y., Deshusses, J. and Buri, P. (2001). Factors and strategies for improving buccal absorption of peptides. *European journal of pharmaceutics and biopharmaceutics*, 51(2), pp.93–109.

Viswanathan, P., Muralidaran, Y. and Ragavan, G. (2017). Challenges in oral drug delivery: A nano-based strategy to overcome. *Nanostructures for Oral Medicine*, 173-201.

Vrdoljak, A., McGrath, M.G., Carey, J.B., Draper, S.J., Hill, A.V.S., O'Mahony, C., Crean, A.M. and Moore, A.C. (2012). Coated microneedle arrays for transcutaneous delivery of live virus vaccines. *Journal of Controlled Release*, 159(1), 34–42.

Waller, D.G. and Sampson, A.P. (2018). Diabetes mellitus In: *Medical Pharmacology and Therapeutics* [Online]. Elsevier, pp.459–473. Available from: http://www.embase.com/search/results?subaction=viewrecord&from=export&id=L351518481.

Waugh, Anne; Grant, A. (2014). Protection and survival In: *Ross and Wilson Anatomy and Physiology in health and illness*. Elsevier Ltd, pp.361–373.

Wright, A., Burden, A.C.F., Paisey, R.B., Cull, C.A. and Holman, R.R. (2002). Sulfonylurea Inadequacy: Efficacy of addition of insulin over 6 years in patients with type 2 diabetes in the U.K. Prospective Diabetes Study (UKPDS 57). *Diabetes Care*. 25(2), 330–336.

Wu, X., Wu, W., Qi, J., Lu, Y., Li, Yang, Chen, Z., Zhu, Q., Li, Ying, Yu, Q. and An, D. (2019). Improving dermal delivery of hydrophilic macromolecules by biocompatible ionic liquid based on choline and malic acid. *International Journal of Pharmaceutics*, 558, 380–387.

Wu, Y., Gao, Y., Qin, G., Zhang, S., Qiu, Y., Li, F. and Xu, B. (2010). Sustained release of insulin through skin by intradermal microdelivery system. *Biomedical Microdevices*, 12(4), 665–671.

Xie, S., Li, Z. and Yu, Z. (2015). Microneedles for transdermal delivery of insulin. *Journal of Drug Delivery Science and Technology*, 28, 11–17.

Yaturu, S. (2013). Insulin therapies: Current and future trends at dawn. *World Journal of Diabetes*, 4(1), 1–7.

Yong, Z., Yingjie, D., Xueli, W., Jinghua, X. and Zhengqiang, L. (2009). Conformational and bioactivity analysis of insulin: Freeze-drying TBA/water co-solvent system in the presence of surfactant and sugar. *International Journal of Pharmaceutics*, 371(1–2), 71–81.

Yu, L. (2001). Amorphous pharmaceutical solids preparation, characterization. *Advanced Drug Delivery Reviews*, 48, 27–42.

Yu, W., Jiang, G., Zhang, Y., Liu, D., Xu, B. and Zhou, J. (2017). Polymer microneedles fabricated from alginate and hyaluronate for transdermal delivery of insulin. *Materials Science and Engineering C*, 80, 187–196.

Zhou, X., Hou, Y. and Lin, J. (2015). A review on the processing accuracy of two-photon polymerization. *API Advances*, (030701-19).

2 CHAPTER

HPLC INSULIN VALIDATION METHOD

2.1 Introduction

High Performance Liquid Chromatography (HPLC) is a powerful analytical method used to separate, identify, and quantify compounds in a mixture. It consists of a stationary phase and a mobile phase. The sample is dissolved in the mobile phase and then forced through an immiscible stationary phase, the column.

Two types of HPLC are used in pharmaceutical analysis, the normal one and the reverse one. In the normal HPLC, the stationary phase is made of highly polar compounds such as triethyleneglycol and the mobile phase is a relatively non-polar solvent such as hexane or iso-propylether. The reverse HPLC consists of a stationary phase made of non-polar hydrocarbons such as C18, C8, phenyl and the mobile phase which is relatively polar such as methanol, water, acetonitrile.

The purpose of this study was to develop and validate a method using a simple, rapid, sensitive, precise, accurate and specific reversed-phase HPLC assay to quantify insulin from coating formulations for the in vitro studies.

2.2 Materials and Methods

2.2.1 Materials

Insulin solution from bovine pancreas (10 mg. mL^{-1}), gelatin type A powder from porcine skin and trehalose dihydrate were ordered from Sigma-Aldrich. Soluplus ® was purchased from BASF. Xylitol (Xylisorb® 90) and mannitol (Pearlitol®) were donated by Roquette Freres (France). Saline Phosphate buffer PBS pH 7.4 was ordered from Sigma-Aldrich. Trifluoroacetic acid (TFA), acetonitrile, deionised water and all the chemical reagents were HPLC grade.

2.2.2 Chromatographic system and conditions

The HPLC system used in the study consisted of an Agilent Technologies 1200 series (Agilent Technologies, Cheshire, UK) equipped with a Phenomenex Jupiter 5 µ c18 300 Å, LC Column (250×4.60 mm, particle size 5 µm, Macclesfield, UK).

Based on the literature review and in some previous tests, the mobile phase used for insulin analysis was water with 0.1% TFA and acetonitrile with 0.1% TFA (64:36 v/v). They were both degassed before running on the HPLC system.

2.2.3 Validation of the method

The validation of HPLC method for insulin was carried out following standard procedures described in the British Pharmacopeia and in the ICH Q2 (R1) (2005). The validation method included specificity, linearity, accuracy, precision (repeatability and reproducibility) limit of detection and limit of quantification.

The analysis was performed in an isocratic elution mode and only after the column had reached the equilibrium (approximately 40-60 min at a flow rate of 1 ml/min). The mobile phase was always filtered and degassed before use. The final flow rate was set to 1 mL/min, and the detector was set to monitor at 214 nm. All the analyses were carried out at 35 °C.

2.2.4 Preparation of the stock solution

Three insulin stock solutions were prepared in two different days by adding 500 µL of insulin to a 50 mL volumetric flask and then diluted with PBS pH 7.4 up to the meniscus. The final concentration was 100 µg/mL, and the stock solutions and the buffer were made and used on the same day.

2.2.5 Specificity

For the specificity test, insulin was tested against all components present in the formulation using the same parameters. For that, all the components were individually added to insulin solution and analysed.

2.2.6 Linearity

The linearity of the developed method was accessed by the preparation of 5 standard solutions in the concentration range of 10 to 50 µg/mL from each stock solution. All the samples were analysed in triplicate and the corresponding peak areas were determined and the calibration curves were plotted.

2.2.7 Precision

2.2.7.1 Repeatability (Intraday analysis)

The repeatability of the method was carried out for insulin by analysing the sample at low (10 µg/mL), medium (30 µg/mL) and high (50 µg/mL) insulin concentrations, six times, in the same day.

2.2.7.2 Reproducibility

The reproducibility of the method was accessed by analysing nine samples of insulin at low (10 µg/mL), medium (30 µg/mL) and high (50 µg/mL) insulin concentration in two different days.

2.2.8 Accuracy

The accuracy of the method was analysed through the mean of the low (10 µg/ml), medium (30 µg/mL) and high (50 µg/mL) insulin concentrations obtained by the previous tests and calculated by the following formula:

$$\text{Accuracy (\%)} = \frac{\text{Concentration mean obtained experimentally}}{\text{Theoretical concentration}}$$

2.2.9 Detection limit and quantification limit

The detection limit and the quantification limit were determined by diluting the insulin stock solution (100 µg/mL) from the initial concentration of 10 µg/mL and

gradually decreasing the concentration down to a point where the analyte could not be detected. The concentration of the insulin samples was 10, 5, 4, 3, 2 and 1 µg/ mL. Each concentration was analysed in triplicate and the detection limit (DL) and the quantification limit (QL) were calculated by the following equations:

$$DL = \frac{3.3 \times SD}{S}$$

$$QL = \frac{10 \times SD}{S}$$

Where SD is the standard deviation of the y-intercepts of the regression lines. S is the slope of the calibration curve.

2.3 Results and discussion

2.3.1 Selection of mobile phase

Good peak symmetry for Insulin was achieved using the mobile phase consisting of water with 0.1% TFA and acetonitrile with 0.1% (64:36 v/v); isocratic mode. Insulin was analysed at 214 nm and its retention time was found to be about 4.42 min.

2.3.2 Specificity

The specificity of the method analyses the ability of the method to measure the drug accurately and specifically in the presence of possible interferences such as the components of the formulation. Figure 2.1 shows the HPLC chromatograms of insulin and the polymers in saline phosphate buffer pH7.4.

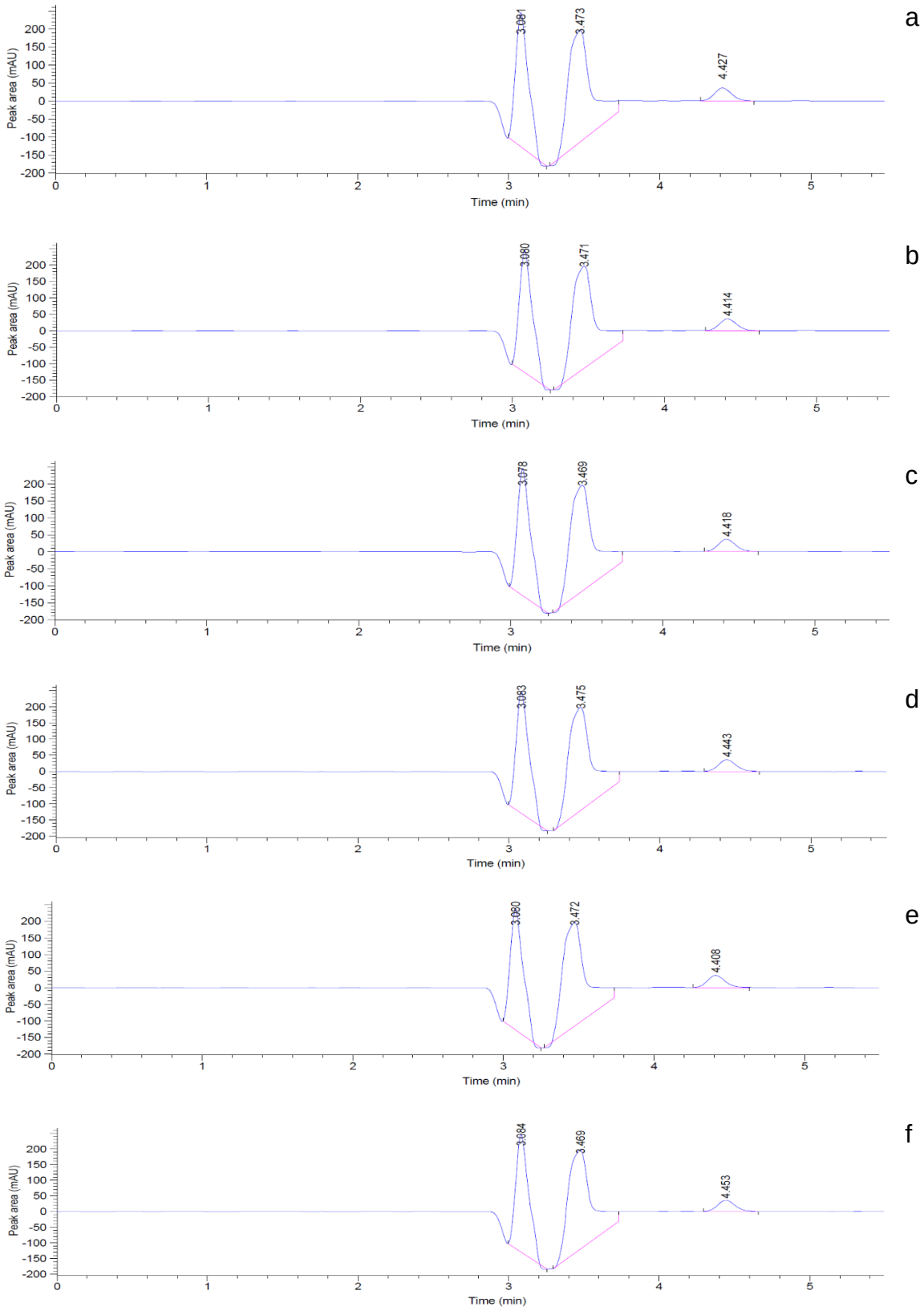

Figure 2.1.Chromatograms of pure insulin and insulin in the presence of different components in milli absorbance units (mAU). (a) pure insulin, (b) insulin:gelatin, (c) insulin:soluplus, (d) insulin:trehalose, (e) insulin:xylitol and (f) insulin:mannitol. The first two peaks are due to the solvents. The third peak is due to the insulin elution.

As the chromatograms show, the polymers used in the formulations do not interfere with the insulin peak at about 4.4 min. Then, the method can be used to quantify insulin in the proposed formulations.

2.3.3 Linearity

Linearity was evaluated through the regression line of the calibration curve in the range of 10 to 50 µg/mL. The linearity details of the insulin calibration curve and the parameters of its linear regression are illustrated in Figure 2.2 and Table 2.1.

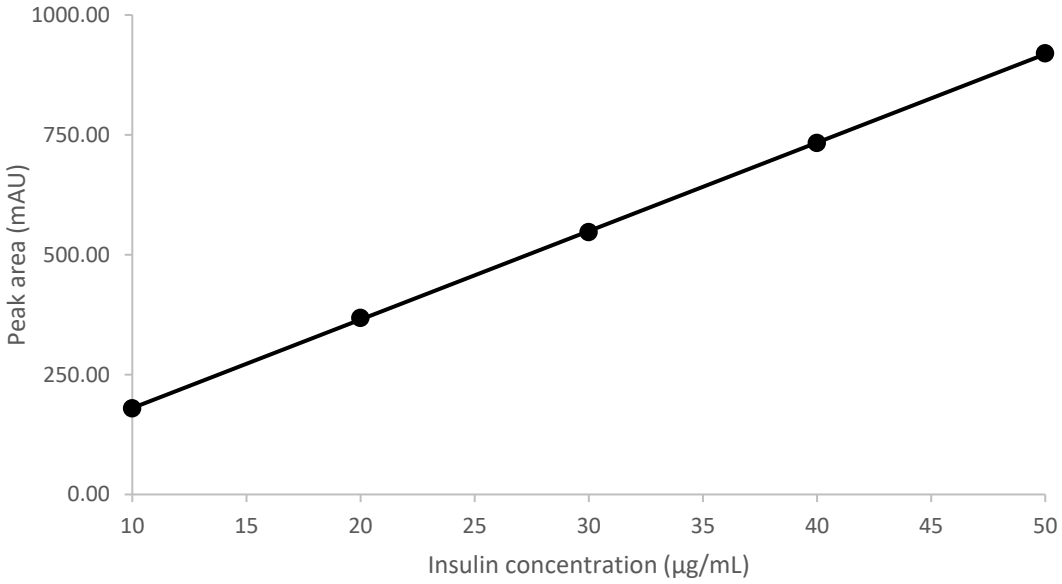

Figure 2.2. Calibration curve of insulin from 10 to 50 µg/mL. Insulin concentration (µg/mL) vs peak area in milli absorbance units (mAU), (n=9).

Table 2.1.Parameters of the linear regression of the calibration curve.

Parameters	Values
Linearity range (µg/mL)	10 to 50
Angular coefficient	18.453
Intercept	-4.330
Coefficient of determination	0.999

The results showed a good coefficient of determination ($R^2 = 0.999$) which is higher than the criteria level chosen for this study (0.990). Good linearity was

achieved by this method in the range analysed and can be employed for the intended application of the method.

2.3.4 Precision

Precision is the level of agreement among individual results. While repeatability analyses the agreement among the individual results in a small period of time with the same instrument and analyst, the reproducibility analyses the agreement of the individual results in different days.

The validation of the method was performed through examining the precision through repeatability and reproducibility. The theoretical insulin concentration, the mean peak areas and their respective standard deviations and the coefficient of variation (CV%) are presented in the Table 2.2 and Table 2.3.

Table 2.2. Repeatability of the method for determination of insulin.

Theoretical concentration (µg/mL)	Mean Peak Area	DP	CV (%)
10	173.863	5.521	3.176
30	547.969	2.404	0.439
50	923.165	4.807	0.521

Table 2.3. Reproducibility of the method for determination of insulin.

Theoretical concentration (µg/mL)	Mean Peak Area	DP	CV (%)
10	178.965	8.706	4.864
30	546.359	14.105	2.582
50	917.852	24.282	2.646

The results obtained can be considered precise as the low CV (%) values obtained for insulin solution in saline phosphate buffer evidence an excellent precision.

2.3.5 Accuracy

Accuracy evaluates the closeness of the individual results are from the true value. Table 2.4 shows the determination of the accuracy of the method.

Table 2.4.Accuracy of the method for determination of insulin.

Theoretical concentration (µg/mL)	Practical mean concentration (µg/mL)	Accuracy (%)
10	178.964	99.158
30	546.359	99.2
50	917.851	99.692

According to the results, the method provides an accuracy of 99.35% on average, which means that the values measured are very close to the true value.

2.3.6 Detection limit and Quantification limit

The detection limit refers to the lowest amount of insulin that can be detected in a sample whereas the quantification limit is the lowest amount of insulin that can be quantitatively determined with suitable precision in a sample.

The determination of the DL and the QL were based on 10, 5, 4 and 3 µg/mL by two approaches based on the standard deviation responses and visual evaluation (see Figure 2.3 and Table 2.5).

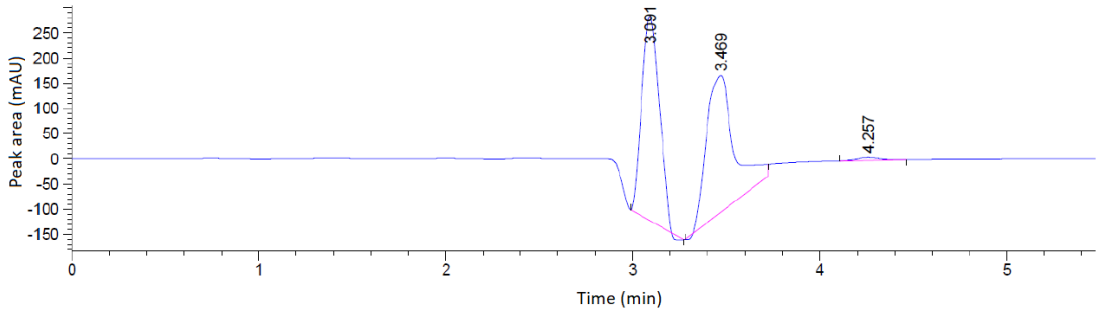

Figure 2.3. Insulin chromatogram in milli absorbance units at 3 µg/mL. The first two peaks are due to the solvents. The third peak is due to the insulin elution.

Table 2.5. DL and QL based on the standard deviation of the response and the slop.

Parameters	Concentration (µg/mL)
Detection Limit	2.107
Quantification Limit	6.385

The minimum concentration able to be detected by this method was 3 µg/mL. Therefore, the DL and QL were determined at a range 10 to 3 µg/mL agrees with

the results obtained once the detection limit is 2.107 but the quantification limit is 6.385 µg/mL

2.4 Conclusion

The validation of the HPLC method for quantification of insulin in the coating formulations was executed following the standard procedures described in the compendial methods of USP and ICH. The retention time obtained for insulin was about 4.42 min and the mobile phase used was water with 0.1% TFA and acetonitrile with 0.1% TFA (64:36 v/v). The selectivity tests showed that the method is able to detect insulin response in the presence of other components of the formulation. The calibration curve measuring the peak area against five insulin concentrations were found to be linear in the range investigated with a regression coefficient (R^2) equal to 0.999. Considerable accuracy and precision were also acquired. Finally, the quantification limit (6.385 µg/mL) is far above the detection limit (2.107 µg/mL). Overall, the validation procedures showed that the developed HPLC method is reliable to identify and quantity insulin in the coating formulations.

2.5 References

British Pharmacopoeia. Vol 1. (2018). Medicinal and Pharmaceutical Substances. London: TSO; 2017. Insulin. pp. I-1211-1218

ICH Harmonised Tripartite Guidelines. Available from: https://www.ich.org/products/guidelines/quality/article/quality-guidelines.html [Accessed 15 January 2019].

ICH Harmonised Tripartite Guideline. Validation of Analytical Procedures: Text and Methodology. [Online]. Available from: https://www.ich.org/fileadmin/Public_Web_Site/ICH_Products/Guidelines/Quality/Q2_R1/Step4/Q2_R1__Guideline.pdf [Accessed 12 December 2018].

3 CHAPTER

METALLIC MICRONEEDLES FOR INSULIN DELIVERY

3.1 Introduction

Transdermal drug delivery has revolutionised the pharmaceutical treatment of many diseases and improved the acceptance therapy of many people. In this sense, a wide range of drugs that are metabolised in the gastrointestinal tract can be now easily administered through transdermal patches (Al-Hanbali *et al.* 2019). However, the transdermal delivery of hydrophilic macromolecules using most of the proposed transdermal drug delivery systems (TDDS) is still a challenge and cannot be easily and quickly released into the systemic circulation due to the protective characteristics of the skin (Prausnitz and Langer 2008).

To overcome the major limitations of the previous TDDS, transdermal microneedles (MNs) have been recently proposed as a new transdermal drug delivery strategy. Their prime advantages rely on the pathways created by the MNs across the skin which allows the easy passage of several different drugs, including high-molecular-weight molecules such as proteins and vaccines (Tuan-Mahmood *et al.* 2013; Liu *et al.* 2019; Choi *et al.* 2012; Tas *et al.* 2012; Sullivan *et al.* 2010; Kommareddy *et al.* 2013; Migalska *et al.* 2011).

Among the variety of microneedles approaches already proposed in the literature (Larrañeta *et al.* 2016; Bariya *et al.* 2012), coated MNs present an interesting strategy for rapid release of drugs to the systemic circulation with the advantage of a single administration process (Ameri *et al.* 2014; Kellerman, Ameri and Tepper 2017; Pere *et al.* 2018; Cormier *et al.* 2004; Harvinder S Gill and Prausnitz 2007). The association of solid MNs made of stainless steel with inkjet printing coating technique is an interesting combination for a promising approach for insulin therapy once it allies the good mechanical properties of the metallic MNs with the accurate coating patterns of the inkjet printing.

Since the inkjet technology was proposed to deposit active pharmaceutical molecules on different substrates in the last few years (Wu *et al.* 1996; Roth *et al.* 2004; Yeo, Basaran and Park 2003; Sandler *et al.* 2011), many advances have been

made in the drug delivery field which also evolved with the application of inkjet printing for fast acquiring accurate and reproducible coatings on small devices (Tarcha *et al.* 2007; Li, Chen and Zhang 2018). Likewise, specific amounts of anticancer drugs (5-fluorouracil, curcumin and cisplatin) (Uddin *et al.* 2015), antifungal agents (miconazole, voriconazole) (Boehm *et al.* 2015; Boehm *et al.* 2014), amphotericin B (Boehm *et al.* 2013) and insulin (Ross *et al.* 2015; Pere *et al.* 2018) were successfully coated onto a wide range of MNs surfaces using inkjet printing.

In this sense, polymeric solutions containing insulin at different ratios were proposed as coating formulations for protecting insulin against degradation as well as to promote a rapid release of the drug. Furthermore, the inkjet printing technique was used to overcome the usual drawbacks presented by the most common coating techniques.

3.2 Material and methods

3.2.1 Materials

Insulin solution from bovine pancreas (10 $mg.mL^{-1}$) and gelatin Type A powder from porcine skin were purchased from Sigma-Aldrich. Soluplus powder, a co-polymer of polyvinyl caprolactame-polyvinyl acetate-polyethylene glycol was ordered from BASF. Phosphate buffer PBS 7.4 (Sigma-Aldrich) and all the solvents used were analytical grades. The metallic microneedles arrays were made according to previous work (Uddin *et al.* 2015; Ross *et al.* 2015) and donated by Prausnitz (Microneedle Systems, LLC).

3.2.2 Penetration studies through porcine skin

For the penetration studies, the metallic microneedles were inserted into the porcine skin samples using a texture analyser (Stable micro system) (n=6). The porcine skin samples were placed in waxed petri dishes at the bottom of the equipment and the MN arrays were mounted on the moving probe using double-

sided adhesive tape. The continuous force and displacement measurements were recorded as the probe moved downward at 0.01 mm/s.

3.2.3 Coating formulations

Gelatin and soluplus were weighed, added to the insulin solution and then left it stirring until complete dissolution. The composition of the coating formulations used is shown in Table 3.1.

Table 3.1. Composition of coating formulations

Formulations	Composition (w/w)
Ins:Sol 2:1	10mg Insulin, 5mg Soluplus
Ins:Sol 1:1	10mg Insulin, 10 mg Soluplus
Ins: Gel 2:1	10mg Insulin, 5 mg Soluplus
Ins:Gel 1:1	10mg Insulin, 10 mg Soluplus

3.2.4 Coating of microneedles through inkjet printing

The MNs were coated using an Inkjet printing Nanoploter II (Gesim, Germany). The arrays were positioned at 45° relative to the dispenser and the formulations were jetted through a piezodriven dispenser (pipette) (PicPip 300) onto the MN surface in the form of fine droplets of approximately 300 pl. For each coating cycle, 5 dots of two droplets of coating formulation were dispensed longitudinally to the axis of each MN. The process was repeated for 130 jetting cycles to coat the desired amounts of 4 IU/array (140µg). The microneedles were left at room temperature for 24hs for drying.

3.2.5 Scanning electron microscopy (SEM)

The metallic microneedle arrays were mounted onto a double-sided carbon adhesive tape on top of an aluminium stub. A Hitachi SU 8030 (Japan) was used to analyse each array by SEM using low accelerating voltage (2.0 kV). The images were digitally taken with different magnifications (30 and 50x).

3.2.6 Quantitative analysis of the amount of insulin coated on the MNs

The metallic microneedles were coated with 4 IU (140 µg/mL) of insulin with insulin:soluplus and insulin:gelatin at 1:1 ratio (w/w) and left to evaporate at room temperature for 24hs. After dried, the coated MNs arrays were individually placed in a glass flask and 4 mL of PBS pH 7.4 was added to the MNs loaded with 4 IU. The vials were placed to sonicate for 5min, filtrated and the amount of insulin analysed by HPLC. The concentration of insulin was calculated using the analytical curve under the same conditions, and the percentage of the coating efficiency (CE%) was then calculated with the following equation:

$$CE\ (\%) = \frac{\text{(The amount of insulin analytically determined)} \times 100}{\text{Theoretical amount of insulin}}$$

3.2.7 Circular Dichroism (CD)

Insulin, gelatin and insulin-polymer solutions were diluted to 1.0 $mg.mL^{-1}$ in saline phosphate buffer pH 7.4 (PBS) whereas their respective films were weighed and solubilized in PBS 7.4 also to 1.0 $mg\ mL^{-1}$ of insulin concentration. The far-UV CD spectra were recorded between 190 and 260 nm on a Chirascan CD spectroscopy (Applied Photophysics, UK) using polarisation certified quartz cells (Hellma). The measurements were carried out at 20 °C using a step size of 1 nm, a bandwidth of 1 nm and an acquisition time of 1 sec. Four scans were recorded for each sample, averaged and the corresponding spectrum of water and polymer concentration, when required, were then subtracted from each spectrum. For estimation of the secondary structure composition of insulin, the CD spectra were evaluated by the CDSSTR method (Sreerama, Venyaminov and Woody 1999; Sreerama and Woody 2000) using Dichroweb website (Whitmore and Wallace 2008; Whitmore and Wallace 2004).

3.2.8 Raman spectroscopy

Insulin and insulin-polymer films were analysed using Raman microscopy (Jobin Yvon LabRam I) with a laser of 532 nm wavelength coupled with an optical microscope with 50x objective. An average of 5 spectra and an acquisition time of 5 seconds were used.

3.2.9 X-Ray Diffraction (XRD)

The X-ray diffraction patterns of the films of the raw materials and the films of insulin-polymer formulations were obtained using a Bruker D8 Advance (Germany) with a Göebel mirror using Cu-Kα radiation and operating at 40 kV and 40 mA. The diffractograms were collected in two-theta (2θ) mode from 5° to 40° with a step size of 0.02° (2θ) and a counting time of 0.2 seconds per step.

3.2.10 Stability of Insulin Films

Circular dichroism and x-ray diffraction were used to study the stability of the insulin in the films at time zero (T_0) and after 30 days (T_{30}) kept in the fridge at 4 ± 1^{o}C using the same parameters as previously described.

3.2.11 Preparation of porcine skin for in vitro release of insulin

A full thickness of abdominal porcine skin was collected from a local slaughterhouse (Forge Farm Ltd, Kent, UK) and stored at 4°C until it was used. The skin was fixed on a polystyrene block previously wiped with 70% ethanol and both the fatty tissue below the abdominal skin area and the abdominal hair were removed. The skin was then treated with dermatome (Padgett dermatome, Integra LifeTMSciences Corporation USA) at an angle of ±45° and tissue samples with 1.0 ± 0.1mm thick were then placed onto filter paper soaked in a small amount of saline phosphate buffer (PBS; pH 7.4) for 2 h before use.

3.2.12 *In vitro* permeation of insulin through porcine skin

The permeation studies were undertaken using Franz diffusion cells (PermeGear, Inc., PA, USA) and abdominal porcine skin. The cells were calibrated with phosphate buffered saline (PBS; pH7.4) at 6-6.5 mL per hour rate using an autosampler (FC 204 fraction collector, Gilson, USA) while the temperature was maintained at 37^{o}C using an automated water bath (Thermo Fisher Scientific, Newington, USA).

The metallic microneedles coated with 4IU of insulin:soluplus at 1:1 ratio (w/w) (n = 6) were inserted into the abdominal porcine skin for 30 s using manual finger pressure and placed on the donor compartment of the Franz diffusion cells with a total diffusion area of 1.1 cm^2. Sample fractions were then collected every 10 minutes, up to 1 h and the amount of insulin was analysed by the validated HPLC method described in chapter 2.

At the end of the experiment, the MNs and the skin were individually placed in a glass flask with 1mL of PBS 7.4 and left it to sonicate for 5 min. After that, they were filtrated and analysed by HPLC in order to determine any remaining insulin on the MNs or in the skin. Statistical analysis for the drug release was performed by using t-test (SPSS software Inc.), and a 0.05 significance level was adopted.

3.3 Results and Discussion

3.3.1 Penetration of the metallic MNs in the porcine skin

To access the required force for the metallic microneedles to pierce the skin, a penetration study using porcine skin was conducted. In this study, all the microneedles successfully pierced the skin with no damage or failure (Figure 3.1).

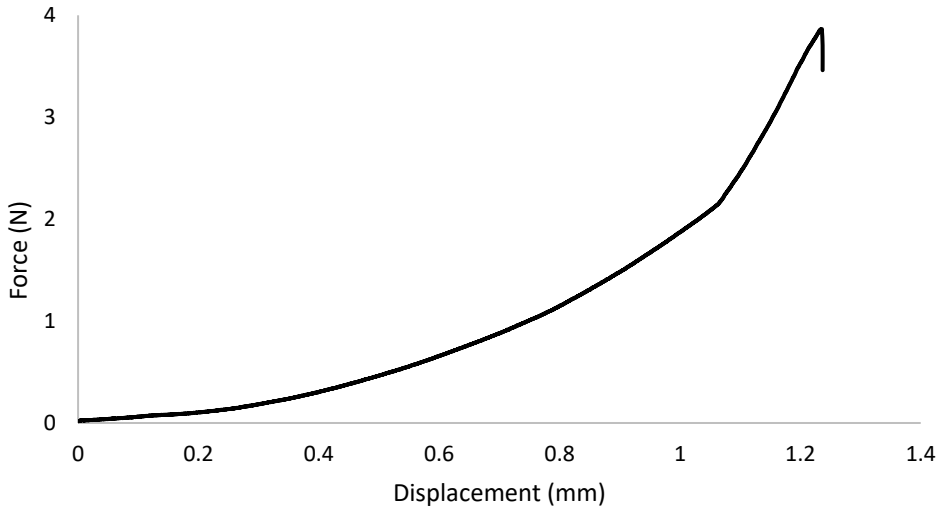

Figure 3.1. Force vs displacement curve for metallic microneedles penetration in the porcine skin. Maximum forces in Newton (N) for the penetration of the metallic microneedles: 3.86 N ± 0.41 (n=6).

Although the fabrication and the physical characteristics of these metallic microneedles are described elsewhere (Ross *et al.* 2015), from this study, it is possible to see that these metallic microneedles, containing 50 needles per array required 3.86 N to pierce the skin.

3.3.2 Scanning electron microscopy (SEM) of the coated MNs

The SEM pictures (Table 3.2) shows that the inkjet printing deposited uniform layers on the surface of the microneedles and reveal that the method can be applied for coating microneedles with high precision and reproducibility without loss of the material on the substrate.

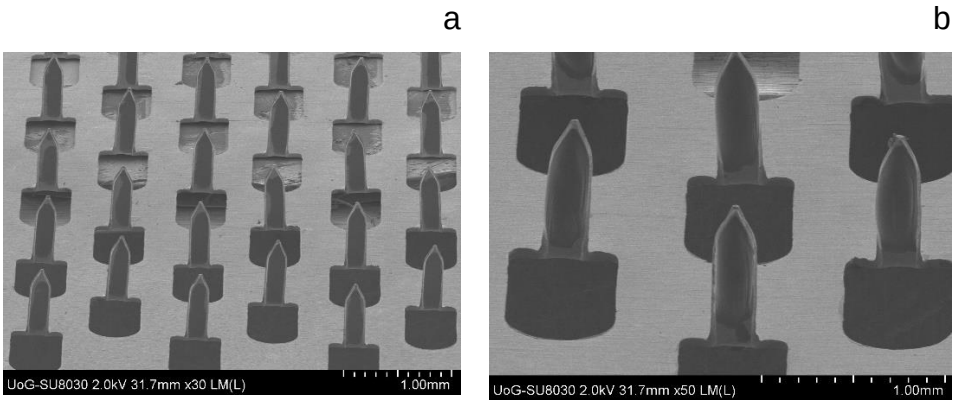

Figure 3.2. SEM images of coated metallic microneedles.

3.3.3 Quantitative analysis of the amount of insulin coated on the MNs

The amount of insulin coated on the MNs (4IU) was quantified by HPLC and the analytical concentration was calculated using the calibration curve. The coating efficiency is showed in Table 3.2.

Table 3.2. Coating efficiency of insulin-polymer formulations using inkjet printing method.

Sample	Theoretical concentration (µg/array)	Analytical concentration (µg/array)	Coating Efficiency (%)
Insulin:soluplus	140.00	139.93± 1.39	101.42 ± 1.54
Insulin:gelatin	140.00	141.99 ± 2.16	99.95 ± 0.99

From the results, it is possible to see that coated method applied for coating the metallic microneedles was very reliable and very close to the desired concentration which allows the delivery of precise doses.

3.3.4 Characterisation of insulin-polymer formulations

3.3.4.1 Circular Dichroism

Circular dichroism (CD) is a spectroscopy technique that measures the difference in absorbance between left- and right-handed circularly polarised light of a chiral sample and generates a signal in terms of ellipticity (θ) in degrees. The secondary structure of proteins can be studied when its peptide bond region is analysed in the far UV CD spectra (Kelly, Jess and Price 2005; Martin and Schilstra 2008).

Once CD gives information about the secondary structure of a molecule, it can be used to study protein denaturation (Kelly, Jess and Price 2005; Greenfield 2007). In this sense, CD spectroscopy was used to investigate the effect of different polymers on the insulin structure as well as its stability. The results were also used to estimate the insulin secondary structure content by CDSSTR method (Sreerama and Woody 2000; Whitmore and Wallace 2008).

Figure 3.3 shows the CD spectra of pure insulin and gelatin at 1.0mg/ mL in saline phosphate buffer pH 7.4 (PBS). Insulin shows a negative double minimum

around 210 and 222 nm which is related to the α-helix and β-sheet structures as already reported by others (Yong *et al.* 2009; Andrade *et al.* 2015; Ettinger, Timasheff and Strycharz 1971). Gelatin, presents a negative peak at 198 nm related to its random coil form which agrees well with the literature (Sakai *et al.* 2018; Gopal *et al.* 2012; Liu *et al.* 2017). As previously studied, in aqueous solution, at a low concentration, gelatin chains tend to form intermolecular hydrogen bonds and adopt a coil conformation (Djabourov *et al.* 1988). As expected, soluplus did not show any CD signal.

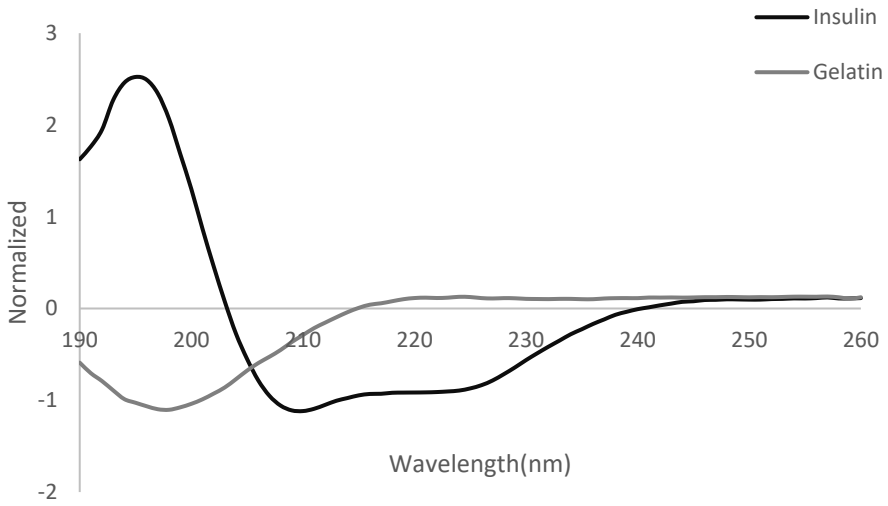

Figure 3.3. CD spectra of insulin solution and gelatin solution at 1.0 mg/mL in PBS 7.4.

Figure 3.4 shows the CD spectra of insulin and insulin-polymer solutions at different ratios (w/w) diluted to 1.0 mg/mL in PBS 7.4. All insulin-polymer solutions showed minima peaks around 210 and 220 nm which are associated with α-helix and β-sheet structures. A reduction in the Molar ellipticity along with changes in the shape of the spectra was noticed for all samples, especially for insulin-gelatin formulations, indicating changes in the secondary structure of insulin. The estimation of the secondary structure content of insulin is summarised in Table 3.3.

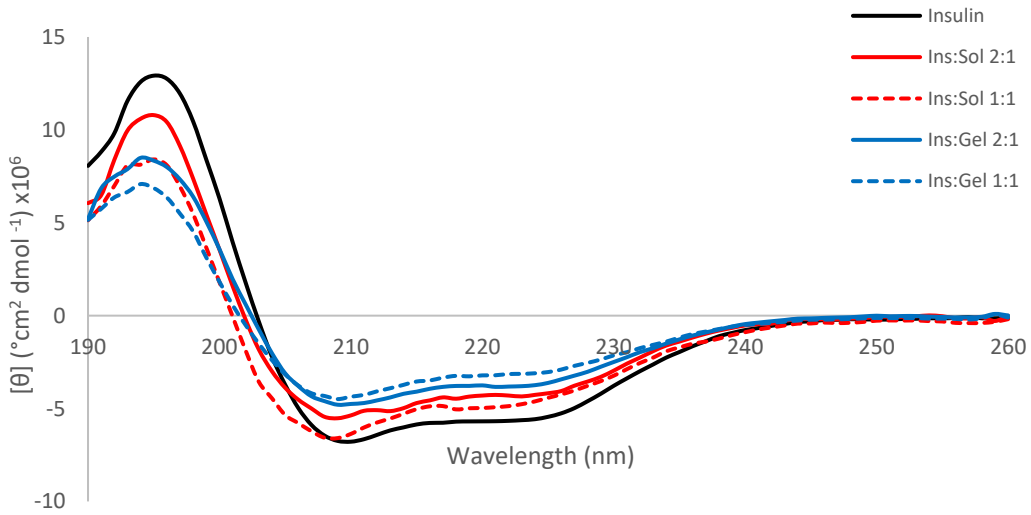

Figure 3.4. CD spectra of insulin solution and insulin-polymer solutions at different ratios (w/w) and 1.0 mg/mL in PBS 7.4.

Table 3.3. Percentage of the secondary structure content of insulin in insulin solution and insulin-polymer solutions at different ratios (w/w).

	Insulin (%)	Ins:Sol (%)		Ins:Gel (%)	
		2:1	1:1	2:1	1:1
Helix	50	43	47	36	32
β-Sheet	10	15	17	20	27
Turn	11	15	17	23	19
Random coil	29	26	18	20	22

In order to evaluate the secondary structure content of insulin after dehydration, the respective films of insulin solution and insulin-polymer formulations were solubilised in PBS 7.4 and analysed by CD. Figure 3.5 shows the CD spectra of insulin solution in comparison with the corresponding films of insulin solution and insulin-polymer formulations at 1.0 mg/mL.

From the spectra and the estimation of the secondary structure of insulin (Table 3.4), it is possible to see that even greater changes occur in the secondary structure of insulin for all samples upon dehydration. For insulin film, a noted decrease in the α-helix content along with an increase in the β-sheet and turn structures during dehydration were noted and it is in agreement with previous studies with insulin dehydration (Zeng *et al.* 2011).

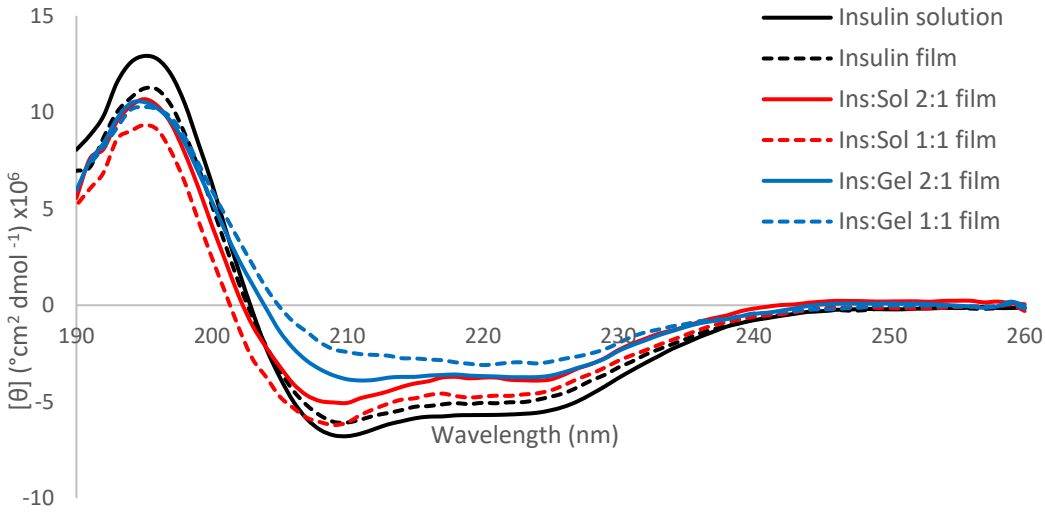

Figure 3.5. CD spectra of insulin solution, insulin film and insulin-polymer films at different ratios (w/w) at 1.0mg/mL in PBS 7.4.

Table 3.4. Percentage of the secondary structure content of insulin in insulin solution, insulin film and insulin-polymer films at different ratios (w/w).

	Insulin solution (%)	Insulin film (%)	Ins:Sol film (%)		Ins:Gel film (%)	
			2:1	1:1	2:1	1:1
Helix	50	46	41	45	32	21
β-Sheet	10	15	18	17	24	34
Turn	11	16	21	17	22	20
Random coil	29	24	20	21	21	25

Many studies have shown that dehydration can lead to significant conformational changes in proteins resulting in partially or completely unfolding and loss of their biological activity even after rehydration (Prestrelski *et al.* 1993; Pierre O Souillac, Middaugh and Rytting 2002; Zeng *et al.* 2011)**.** During drying, the removal of the water from the vicinity of the protein often perturbs its structure and force them to rearrange in order to compensate the lost hydrogen-bonds which is also affected by the dynamic and interactions among the molecules in the system (Ohtake, Kita and Arakawa 2011).

In this sense, once insulin presents a tendency to lose its native secondary structure upon dehydration, many studies have been done with different additives and strategies in order to stabilise and protect insulin molecule from denaturation (Zhang *et al.* 2010; Hosseinzadeh *et al.* 2017; Zhang *et al.* 2018).

All insulin-soluplus samples showed a slight shift to 208 nm and a decrease in the Molar ellipticity intensity, compared to the insulin solution sample. From the results, it is possible to see that a higher amount of soluplus prevented bigger changes in the secondary structure of insulin for both solution and film samples (Figure 3.3 and Figure 3.5). Furthermore, insulin:soluplus 1:1 ratio (w/w) film presented almost the same insulin structure content as the pure insulin film at time zero.

Both insulin-gelatin ratios presented expressive changes in the secondary structure of insulin (Figure 3.4) with a further decrease in the Molar ellipticity upon dehydration (Figure 3.5). Moreover, the estimation of the insulin secondary structure content (Table 3.3 and Table 3.4) indicate a clear reduction in the α-helix content followed by an increase in the β-sheet and turn structures for all samples.

Additionally, it was also noted that the higher the gelatin concentration, the bigger the reduction of the Molar ellipticity, indicating a decrease of the native insulin molecules in the system. These results might be due to intermolecular interactions and aggregation between insulin and gelatin and agrees well with other reported results regarding the reduction of the native conformation of proteins in the presence of gelatin (Gopal *et al.* 2012).

Overall, although many studies have shown that hydrophilic polymers can interact and protect proteins through many specific and non-specific mechanisms, they can also enhance self-association and aggregation (Kamerzell *et al.* 2011; Ohtake, Kita and Arakawa 2011). Moreover, even though it is suggested that gelatin interacts with proteins in a specific protein-manner with electrostatic interactions playing an important role, the mechanisms by which gelatin interacts with proteins still not completely understood yet (Young *et al.* 2005; Thyagarajapuram, Olsen and Middaugh 2007; Olsen *et al.* 2003; Wang 2005).

3.3.4.2 Raman Spectroscopy

In the Raman spectroscopy, the scattered light is used to interrogate the nature of the sample within an irradiated volume. Basically, the energy from the excitation light can be absorbed, transmitted or scattered, which can be further classified as elastic or inelastic according to its properties. The elastic scattered light

or Rayleigh is the majority of the scattered photons whereas the inelastic scattered light, known as Raman scattering, is a rare event that occurs due to its interaction with the molecules in an irradiated sample (Smith *et al.* 2015).

The pattern of Raman scattering can give important information about the identity of the molecules according to how those molecules interact with the electric field of the laser. Furthermore, the more easily the compound can be polarised the more intense the Raman signal will be (Goh, Ismail and Ng 2017).

Amide I and III are important features in the Raman spectra regarding the secondary structures of proteins. According to Liu at al. (1972), the denaturation of insulin can be clearly investigated through the observation of the amide I peak in the Raman spectra between 1600 and 1700 cm^{-1}. Liu and his colleagues demonstrated that the native insulin shows a broad peak band at around 1662 cm^{-1} and a shoulder near 1685 cm^{-1} assigning the α-helix structure and the random coil form. However, denaturated insulin has its amide I peak sharpened and shifted to lower frequencies (1673 cm^{-1}) and no shoulder regarding the random coil form can be seen.

In this research, the spectra of pure insulin (Figure 3.6) shows the amide I band at 1661 cm^{-1} and a shoulder near 1682 cm^{-1} related to the α-helix and the random coil form respectively, indicating the native form of insulin in the film. Peaks at 1242 cm^{-1} and 1273 cm^{-1} regarding amide III in the native insulin conformation can also be seen in the spectra and are related to random coil and α-helix structures, respectively.

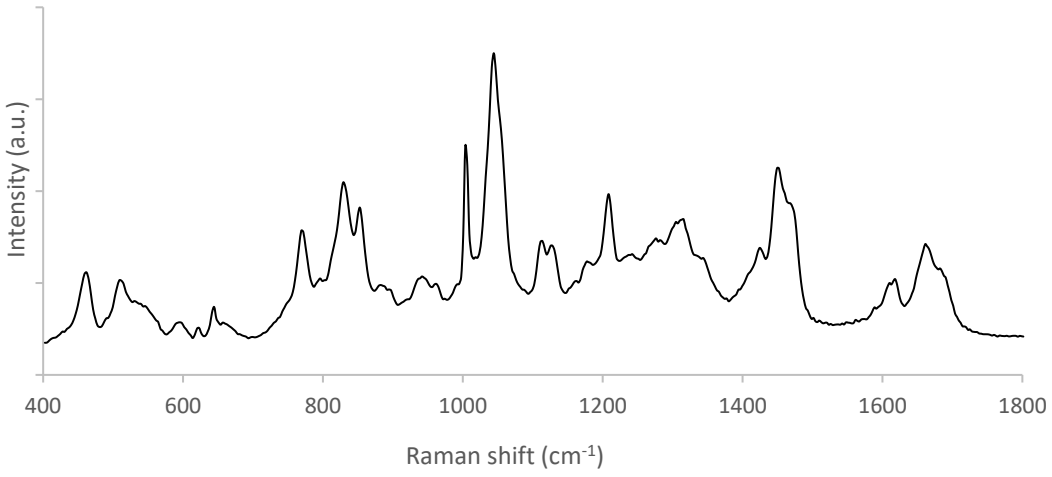

Figure 3.6. Raman spectrum of pure insulin film.

Figure 3.7 shows the Raman spectra for all insulin-polymer films at different ratios (w/w). All films showed amide I peak around 1662 cm^{-1} and a shoulder near 1685 cm^{-1} which correspond to the α-helix and random coil form assignments. Insulin-gelatin films did not show any distinctive peaks of gelatin whereas insulin-soluplus films show the distinctive peaks of soluplus at 699, 1087 and 1738 cm^{-1}.

For both insulin-soluplus films, amide III bands slightly shift to higher frequencies around 1237 and 1271cm^{-1} whereas insulin-gelatin samples showed amide III peaks about the same frequency as the pure insulin film with however less resolved peaks. Similar behaviour was reported by Zeng et al. (2011) during insulin dehydration. They noted that amide III peaks become gradually unresolved and amide I band becomes wider as the relative humidity is reduced and the water is removed.

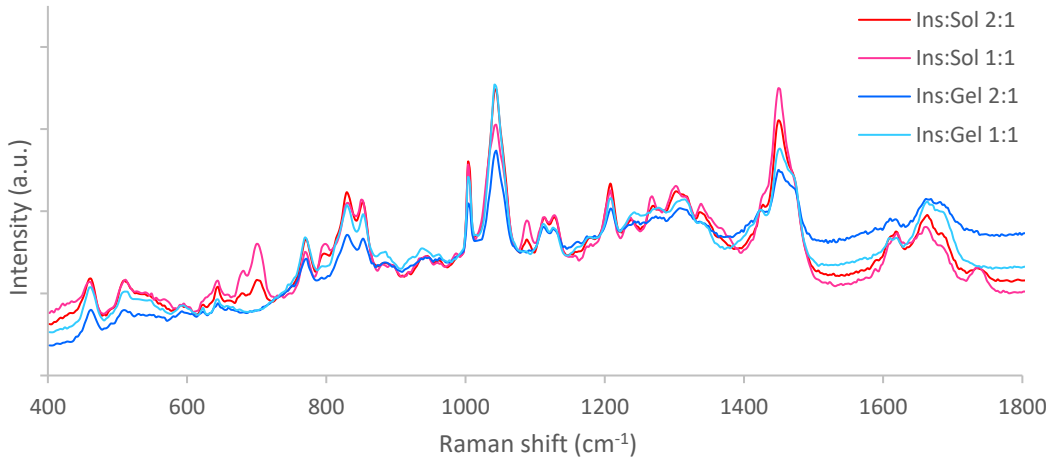

Figure 3.7. Raman spectra of insulin and insulin polymer-formulations films at 2:1 and 1:1 ratios (w/w).

Insulin has three disulphide bonds, one between A6 and A11 and other two that connect A and B chains, A7-B7 and A20-B19. These bonds are formed during the folding process and there are very important for stabilising the folded structure of insulin. The S-S bonds are also very sensitive to conformational changes in the molecule and their vibrations appear in the range of 500 - 550 cm^{-1} (Tensmeyer, Shields and Lilly 1990; Ortiz *et al.* 2004). From the spectra, all insulin and insulin-polymer films show similar Raman bands at about 509 cm^{-1} suggesting that the disulphide bonds of insulin adopt the most stable conformation in the dehydrated state, protecting its hydrophobic surfaces inside of its three-dimensional structure.

Among all insulin residues, Tyrosine (Tyr) is one of the most sensitive residues to the environmental changes. The doublet band located approximately at 830 cm^{-1} and 850 cm^{-1} and its relative intensity of I_{850}/I_{830} is sensitive to the hydrogen bonding of the phenolic hydroxyl group of the Tyr residues and can be used as an indicator of the state of the Tyr residues (Tensmeyer, Shields and Lilly 1990; Siamwiza *et al.* 1975; Zeng *et al.* 2011). From our study (Table 3.5), it is possible to see that all insulin-polymers showed an increase in the I_{850}/I_{830} when compared with insulin film alone indicating that more Tyr residues are exposed, and more hydrogen bonds are formed when the polymer is present.

Table 3.5. Relative intensity of Tyr residues of insulin and insulin-polymer films at different ratios (w/w).

	Insulin Film	Ins:Sol 2:1	Ins:Sol 1:1	Ins:Gel 2:1	Ins:Gel 1:1
I_{852}/I_{830}	0.91	0.97	1.01	0.99	0.97
I_{1174}/I_{1206}	0.77	0.82	0.81	0.93	0.89

Another interesting Raman bands that involve Tyr residues are the peaks at 1174 cm^{-1} and 1206 cm^{-1} and its relative intensity ratio I_{1174}/I_{1206}. Zeng et al. (2011) have demonstrated that its intensity ratio decreases as the water is removed from insulin crystals. It is interesting to note that insulin alone shows a significant water loss while more molecules of water were retained in the films containing the polymers.

Overall, all the films showed an increase in the hydrogen bonding of insulin as well as an increase in their content of water in the dehydrated state. Although the circular dichroism studies point to a decrease in the native state of insulin, no specific signs of insulin degradation can be seen in the Raman spectra.

3.3.4.3 X-ray diffraction (XRD)

Insulin, the isolated polymers and insulin-polymer films were studied by X-ray diffraction. Figure 3.8 shows the diffractogram of insulin which is predominantly amorphous with a small peak at 31.79°. Soluplus showed characteristics peaks at 9.97°, 20.44°, 24,56° and 29.54° whereas Gelatin showed no crystalline peaks, indicating its amorphous nature.

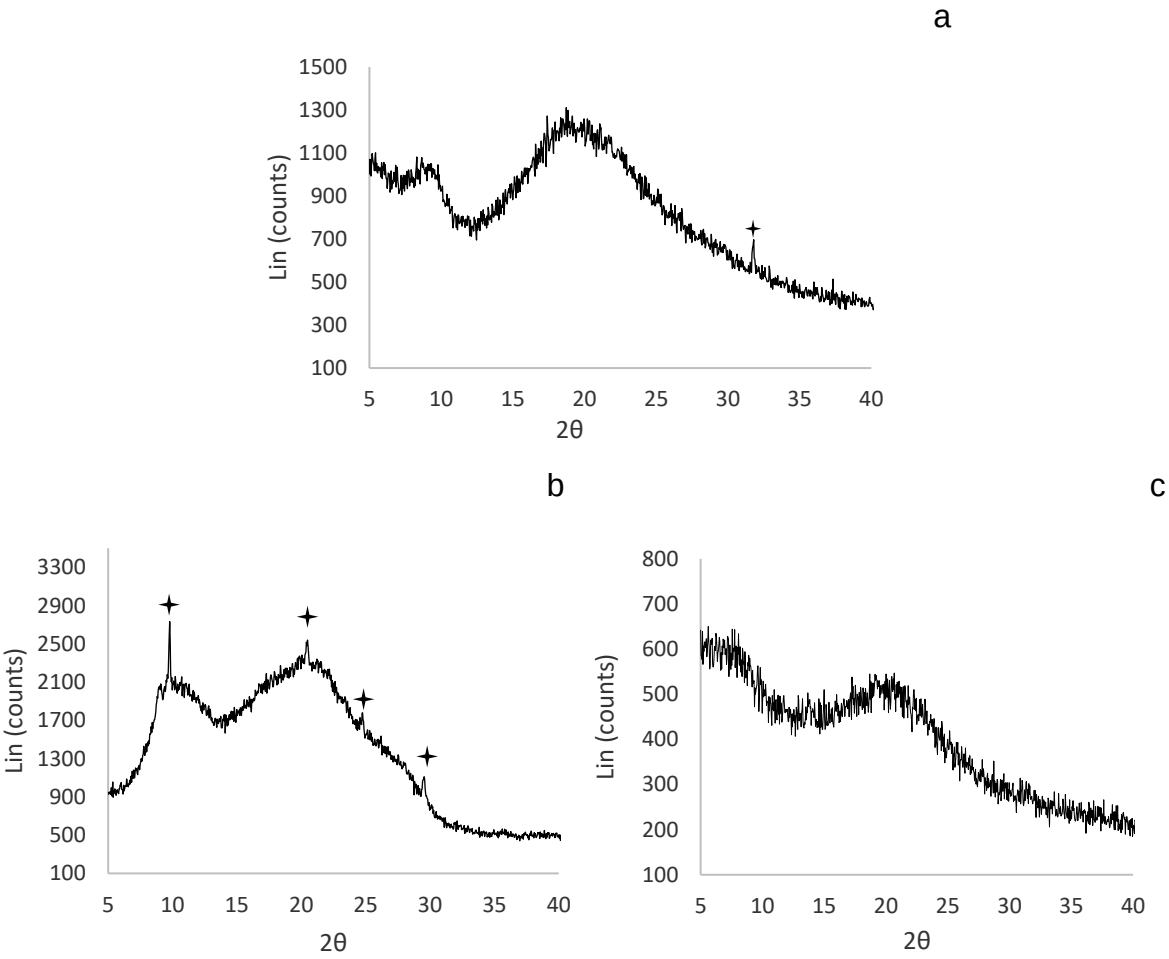

Figure 3.8. Diffractograms of the films of the components of the formulations: (a) insulin, (b) soluplus and (c) gelatin.

Figure 3.9 shows the diffractograms of insulin-polymer films. Insulin:soluplus (Figure 3.9, a) at 2:1 ratio showed crystalline peaks at 26.56° and 28.39° whereas the 1:1 ratio presented more crystalline regions with peaks at 18.22°, 20.16°, 26.56°. 28.31° and 31.68°. It is interesting to note that the insulin characteristic peak only strongly appears in the 1:1 ratio film.

a

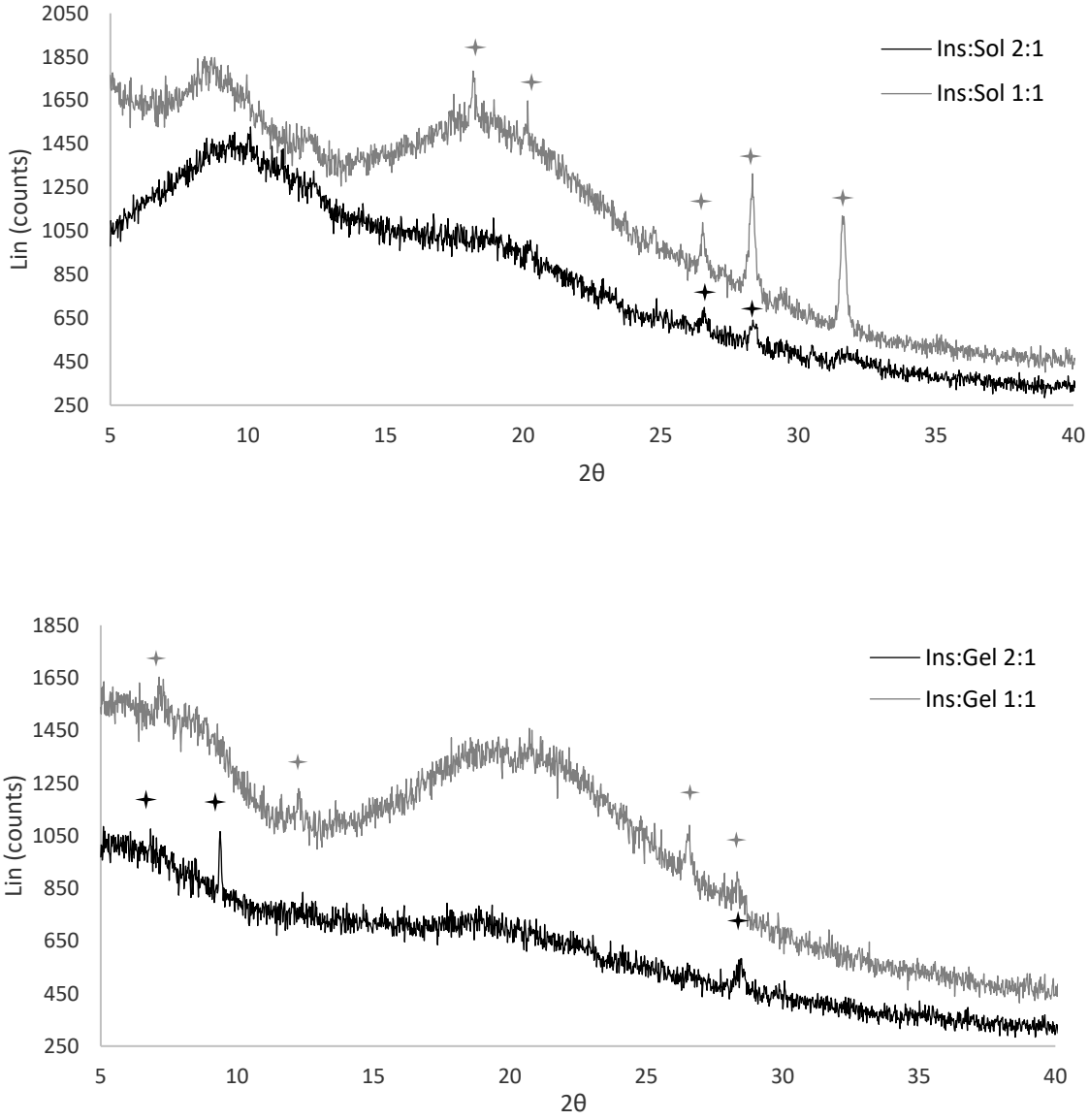

Figure 3.9. Diffractograms of insulin-polymer films at different ratios (w/w).

Insulin-gelatin films (Figure 3.9, b) show a predominant amorphous state with some regions of crystallinity. The 2:1 ratio film showed peaks 6.82° 9.33° and 28.54° while the 1:1 insulin: gelatin showed more crystalline regions with peaks at 7.10°, 12.35°, 26.54° and 28.40°.

From the spectra, it is possible to see that the random coil form of gelatin is maintained after the dehydration of the pure gelatin solution, however, when gelatin and insulin are combined, gelatin presents a tendency to form a triple helix structure after dehydration, which is indicated by the formation of the characteristic peak near 7°. It was also noted that the increase of gelatin concentration in the film leads to an increase of the ~7° peak intensity, indicating an increase of gelatin triple helix

content. Furthermore, a shift of the triple helix peak towards greater 2θ values also may indicate the presence of stronger interactions between gelatin and insulin molecules, especially by electrostatic interaction. Besides that, the 31.79° peak of insulin completely disappears in the presence of gelatin. These results also agree with Raman and circular dichroism findings, indicating a strong interaction between insulin and gelatin molecules.

3.3.5 Insulin stability

Circular dichroism and x-ray diffraction were used to study the stability of insulin and insulin-polymer films during the time. The samples were analysed using the same parameters as before at time zero (T0) and after thirty days (T30) kept in the fridge at 4 ± 1°C.

Figure 3.10 shows the CD spectra of insulin film at T0 and T30 at 1.0 mg/mL in PBS 7.4. The spectra of insulin show a double minimum around 210 and 222 nm which are related with α-helix and β-sheet structures as already reported by others (Correia *et al.* 2012; Zhang *et al.* 2010). The main difference between the two insulin spectra is due to the decrease of the Molar ellipticity for the T30 samples which suggest changes in the secondary structure of insulin with reduction of the α-helix structure. The estimation of the secondary structure content of insulin (Table 3.6) indicates a decrease in the α-helix content while new β-sheet structures were formed.

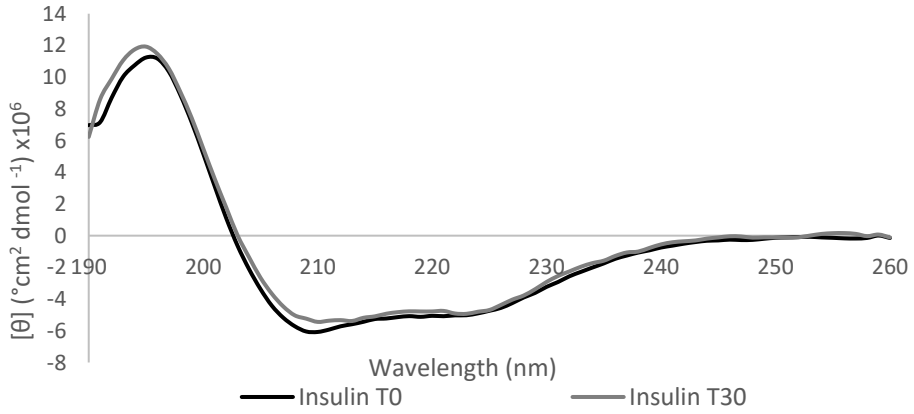

Figure 3.10. CD spectra of insulin film at time zero (T0) and after 30 days (T30) at 1.0mg/mL in PBS 7.4.

Table 3.6. Percentage of the secondary structure content of insulin of insulin films and insulin-polymer films at different ratios (w/w).

	Insulin (%)		Ins:Sol T0 (%)		Ins:Sol T30 (%)		Ins:Gel T0 (%)		Ins:Gel T30 (%)	
	T0	T30	2:1	1:1	2:1	1:1	2:1	1:1	2:1	1:1
Helix	46	44	41	45	44	45	32	21	33	19
β-sheet	15	19	18	17	16	19	24	34	26	36
Turn	16	14	21	17	21	18	22	20	23	23
Random coil	24	23	20	21	19	18	21	25	19	22

Figure 3.11 and Table 3.6 compares the CD spectra of the insulin-polymer films at T0 and T30 with the CD spectra of the pure insulin film after T30.

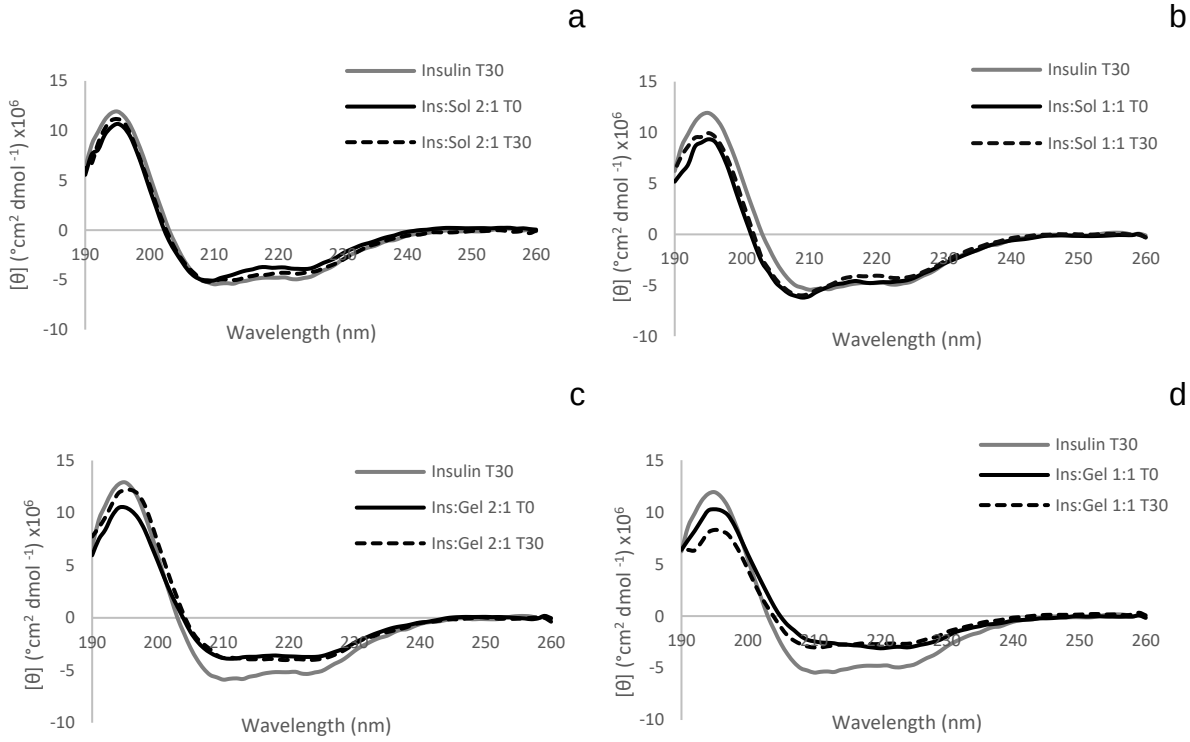

Figure 3.11. CD spectra of insulin film and insulin-polymer films at different ratios (w/w) at time zero (T0) and after 30 days stored in the fridge at 4°C (T30) at 1.0mg/mL in PBS 7.4.

From the results, it is possible to see that the secondary structure content of insulin slightly changed during the time for both insulin:soluplus ratios (w/w). Insulin:soluplus 2:1 ratio presented an increase in the α-helix structure along with a decrease in β-sheet content whereas insulin:soluplus 1:1 ratio maintained the same amount of α-helix content accompanied with the formation of more β-sheet and turn structures.

As previously discussed, greater changes occur in the secondary structure content of insulin for insulin-gelatin formulations. From Figure 3.11 (b, c) and Table 3.6, it is possible to see that insulin:gelatin 2:1 presented almost the same α-helix content during the time with however an increase in the β-sheet structures. As it

shows, insulin:gelatin 1:1 also showed changes during the time, with a decrease in the α-helix content and an even greater increase in the β-sheet and turn structures.

As mentioned earlier, the X-ray diffraction was also used to study the stability of the samples during the time.

Overall, insulin presents a predominant amorphous nature with some regions of crystallinity which increase during the time. Figure 3.12 shows the diffractogram of insulin films at T0 and T30 kept in the fridge at 4 ± 1°C. At T0 insulin shows a small peak at 31.79° which has increased and shifted to 31.66° after 30 days in the fridge. Furthermore, a small peak at 28.33° was also present at T30 indicating the formation of new crystalline regions. These changes in the insulin diffractogram during the time may be due to expected changes in the freshly prepared amorphous system as already reported by others (Abdul-fattah *et al.* 2007).

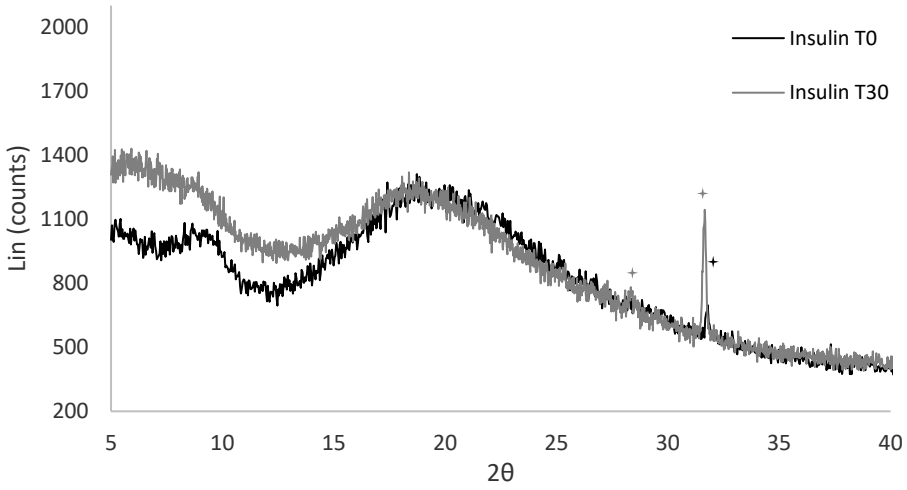

Figure 3.12. Diffractograms of insulin films at time zero (T0) and after 30 days (T30).

Insulin:soluplus films showed a predominance of amorphous phase for both ratios at both times (Figure 3.13 a, b). At time zero, the 2:1 ratio showed small peaks at 26.42° and 28.27° which were slightly shifted to 26.56° and 28.39° after 30 days. Moreover, the intensity of the peak at ~28° increases and a new peak is formed at 18.61°. The 1:1 ratio at time zero showed small peaks at 18.22° and 20.16° and higher peaks at 26.56°, 28.31° and 31.68° while the films after 30 days showed only the bigger peaks which were shifted to 26.32°, 28.39° and 31.69° respectively. The diffractogram also shows that the intensity of the characteristic peak of insulin near

31° is also reduced during the time which may be due to the changes in the lattice order of the molecule.

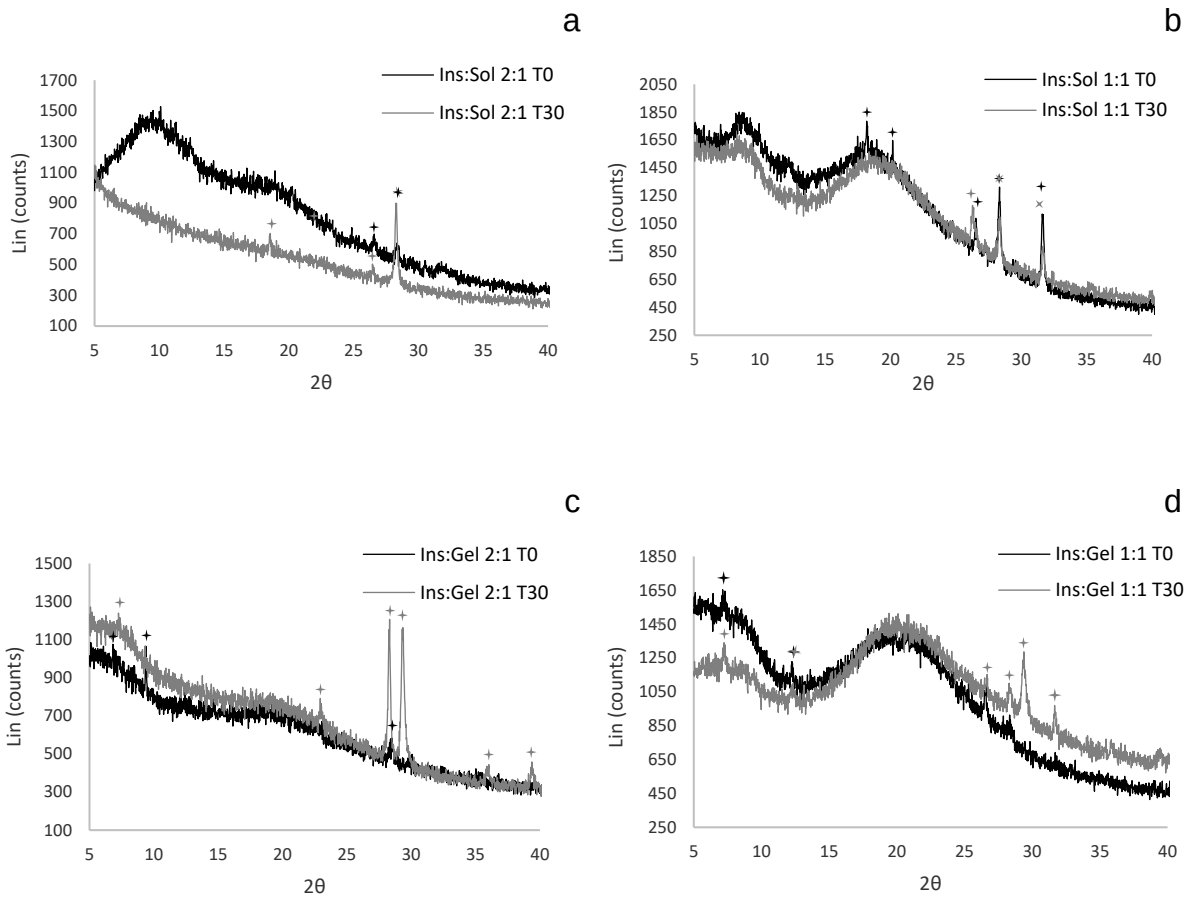

Figure 3.13. Diffractograms of insulin-polymer films at different ratios (w/w) at T0 and T30.

It is possible to see from the diffractogram of insulin:gelatin 2:1 (Figure 3.13, c) that the peak at 6.82°and 28.54° at T0 has shifted to 7.21° and 28.27°, respectively during the time, while the peak at 9.33° disappears and new ones are formed at 22.98°, 29.28°, 36.01° and 39.45°. The absence of the insulin peak and the shift of the gelatin triple helix peak (~7°) suggest stronger interaction between insulin and gelatin molecules in the films. Likewise, Insulin:gelatin 1:1 ratio also showed an increase in the crystallinity regions of the films during the time. Both samples, T0 and T30, showed similar peaks around 7.2°, 12.3°, 26.5° and 28.4° however with higher intensities for the samples kept in the fridge for 30 days which also presented new peaks at 29.40° and 31.68°.

Overall, all the samples showed changes in the crystalline structure of the molecules as well as in the secondary structure content of insulin as showed by the

CD results. These events may be due to the fact that the freshly prepared samples need time to reach their thermodynamic equilibrium (Abdul-fattah *et al.* 2007). Furthermore, we conclude that the insulin:soluplus 1:1 formulation offered the best protective properties to maintain the secondary structure of insulin in its native conformation during the time.

In this sense, insulin:soluplus 1:1 was selected as coating formulation for the *in vitro* release studies.

3.3.6 Insulin permeation studies

The permeation profile of insulin from the microneedles coated with insulin:soluplus 1:1 was studied using porcine skin and Franz diffusion cells. The metallic microneedles were coated with 4IU of insulin and the collected samples quantified by HPLC.

The permeation profile of insulin from the coated MNs are shown in Figure 3.14. The graph shows that 50% of the dose was released in about 15 min and 80% in about 30 min.

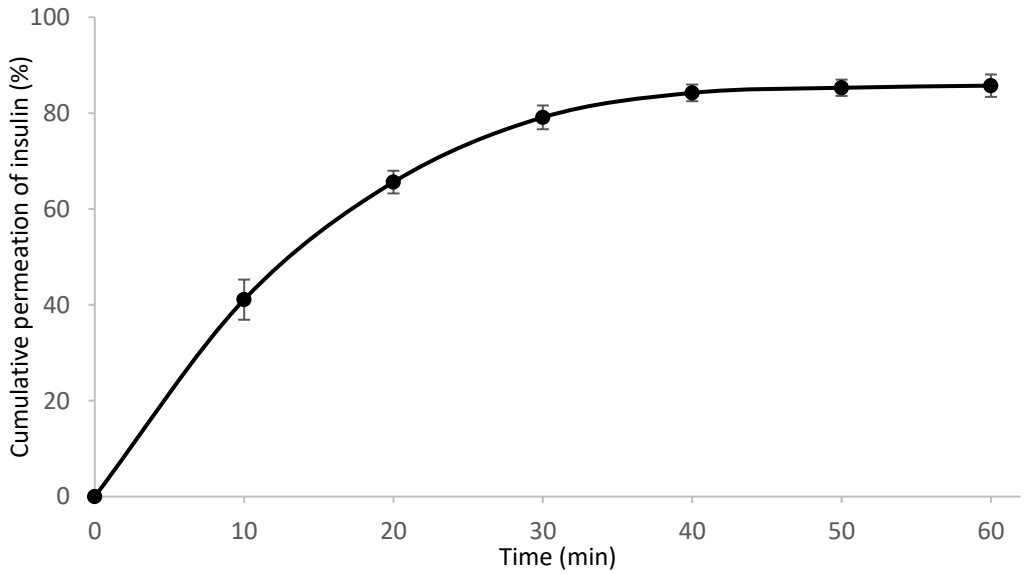

Figure 3.14. *In vitro* permeation profile of insulin from the insulin:soluplus 1:1 coated microneedles (n=6).

Therefore, the results show that the coated microneedles with insulin:soluplus 1:1 allows a relatively fast release of the insulin molecules from the coated microneedles and could be potentially used for the treatment of diabetes.

3.4 Conclusions

In this study, gelatin and soluplus at different ratios were proposed to increase the stability of insulin in the dried state and to be used as coating formulations for metallic microneedles. Although, both of them are successfully used as stabilizers for many drugs, only soluplus at 1:1 ratio (w/w) presented the ability to maintain the most native structure of insulin during the time. The inkjet printing provided uniform, precise and reproducible coating layers on the metallic MNs without any material loss during the coating process. Furthermore, the permeation studies showed that most of the insulin dose permeates the skin within 30 min after the MN application.

3.5 References

Abdul-fattah, A.M., Dellerman, K.M., Bogner, R.H., Pikal, M.J. (2007). The Effect of Annealing on the Stability of Amorphous Solids: Chemical Stability of Freeze-Dried Moxalactam. *Journal of Pharmaceutical Sciences*, 96(5), 1237–1250.

Al-Hanbali, O. A., Khan, H.M.S., Sarfraz, M., Arafat, M., Ijaz, S., Hammed, A. (2019). Transdermal patches: Design and current approaches to painless drug delivery. *Acta Pharmaceutica*, 69(1), 1-19.

Ameri, M., Kadkhodayan, M., Nguyen, J., Bravo, J. A., Su, R., Chan, K., Daddona, P. E. (2014). Human growth hormone delivery with a microneedle transdermal system: Preclinical formulation, stability, delivery and PK of therapeutically relevant doses. *Pharmaceutics*, 6(2), 220–234.

Andrade, F., Fonte, P., Oliva, M., Videira, M., Ferreira, D., Sarmento, B. (2015). Solid state formulations composed by amphiphilic polymers for delivery of proteins: characterization and stability. *International Journal of Pharmaceutics*, 486(1–2), 195–206.

Bariya, S.H., Gohel, M.C., Mehta, T.A., Sharma, O.P. (2012). Microneedles: an emerging transdermal drug delivery system. *Journal of Pharmacy and Pharmacology*, 64(1), 11–29.

Boehm, R.D., Daniels, J., Stafslien, S., Nasir, A., Lefebvre, J., Narayan, R.J., Lefebvre, J. (2015). Polyglycolic acid microneedles modified with inkjet-deposited antifungal coatings. *Biointerphases*, 10(1).

Boehm, R.D., Miller, P.R., Daniels, J., Stafslien, S., Narayan, R.J. (2014). Inkjet printing for pharmaceutical applications. *Biochemical Pharmacology*, 17(5), 247–252.

Boehm, R.D., Miller, P. R., Schell, W.A., Perfect, J.R., Narayan, R.J. (2013). Inkjet printing of amphotericin B onto biodegradable microneedles using piezoelectric inkjet printing. *Jom*, 65(4), 525–533.

Choi, H.J., Yoo, D.G., Bondy, B.J., Quan, F.S., Compans, R. W., Kang, S.M., Prausnitz, M.R. (2012). Stability of influenza vaccine coated onto microneedles. *Biomaterials*, 33(14), 3756–3769.

Cormier, M., Johnson, B., Ameri, M., Nyam, K., Libiran, L., Zhang, D.D., Daddona, P. (2004). Transdermal delivery of desmopressin using a coated microneedle array patch system. *Journal of Controlled Release*, 97(3), 503–511.

Correia, M., Neves-Petersen, M.T., Jeppesen, P.B., Gregersen, S., Petersen, S.B. (2012). UV-Light Exposure of Insulin: Pharmaceutical Implications upon Covalent Insulin Dityrosine Dimerization and Disulphide Bond Photolysis. *PLoS ONE*, 7(12).

Djabourov, M., Leblond, J., Papon, P., Djabourov, M., Leblond, J., Papon, P. (1988). Gelation of aqueous gelatin solutions. I. Structural investigation To cite this version: Gelation of aqueous investigation. *Journal de Physique*, 49(2), 319–332.

Ettinger, M.J., Timasheff, S.N. and Strycharz, G.D. (1971). Optical Activity of Insulin. I. On the Nature of the Circular Dichroism Bands. *Biochemistry*, 10(5), 824–831.

Gill, H.S. and Prausnitz, M.R. (2007). Coated microneedles for transdermal delivery. Journal of Controlled Release, 117(2), 227–237.

Goh, P.S., Ismail, A.F. and Ng, B.C. (2017). Raman Spectroscopy. *In Membrane Characterization*, pp. 31-46. Available from: https://linkinghub.elsevier.com/retrieve/pii/B9780444637765000024 [Accessed 12 January 2019].

Gopal, R., Park, J.S., Seo, C.H., Park, Y. (2012). Applications of circular dichroism for structural analysis of gelatin and antimicrobial peptides. *International Journal of Molecular Sciences*, 13(3), 3229–3244.

Greenfield, N. (2007). Using circular dichroism spectra to estimate protein secondary structure. *Nature Protocols*, 1(6), 2876–2890.

Hosseinzadeh, G., Maghari, A., Farniya, S.M.F., Keihan, A. H., Moosavi-Movahedi, A.A. (2017). Interaction of insulin with colloidal ZnS quantum dots functionalized by various surface capping agents. *Materials Science and Engineering: C*, 77, 836–845.

Kamerzell, T.J., Esfandiary, R., Joshi, S.B., Middaugh, C.R., Volkin, D.B. (2011). Protein-excipient interactions: Mechanisms and biophysical characterization applied to protein formulation development. *Advanced Drug Delivery Reviews*, 63(13), 1118–1159.

Kellerman, D.J., Ameri, M. and Tepper, S.J. (2017). Rapid systemic delivery of zolmitriptan using an adhesive dermally applied microarray. *Pain Management*, 7(6), 559–567.

Kelly, S.M., Jess, T.J. and Price, N.C. (2005). How to study proteins by circular dichroism. *Biochimica et Biophysica Acta - Proteins and Proteomics*, 1751(2), 119–139.

Kommareddy, S., Baudner, B.C., Bonificio, A., Gallorini, S., Palladino, G., Determan, A.S., O'Hagan, D.T. (2013). Influenza subunit vaccine coated microneedle patches elicit comparable immune responses to intramuscular injection in guinea pigs. *Vaccine*, 31(34), 3435–3441.

Larrañeta, E., McCrudden, M.T.C., Courtenay, A.J., Donnelly, R.F. (2016). Microneedles: A New Frontier in Nanomedicine Delivery. *Pharmaceutical Research*, 33(5), 1055–1073.

Li, K., Chen, W. and Zhang, L. (2018). Controllable printing droplets on demand by piezoelectric inkjet: applications and methods. *Microsystem Technologies*, 24(2), 879–889.

Liu, F., Chiou, B. Sen, Avena-Bustillos, R. J., Zhang, Y., Li, Y., McHugh, T. H., Zhong, F. (2017). Study of combined effects of glycerol and transglutaminase on properties of gelatin films. *Food Hydrocolloids*, 65, 1–9.

Liu, M., Ji, J., Zhai, Y., Du, X., He, S., Cheng, H., Zhai, G. (2019). Recent progress of micro-needle formulations: Fabrication strategies and delivery applications. *Journal of Drug Delivery Science and Technology*, 50, 18–26.

Martin, S.R. and Schilstra, M.J. (2008). Circular Dichroism and Its Application to the Study of Biomolecules. *Methods in Cell Biology*, 84(07), 263–293.

Migalska, K., Morrow, D. I. J., Garland, M. J., Thakur, R., Woolfson, A. D., Donnelly, R. F. (2011). Laser-engineered dissolving microneedle arrays for transdermal macromolecular drug delivery. *Pharmaceutical Research*, 28(8), 1919–1930.

Ohtake, S., Kita, Y. and Arakawa, T. (2011). Interactions of formulation excipients with proteins in solution and in the dried state. *Advanced Drug Delivery Reviews*, 63(13), 1053–1073.

Olsen, D., Yang, C., Bodo, M., Chang, R., Leigh, S., Baez, J., Polarek, J. (2003). Recombinant collagen and gelatin for drug delivery. *Advanced Drug Delivery Reviews*, 55(12), 1547–1567.

Ortiz, C., Zhang, D., Xie, Y., Davisson, V. J., Ben-Amotz, D. (2004). Identification of insulin variants using Raman spectroscopy. *Analytical Biochemistry*, 332(2), 245–252.

Pere, C.P.P., Economidou, S.N., Lall, G., Ziraud, C., Boateng, J.S., Alexander, B. D., Douroumis, D. (2018). 3D printed microneedles for insulin skin delivery. *International Journal of Pharmaceutics*, 544(2), 425–432.

Prausnitz, M.R. and Langer, R. (2008). Transdermal drug delivery. *Nature Biotechnology*, 26(11), 1261–1268.

Prestrelski, S.J., Tedeschi, N., Arakawa, T., Carpenter, J.F. (1993). Dehydration-induced conformational transitions in proteins and their inhibition by stabilizers. *Biophysical Journal*, 65(2), 661–671.

Ross, S., Scoutaris, N., Lamprou, D., Mallinson, D., Douroumis, D. (2015). Inkjet printing of insulin microneedles for transdermal delivery. *Drug Delivery and Translational Research*, 5(4), 451–461.

Roth, E.A., Xu, T., Das, M., Gregory, C., Hickman, J.J., Boland, T. (2004). Inkjet printing for high-throughput cell patterning. *Biomaterials*, 25(17), 3707–3715.

Sakai, A., Murayama, Y., Fujiwara, K., Fujisawa, T., Sasaki, S., Kidoaki, S., Yanagisawa, M. (2018). Increasing Elasticity through Changes in the Secondary Structure of Gelatin by Gelation in a Microsized Lipid Space. *ACS Central Science*, 4(4), 477–483.

Sandler, N., Maattanen, A., Ihalainen, P., Kronberg, L., Meierjohann, A., Viitala, T., Peltonen, J. (2011). Inkjet Printing of Drug Substances and Use of Porous Substrates-Towards Individualized Dosing. *Journal of Pharmaceutical Sciences*, 100(8), 3386–3395.

Siamwiza, M.N., Lord, R. C., Chen, M. C., Takamatsu, T., Harada, I., Matsuura, H., Shimanouchi, T. (1975). Interpretation of the doublet at 850 and 830 cm^{-1} in the Raman spectra of tyrosyl residues in proteins and certain model compounds. *Biochemistry*, 14(22), 4870–4876.

Smith, G.P.S., McGoverin, C.M., Fraser, S.J., Gordon, K.C. (2015). Raman imaging of drug delivery systems. *Advanced Drug Delivery Reviews*, 89, 21–41.

Souillac, P.O., Middaugh, C.R. and Rytting, J.H. (2002). Investigation of protein / carbohydrate interactions in the dried state. 2. Diffuse reflectance FTIR studies. *International Journal of Pharmaceutics*, 235, 207–218.

Sreerama, N, Venyaminov, S. Y. and Woody, R. W. (1999). Estimation of the number of alpha-helical and beta-strand segments in proteins using circular dichroism spectroscopy. *Protein Science*, 8(2), 370–380.

Sreerama, N., Venyaminov, S.Y. and Woody, R.W. (2000). Estimation of protein secondary structure from circular dichroism spectra: Comparison of CONTIN, SELCON, and CDSSTR methods with an expanded reference set. *Analytical Biochemistry*, 287(2), 252–260.

Sullivan, S.P., Koutsonanos, D.G., Del Pilar Martin, M., Lee, J.W., Zarnitsyn, V., Choi, S.O., Prausnitz, M.R. (2010). Dissolving polymer microneedle patches for influenza vaccination. *Nature Medicine*, 16(8), 915–920.

Tarcha, P.J., Verlee, D., Hui, H.W., Jetesak, J., Antohe, B., Radulescu, D., Wallace, D. (2007). The Application of Ink-Jet Technology for the Coating and Loading of Drug-Eluting Stents. *Annals of Biomedical Engineering*, 35(10), 1791–1799.

Tas, C., Mansoor, S., Kalluri, H., Zarnitsyn, V.G., Choi, S.O., Banga, A.K., Prausnitz, M.R. (2012). Delivery of salmon calcitonin using a microneedle patch. *International Journal of Pharmaceutics*, 423(2), 257–263.

Tensmeyer, L.G., Shields, J.E. and Lilly, E. (1990). The Raman Spectra of Crystalline 4Zn, 2Zn, and Na Insulin. *Raman and Luminescence Spectroscopies in Technology II*, 1336, 222–234.

Thyagarajapuram, N., Olsen, D. and Middaugh, R. (2007). Stabilization of Proteins by Recombinant Human Gelatins. *Journal of Pharmaceutical Sciences*, 96(12), 3304–3315.

Tuan-Mahmood, T.M., McCrudden, M.T.C., Torrisi, B.M., McAlister, E., Garland, M.J., Singh, T.R.R., Donnelly, R.F. (2013). Microneedles for intradermal and transdermal drug delivery. *European Journal of Pharmaceutical Sciences*, 50(5), 623–637.

Uddin, M.J., Scoutaris, N., Klepetsanis, P., Chowdhry, B., Prausnitz, M.R., Douroumis, D. (2015). Inkjet printing of transdermal microneedles for the delivery of anticancer agents. *International Journal of Pharmaceutics*, 494(2), 593–602.

Wang, W. (2005). Protein aggregation and its inhibition in biopharmaceutics. *International Journal of Pharmaceutics*, 289(1–2), 1–30.

Whitmore, L. and Wallace, B.A. (2004). DICHROWEB, an online server for protein secondary structure analyses from circular dichroism spectroscopic data. *Nucleic Acids Research*, 32, 668–673.

Whitmore, L. and Wallace, B.A. (2008). Protein secondary structure analyses from circular dichroism spectroscopy: Methods and reference databases. *Biopolymers*, 89(5), 392–400.

Wu, B.M., Borland, S.W., Giordano, R. A., Cima, L.G., Sachs, E.M., Cima, M. (1996). Solid free-form fabrication of drug delivery devices. *Journal of Controlled Release*, 40(1–2), 77–87.

Yeo, Y., Basaran, O.A. and Park, K. (2003). A new process for making reservoir-type microcapsules using ink-jet technology and interfacial phase separation. *Journal of Controlled Release*, 93(2), 161–173.

Yong, Z., Yingjie, D., Xueli, W., Jinghua, X., Zhengqiang, L. (2009). Conformational and bioactivity analysis of insulin: Freeze-drying TBA/water co-solvent system in the presence of surfactant and sugar. *International Journal of Pharmaceutics*, 371(1–2), 71–81.

Young, S., Wong, M., Tabata, Y., Mikos, A. G. (2005). Gelatin as a delivery vehicle for the controlled release of bioactive molecules. *Journal of Controlled Release*, 109(1–3), 256–274.

Zeng, G., Shou, J.J., Li, K.K., Zhang, Y.H. (2011). *In-situ* confocal Raman observation of structural changes of insulin crystals in sequential dehydration process. *Biochimica et Biophysica Acta*, 1814(12), 1631–1640.

Zhang, N., Li, J., Jiang, W., Ren, C., Li, J., Xin, J., Li, K. (2010). Effective protection and controlled release of insulin by cationic β-cyclodextrin polymers from alginate/chitosan nanoparticles. *International Journal of Pharmaceutics*, 393(1–2), 213–219.

Zhang, Y., Jiang, G., Yu, W., Liu, D., Xu, B. (2018). Microneedles fabricated from alginate and maltose for transdermal delivery of insulin on diabetic rats. *Materials Science and Engineering: C*, 85, 18–26.

4 CHAPTER

3D PRINTED MICRONEEDLES FOR INSULIN DELIVERY

4.1 Introduction

Undeniably, many researchers have shown that coated microneedles can be an excellent strategy for transdermal delivery of drugs locally (Gittard *et al.* 2011; Zhang *et al.* 2012; Baek, Shin and Kim 2017) and systemically (Harvinder S Gill and Prausnitz 2007; Ameri *et al.* 2014; Cormier *et al.* 2004; Uddin *et al.* 2015; Boehm *et al.* 2014). Nevertheless, the selection of the materials, the delivery approach and the MNs processing are the most important factors that will determine its success.

Even though many studies have been done with a wide range of materials, the metallic microneedles usually offer the best piercing properties due to the inherent characteristics of the used materials (Larraneta *et al.* 2016; Tuan-Mahmood *et al.* 2013). However, the usual two-step administration process, the limited coating area, the required time and the fabrication process usually limit the potential application of those MNs (Bariya *et al.* 2012; Kim, Park and Prausnitz 2012)

3D printing is a family of techniques that have been opportunely applied for rapid fabrication of customised pharmaceutical systems (Chimate and Koc 2014; Goyanes *et al.* 2014; Goyanes, Buanz, *et al.* 2015; Jamróz *et al.* 2017; Herwadkar and Banga 2012; Doraiswamy *et al.* 2006). Their greatest advantages are the capability that those apparatuses have to create unique small and complex objects with fine details, with a small time-required process and an easy scale-up production (Economidou, Lamprou and Douroumis 2018; Park *et al.* 2018; Jamróz *et al.* 2018).

Recently, different 3D printing technologies have been applied for the fabrication of transdermal microneedles. Micro-stereolithography of digital light processing (DLP) was used to indirect obtain Gantrez biodegradable microneedles from 3D printed moulds (Boehm *et al.* 2011; Boehm *et al.* 2013; Boehm *et al.* 2012). In another work, Gittard et al. (2011) directly printed a Class-IIa biocompatible polymer MNs arrays through DLP processes to be coated with silver and zinc oxide films for antimicrobial attributes. Two-Photon polymerisation (2PP) printers have also been applied for the fabrication of hybrid organic-inorganic hollow MNs

(Ovsianikov *et al.* 2007; Doraiswamy *et al.* 2006). Finally, biodegradable MNs made of polylactic acid were directly printed using fused deposition modelling (FDM) technology, however the resolution of the FDM printers is still a limiting factor for MNs fabrication (Luzuriaga *et al.* 2018).

In this sense, different designs of 3D printed MNs made of biocompatible material class I approved by FDA and fabricated by Stereolithography were combined with inkjet printing technique for the deposition of uniform and accurate coatings of a highly dissolvable insulin-sugar formulations for rapid insulin release.

4.2 Material and methods

4.2.1 Materials

Insulin solution from bovine pancreas (10 mg. mL^{-1}) and trehalose dihydrate were purchased from Sigma-Aldrich (Gillingham, UK). Xylitol (Xylisorb® 90) and mannitol (Pearlitol®) were donated by Roquette Freres (France). The resin used to fabricate the MNs was the biocompatible Class I resin, Dental SG, purchased from Formlabs. Streptozocin (≥75% α-anomer basis, ≥98%) and citric acid were both purchased from Merck Chemical Co. (Darmstadt, Germany). Saline phosphate buffer pH 7.4 was purchased from Sigma-Aldrich. All solvents used were of analytical grades.

4.2.2 3D printing of microneedles

The microneedles` designs were developed using appropriate engineering software (SolidWorks by Dassault Systems) and built on a solid 15x15x1 mm substrate. The needles` length and the interspace distance between them (measured from tip to tip) were 1.0 mm and 1.85mm, respectively. A Form 2 SLA printer with high-resolution capability was used to print the MNs arrays. Following the printing, all MNs were washed and cured under UV radiation for 60 min at 40^{o}C to improve its mechanical properties.

Due to the flexibility of the technique, the number of needles per array can be easily changed and straightforwardly printed. Therefore, all printed designs used in this work are composed of 48 (6x8) needles per array, unless otherwise stated.

4.2.3 Penetration studies through porcine skin

A texture analyser (Stable micro system) was used for the penetration studies where the MN arrays were mounted on the bottom of the moving probe using double-sided adhesive tape and the porcine skin samples were placed in waxed petri dishes at the bottom of the equipment. The probe was then moved at 0.01 mm/s and the continuous force and displacement measurements were recorded to identify the point of needle insertion.

4.2.4 Coating formulations

Trehalose, xylitol and mannitol were weighed, added to the insulin solution and then left it stirring until complete dissolution. The composition of the coating formulations used is shown in Table 4.1.

Table 4.1. Composition of coating formulations.

Formulations	Composition (w/w)
Ins:Treh 5:1	10mg Insulin, 2mg Trehalose
Ins:Treh 3:1	10mg Insulin, 3.33mg Trehalose
Ins: Xy 5:1	10mg Insulin, 2mg Xylitol
Ins:Xy 3:1	10mg Insulin, 3.33mg Xylitol
Ins:Man 5:1	10mg Insulin, 2mg Mannitol
Ins:Man 3:1	10mg Insulin, 3.33mg Mannitol

4.2.5 Coating of microneedles through inkjet printing

The coating process was performed with an Inkjet printing Nanoploter II (Gesim, Germany). The MNs were positioned at 45º relative to the dispenser and the formulations were jetted through a piezodriven dispenser (pipette) (PicPip 300) onto the MN surface in the form of fine droplets of approximately 300 pl. The

microneedles were coated through various coating cycles. For each coating array, two droplets and 10 spots of a coating formulation were dispensed on each needle's longitudinal axis, and the number of cycles was adjusted to achieve the appropriate amount for a required experiment. The coated arrays were then incubated at room temperature for 24 hours to allow the evaporation of the solvent (deionised water) and the formation of uniform films.

4.2.6 Scanning electron microscopy (SEM)

The microneedle arrays were placed on a double-sided carbon adhesive tape on top of an aluminium stub. The MNs were then analysed by SEM (Hitachi SU 8030, Japan) using low accelerating voltage (1.0 kV) to avoid electrical charges on the microneedles. The images were digitally taken with different magnifications (from 30 to 120x).

4.2.7 X-ray computed microtomography (μ-CT)

X-ray computed microtomography scans were performed on pyramid 3D printed microneedles coated with insulin:xylitol, insulin:trehalose and insulin:mannitol at 5:1 ratios. The analysis was performed using a Bruker Skyscan 1172, with an SHT 11 Megapixel camera and a Hamamatsu 80kV (100μA) source. The samples were mounted vertically on a portion of dental wax and positioned at 259.4 mm from the source. No filter was applied to the X-ray source, and a voltage of 80 kV was applied for an exposure time of 1050 ms. Followed the scans of the coated arrays, the MNs were inserted in 8-ply strips of parafilm, with an applying force of 5 N, to examine the performance of the coatings during piercing and to investigate whether any coating material would be detached from the MN and stay on the parafilm surface.

4.2.8 Quantitative analysis of the amount of insulin coated on the MNs

Pyramid MNs were coated with 10 IU (350μg) of insulin for each 5:1 formulation ratio in triplicate. The MNs were left to completely dry at room temperature for 24 hours and kept in the fridge at 4 °C until the experiment.

The coated MNs were individually placed in a glass flask and 8 mL of saline phosphate buffer pH 7.4 (PBS pH 7.4) was added to each MN. The vials were placed to sonicate for 5min, filtrated and the amount of insulin analysed by HPLC. The concentration of insulin was calculated using the analytical curve under the same conditions, and the percentage of the coating efficiency (CE%) was then calculated with the following equation:

$$CE\ (\%) = \frac{\text{(The amount of insulin analytically determined)}}{\text{Theoretical amount of insulin}} \times 100$$

4.2.9 Circular Dichroism (CD)

Insulin and insulin-sugar solutions were diluted to 1.0 mg. mL^{-1} in PBS 7.4 whereas their respective films were weighed and solubilized in PBS 7.4 to 1.0 mg. mL^{-1} of insulin concentration. All the spectra were recorded at 20 °C between 190 and 260 nm by CD (Chirascan, Applied Photophysics, UK) using a 0.1 mm polarization certified quartz cell (Hellma) and recorded using a step size of 1 nm, a bandwidth of 1 nm and an acquisition time of 1 sec. Four scans were recorded for each sample, averaged and the corresponding spectrum of water and sugar concentration, when required, were then subtracted from each spectrum. For estimation of the secondary structure composition of insulin, the CD spectra were evaluated by the CDSSTR method (Sreerama, Venyaminov and Woody 1999; Sreerama and Woody 2000) using Dichroweb website (Whitmore and Wallace 2008; Whitmore and Wallace 2004).

4.2.10 Raman spectroscopy

Insulin and insulin-sugar films were analysed using Raman microscopy (Jobin Yvon LabRam I) with a laser of 532 nm wavelength coupled with an optical microscope with 50x objective. An average of 5 spectra and an acquisition time of 5 seconds were used.

4.2.11 X-Ray Diffraction (XRD)

The X-ray diffraction patterns of the films of the raw materials and the films of insulin-sugar formulations were obtained using a Bruker D8 Advance (Germany) with a Göebel mirror using Cu-Kα radiation and operating at 40 kV and 40 mA. The diffractograms were collected in two-theta (2θ) mode from 5° to 40° with a step size of 0.02° (2θ) and a counting time of 0.2 seconds per step.

4.2.12 Stability of Insulin Films

The stability of the insulin-sugar films was accessed by the study of the films through circular dichroism and X-ray diffraction at time zero (T_0) and after 30 days (T_{30}) kept in the fridge at 4 ± 1 ^oC.

4.2.13 Preparation of porcine skin for in vitro release of insulin

Untreated abdominal porcine skin was obtained from a slaughterhouse (Forge Farm Ltd, Kent, UK) and stored at 4° until it was used. The skin was fixed on a polystyrene block previously wiped with 70% ethanol. The skin was shaved with a razor blade and the fatty tissue below the abdominal skin area was removed with a scalpel. Once ready, the skin was then treated with dermatome (Padgett dermatome, Integra LifeTMSciences Corporation USA) at an angle of ±45°. The thickness of the skin was measured using a calliper, and the tissue samples of 1.0 ± 0.1mm thick were cut at the required dimensions for the Franz diffusion cells. The skin samples were then placed onto filter paper soaked in a small amount of PBS pH 7.4 for 2 h before use.

4.2.14 *In vitro* permeation of insulin through porcine skin

The transdermal permeation of insulin from the coated MNs through the abdominal porcine skin was studied using Franz diffusion cells (PermeGear, Inc., PA, USA). The cells were calibrated with PBS pH 7.4 at 6-6.5 mL per hour rate using an autosampler (FC 204 fraction collector, Gilson, USA) while the temperature was maintained at 37°C using an automated water bath (Thermo Fisher Scientific,

Newington, USA). A total diffusion area of 1.1 cm^2 was used to access the insulin release.

Each design of MN (pyramid, cone and spear) was coated with 10 IU of the three different formulations, insulin:xylitol, insulin:trehalose and insulin: mannitol at 5:1 ratio (n = 6). The MNs were inserted into the abdominal porcine skin for 30 s using manual finger pressure. The pierced skin with the MN was then mounted on the donor compartment of the Franz diffusion cells previously equilibrated at 37°C with PBS 7.4. Sample fractions were then collected up to 1 h, and the amount of insulin was analysed by a validated HPLC method (chapter 2). At the end of the experiment, the MNs and the skin were individually placed in a glass flask with 1mL of PBS 7.4 and left it to sonicate for 5 min. After that, they were filtrated and analysed by HPLC in order to determine any remaining insulin on the MNs or in the skin. Statistical analysis for the drug release was performed by using ANOVA (SPSS software Inc.), and a 0.05 significance level was adopted.

4.2.15 Animal studies

The protocol for the animal experiments were submitted and approved by the Research Ethics Committee (reference number 0003/17, Department of Pharmacy, Southern University Bangladesh) and conducted according to the Southern University Bangladesh policy for the protection of Vertebrate Animals used for Experimental and Other Scientific Purposes, with implementation of the principle of the 3Rs (replacement, reduction, refinement).

4.2.15.1 Diabetic mice model

To generate the diabetic animal model, Swiss albino female mice (130 ± 10g) were allowed to free access to food and water for 3 days prior to diabetes therapy. Streptozotocin (70 mg/kg) in citric acid buffer (pH 4.5) was subcutaneously injected on the flank of the animals. To verify the induction of diabetes, fasting blood glucose level was measured for each animal at scheduled times using a one-touch glucometer (ACCU-CheckVR Active, Roche, Germany). After 7 days of

streptozotocin administration, mice with blood glucose exceeding 300 mg/dl were considered as diabetic.

4.2.15.2 Insulin transdermal delivery in diabetic mice

The diabetic mice were randomly divided into three groups containing 3 mice each: (1) untreated group as negative control; (2) subcutaneous injection (SC) (0.2 IU/animal) as positive control and (3) 3D printed MN coated with Insulin:Xylitol 5:1 (0.2 IU/animal) as experimental group.

Preceding the experiment, diabetic mice were anaesthetized and carefully shaved at the area of application using an electric razor (Panasonic, USA) 24 hours before the experiment. Then, the animals were left for fasting for 12 hours prior to the beginning of the study.

Subcutaneous injection of insulin solution was administered into the dorsal skin using a hypodermic needle while the 3D printed MNs coated with insulin were applied onto the dorsal skin of the animals, and an adhesive tape (3M, USA) was used to prevent any dislodgement during therapy.

The microneedles were then removed from the mice skin after 2 hours. For all groups, blood samples were collected from jugular vein at 0, 1, 2, 3 and 4 hours after the administration and centrifuged at 3000 r.p.m. for 5 min to immediately separate the plasma. Plasma glucose levels were measured with a glucometer (ACCU-CheckVR Active, Roche, Germany) whereas insulin plasma concentrations were determined using insulin ELISA kit.

4.2.15.3 Pharmacodynamic and pharmacokinetic analyses of insulin after application of insulin-3D printed Microneedles

The minimum glucose level (Cmin) and the time point of minimum glucose level (Tmin) were calculated from the respective curves of the blood glucose level over time. The relative pharmacological availability (RPA) was calculated with the following equation:

$$RPA\ (\%) = \{(AAC_{3DMN}) \times (Dose_{sc})\} / \{(AAC_{sc}) \times (Dose_{3DMN})\} \times 100$$

Where AAC_{3DMN} indicates the area above the curve after the application of the 3D printed MNs, and AAC_{sc} shows the area above the curve after the subcutaneous injection of insulin.

The maximum plasma insulin concentration (C_{max}) and the time point of maximum plasma insulin concentration (T_{max}) were calculated from the curve of the plasma insulin concentration (µIU/ml) over time curve. The relative bioavailability (RBA) was determined using the following equation.

$$RBA\ (\%) = \{(AUC_{3DMN}) \times (Dose_{sc})\} / \{(AUC_{sc}) \times (Dose_{3DMN})\} \times 100$$

Where AUC_{3DMN} indicates the area under the curve after the application of the 3D printed MNs, and AUC_{sc} shows the area under the curve after the subcutaneous injection of insulin.

Furthermore, the comparison of the plasma glucose level and plasma insulin level for the SC injection group and the 3D printed MNs group were performed by a t-test (SPSS software Inc.), and a 0.05 significance level was adopted.

4.3 Results and Discussion

4.3.1 Manufacture and printability of microneedles

Pyramid, cone and spear MNs were successfully printed using a biocompatible resin Class I, FDA approved and a commercial stereolithography (SLA) printer, whose laser beam solidifies the resin in a layer by layer manner, originating then the 3D structure. The Dental SG resin applied in this work is one of the few biocompatible resins that are commercially available and compatible with SLA printers and the only Class I compatible with the Form 2 system, which reduces the risks of possible side effects caused by the MNs` material.

4.3.2 Scanning electron microscopy (SEM) of the printed MNs

From the SEM results (Figure 4.1), it is possible to see that the printer allowed the fabrication of the MNs with excellent details. Uniform and reproducible arrays were obtained for all pyramid, cone and spear microneedles designs. SEM analysis

shows sharp needle tips, revealing the high-resolution capability of the printer and a consistent and reproducible formation of the build layers on all MNs.

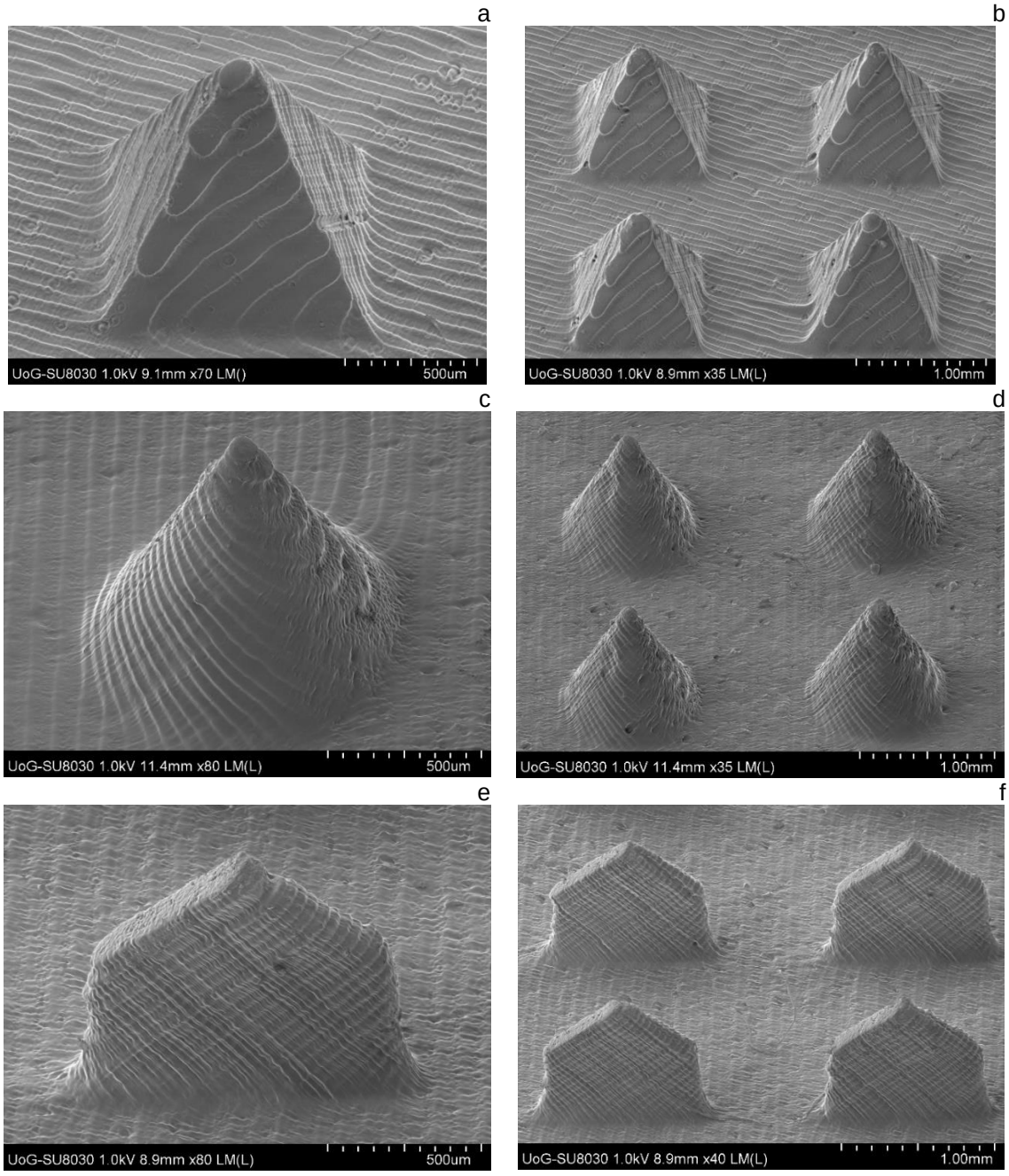

Figure 4.1. SEM images of coated 3D printed microneedles (a) and (b) pyramids, (c) and (d) Cones and (e) and (f) Spears.

4.3.3 Penetration of the MN in the porcine skin

Once the material and the geometry of the microneedles affects the force required to pierce the skin (Davis *et al.* 2004), penetration studies using porcine skin were conducted. Similar tests are previously reported in the literature for metallic

and polymeric MNs (Donnelly *et al.* 2012; Pere *et al.* 2018; McCrudden, Alkilani, Cian M. McCrudden, *et al.* 2014).

In this study, all microneedles successfully pierced the skin with no damage or failure. Furthermore, the force against displacement data was measured throughout the penetration test (Figure 4.2).

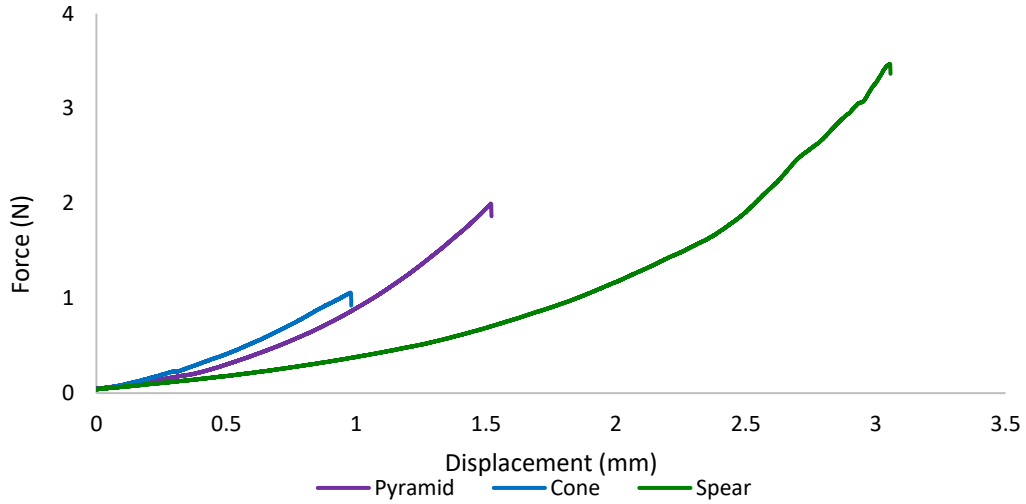

Figure 4.2. Force vs displacement curves for MN penetration in the porcine skin. Maximum forces in Newton (N) for the MN penetration in the porcine skin: pyramid (2.288N ± 0.23), cone (1.028N ± 0.04) and spear (3.360N ±0.03) (n=6).

It is possible to see that all microneedles designs presented a linear behaviour at the beginning (displacement < 3.5 mm), however, as the MN continues to penetrate the skin, a non-linear connection between the developed forces and the penetration depth is revealed. As proposed by Gittard et al. (2013), this behaviour indicates that the process of MN penetration in the skin is not a mere single event; instead it should be viewed as a series of sequential penetrations.

As the load increases, the MNs penetrates deeper through the skin until a threshold force is reached and the insertion becomes abrupt. At this point, a steep drop of the force is observed, indicating that the MN insertion was successful. Therefore, the graph shows that cone MN designs require the least force to successfully penetrate the skin, followed by the pyramid and spear designs.

Overall, the SLA technique has been proved to be an attractive process for fabrication of identical and reproducible biocompatible MNs with high-resolution characteristics. Furthermore, it offers the advantage of the low cost of the printing

material and fast production than other techniques of MNs fabrication (Larraneta *et al.* 2016; Park, Allen and Prausnitz 2005).

Although all the designed MNs presented excellent results and promising applications, the pyramid MN design was selected to be used for transdermal delivery of insulin for the animal studies. Its selection was based on the relatively small force required to pierce and skin and due to the bigger surface area for coating (2.24 mm^2) when compared with the cone ones (1.76 mm^2).

4.3.4 Inkjet printing of insulin formulations onto the microneedles

Inkjet printing is a technology that can be employed for 2D and 3D printing purposes (Economidou, Lamprou and Douroumis 2018; Boehm *et al.* 2014; Singh *et al.* 2010). It this research, it was used to apply the selected formulations onto the 3D printed MNs once the same technique was successfully used before for coating MNs (Ross *et al.* 2015; Uddin *et al.* 2015; Boehm *et al.* 2015; Haj-Ahmad *et al.* 2015).

The dispenser's tip was kept close to the microneedle surface to avoid losses of the coating material. Upon voltage appliance, the solution was jetted in the form of fine droplets (300 pl) onto the MN surface (Figure 4.3). Due to the flexibility of the system, the amount of insulin required for specific tests could be easily adjusted in a few clicks by changing the number of dots and cycles required.

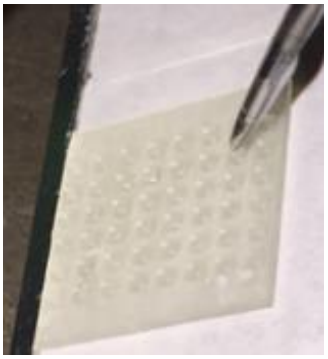

Figure 4.3. Inkjet coating process of the 3D printed microneedles.

The evaluation of the characteristics of the coatings as well as the quality of the coating process was accessed by scanning electron microscopy (SEM) and X-ray computer micro tomography (μCT) as described below.

4.3.5 Scanning electron microscopy (SEM) of the coated MNs

Initially, the coatings of the MNs were analysed for all three MNs` designs (Figure 4.4). It is possible to see that uniform layers were deposited onto the MN`s surfaces with high precision and reproducibility. No loss of material in the form of satellite droplets on the substrate nor the creation of bulky coatings that are observed in conventional techniques such as dip coating could be seen (Haj-Ahmad *et al.* 2015). Moreover, the smooth morphology of the films provided by the technique is more likely to prevent losses of the drug during MN insertion, which can occur when bulky coatings remain on the skin surface.

The MN arrays were also measured as having an average and standard deviation base, needle height and interspacing between the needles` tips of 1.06±0.003 mm^2, 1.03±0.03 mm^2 and 1.84±0.04 mm^2 respectively, which are very close to the designed dimensions.

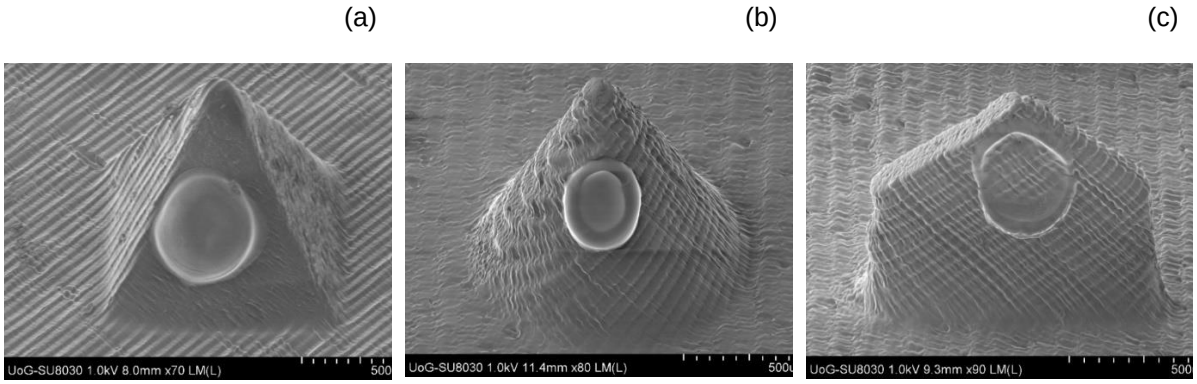

Figure 4.4. SEM images of coated 3D printed microneedles (a) pyramid, (b) Cone and (c) Spear.

4.3.6 X-ray computed microtomography (µ-CT)

The coated microneedles and the performance of the coatings during piercing were also investigated by µ-CT.

A total of 962 µCT images were taken in 0.2º steps around one hemisphere of the sample with an average of 4 frames taken at each rotation step. The images generated were 2664 x 4000 pixels with a resolution of 6.75 µm per pixel, which were reconstructed by Bruker's *CTvol* software.

Figure 4.5 (a) shows an overview of the inkjet coatings onto a printed pyramid microneedle. A coffee ring effect in the density of the coating material deposition

was noticed for all coated samples and a fringe layer of 10-15µm was more pronounced for insulin: xylitol coatings (b). Furthermore, the relative density of all coated microneedles showed to be 200 HU higher than the uncoated microneedles.

(a) (b)

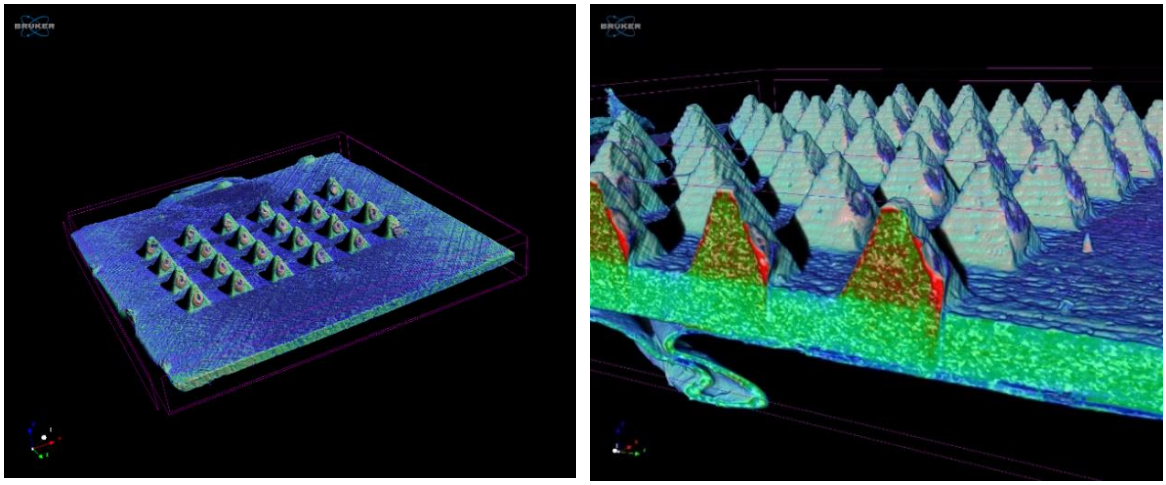

Figure 4.5. µ-CT scan of the coated pyramid microneedles (a) superior overview and (b) cross-section overview.

Scans were taken from the side and the back of the coated MNs (Figure 4.6) presented thin coated layers for all insulin-sugar formulations being in accordance with previous SEM data.

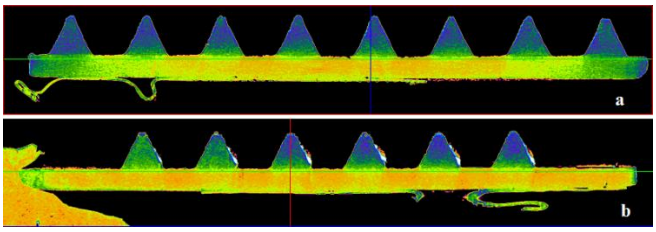

Figure 4.6. µ-CT images of (a) the back and (b) the side of the pyramid microneedle arrays.

The performance of the coatings during the piercing was accessed through a penetration experiment where a 5 N force was applied on the base of the coated MNs against 8-ply strips of parafilm. The cross-section of the pierced strips (Figure 4.7) demonstrates that the films stay on the MNs surfaces during the piercing. Furthermore, the averaged depth measured for all pyramid MNs was 650mm which means that almost 2/3 of the MNs successfully penetrate the skin.

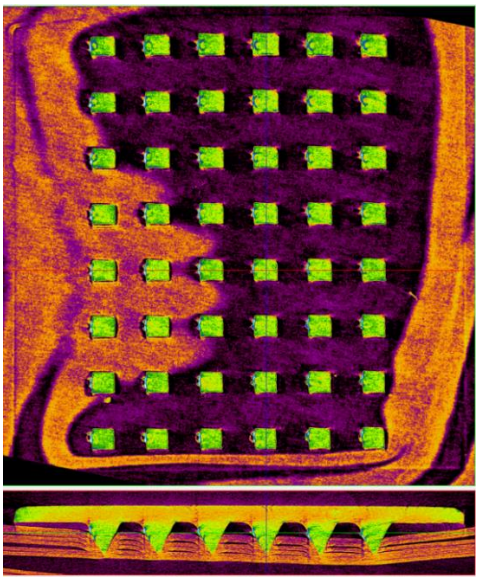

Figure 4.7. µ-CT image of a cross-section of MN array penetration through an 8-ply strip of parafilm.

Overall, inkjet printing demonstrated to be a powerful technique for precise and reproducible coating method for 3D printed MNs. Furthermore, the coatings provided by this technique demonstrated to be very thin and stay on the MN surface during piercing with no loss during the process.

4.3.7 Quantitative analysis of the amount of insulin coated on the MNs

The amount of insulin coated on the MNs (10 IU) was quantified by HPLC and the analytical concentration was calculated using the calibration curve (Table 4.2).

Table 4.2. Coating efficiency of insulin-sugar formulations using inkjet printing method.

Sample	Theoretical concentration (µg/array)	Analytical concentration (µg/array)	Coating Efficiency (%)
Ins:Trehalose	350.00	345.20 ± 4.14	98.63 ± 1.18
Ins:Xylitol	350.00	342.53 ± 4.56	97.89 ± 1.30
Ins:Mannitol	350.00	352.34 ± 4.82	100.67 ± 1.37

From the results, it is possible to see that inkjet printing is a reliable method for coating microneedles with specific doses.

4.3.8 Characterisation of insulin-sugar formulations

4.3.8.1 Circular Dichroism

Circular dichroism (CD) spectroscopy can be used to study the secondary structure conformation of a molecule in a sample, giving important information about protein denaturation and protein-ligand interactions (Kelly, Jess and Price 2005). Accordingly, in this research, CD was used to investigate the effect of different sugars on the insulin structure as well as its stability.

The spectrum of pure insulin (Figure 4.8) at 1.0 mg/mL in PBS 7.4 shows two minima peaks around 210 and 222 nm associated with α-helix and β–sheet, respectively, which are in accordance with previous studies (Ettinger and Timasheff 1971; Sarmento *et al.* 2007; Andrade *et al.* 2015).

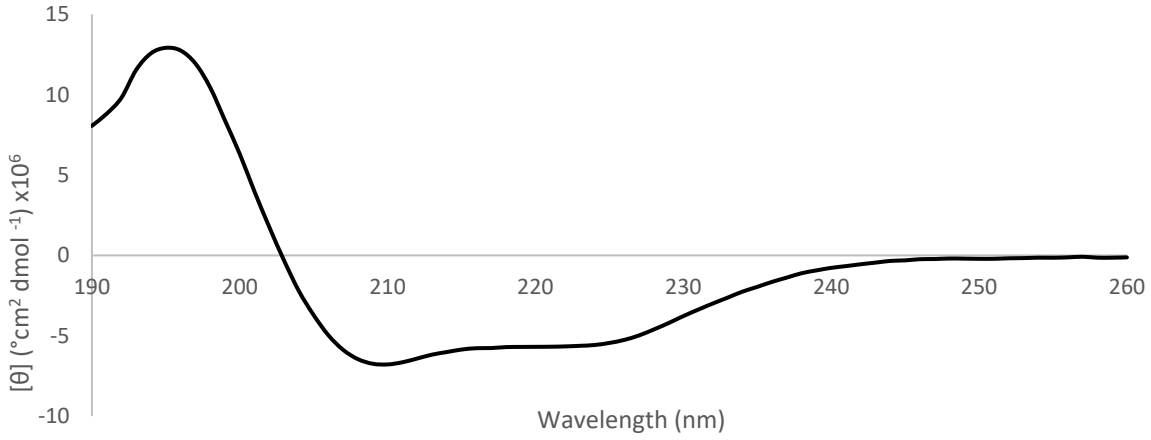

Figure 4.8. CD spectrum of insulin solution at 1.0 mg/mL in PBS 7.4.

Insulin and insulin-sugar solutions were analysed to understand the conformational behaviour of insulin in those systems, especially in the presence of sugars. The spectra of insulin, insulin-xylitol (Ins:Xy), insulin-trehalose (Ins:Treh) and insulin-mannitol (Ins:Man) in solution (Figure 4.9) were found to be quite similar showing two negative minima around 210 and 222 nm which is a typical predominant feature of α-helix structures as already reported in the literature (Wu and Yang 1981; Ettinger, Timasheff and Strycharz 1971; Correia *et al.* 2012). Moreover, the estimation of insulin content by CDSSTR is quantitatively summarised in Table 4.3.

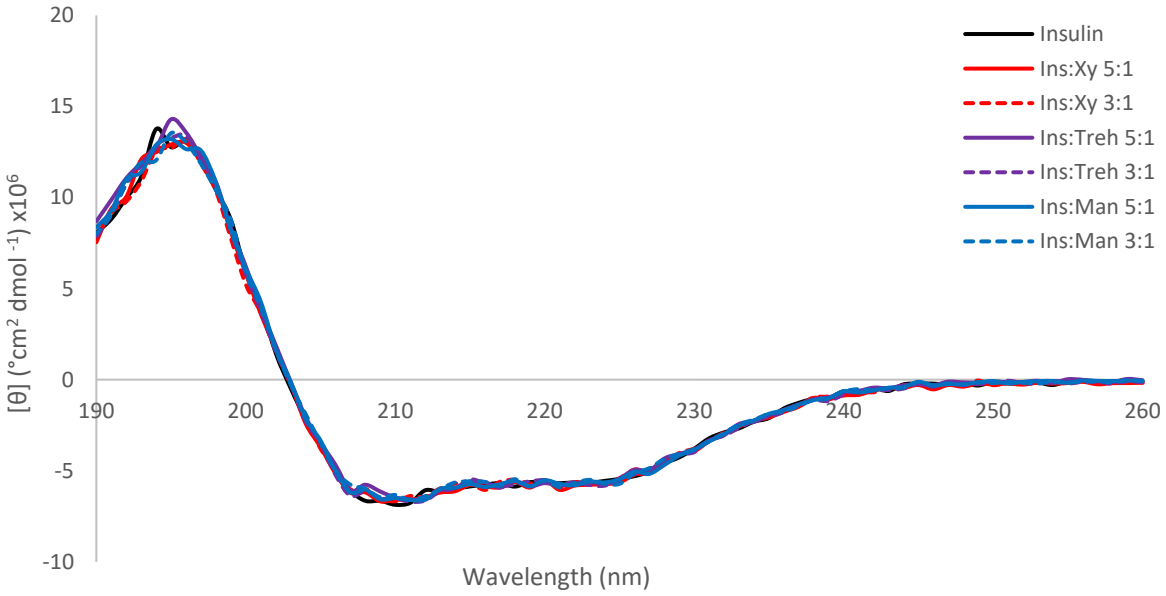

Figure 4.9. CD spectra of insulin and insulin-sugar formulations in solution at different ratios (w/w) at 1.0 mg/mL in PBS 7.4.

Table 4.3. Percentage of secondary structure estimation of insulin and insulin formulations in solution at different ratios (w/w).

	Insulin (%)	Ins:Xy (%)		Ins:Man (%)		Ins:Treh (%)	
		5:1	3:1	5:1	3:1	5:1	3:1
α-helix	51	50	49	49	49	49	49
β-sheet	11	10	11	13	10	12	11
Turn	9	10	11	13	11	11	12
Random coil	30	29	30	25	28	27	28

The CD spectra and the estimation of the secondary structure of insulin suggest that the sugars, in solution, do not alter the secondary structure of insulin which showed to be very similar to the pure insulin solution. It is likely that xylitol, trehalose and mannitol in solution possess a similar effect on the hydrogen bond network of water for all concentrations analysed in this work. Similar results were also found for different concentrations of trehalose, sucrose and maltose solutions below 30% (Lerbret *et al.* 2005).

It is well known that in aqueous solution proteins are preferentially hydrated, which helps to maintain their three-dimensional structure. In the presence of sugars, such as trehalose, the water network is disrupted, and strong hydrogen-bonds are created between trehalose and water (Branca *et al.* 2005; Lerbret *et al.* 2005; Ohtake, Kita and Arakawa 2011). Therefore, it is suggested that sugars do not interact directly with proteins; instead, they may interact with water and form a

hydrated shell around proteins protecting them (Jain and Roy 2009; Castro *et al.* 2015).

Figure 4.10 shows the CD spectra of insulin solution in comparison with the respective films of insulin solution and insulin-sugar formulations at 1.0mg/mL. All the samples display similar CD spectra showing two minima peaks around 210 and 222 nm, which are associated with α-helix and β-sheet content.

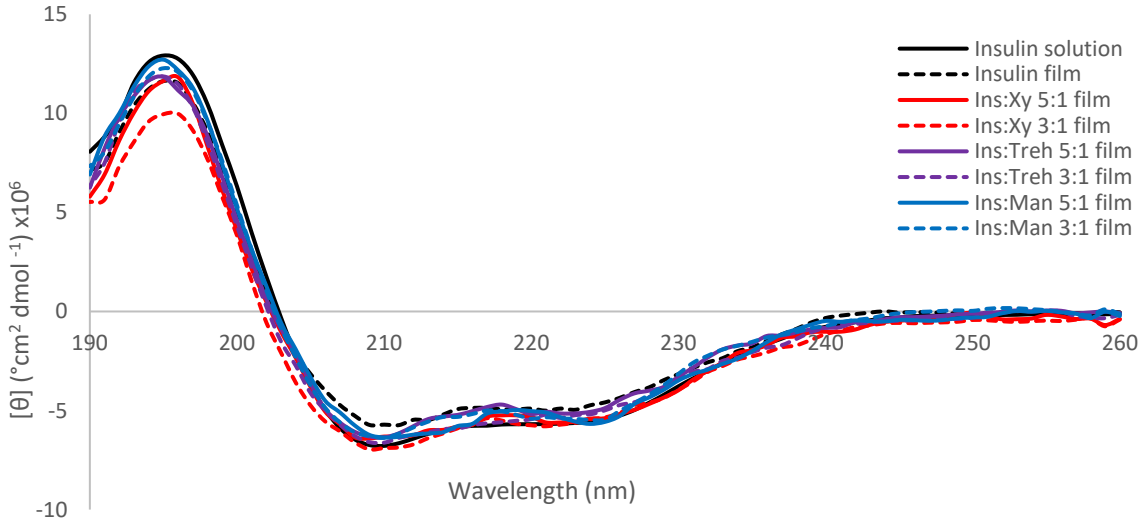

Figure 4.10. CD spectra of insulin solution, insulin film and insulin-sugar films at different ratios (w/w) at 1.0 mg/mL in PBS 7.4.

The pure insulin film showed a notable reduction in the Molar ellipticity (Figure 4.10) accompanied by changes in the spectra. It was noted that the dehydration led to a decrease in α-helix content of insulin whereas the β-sheet and turn structures were raised (Table 4.4). Analogous results were found by Zeng et al. (2011) upon insulin dehydration where relative humidity (RH) was decreased from 92% to 2%.

Table 4.4. Percentage of secondary structure estimation of insulin solution, insulin film and insulin-sugar films.

	Insulin solution	Insulin film (%)	Ins:Xy film (%)		Ins:Treh film (%)		Ins:Man film (%)	
			5:1	3:1	5:1	3:1	5:1	3:1
α-helix	51	47	52	54	48	49	48	49
β-sheet	11	15	20	12	14	8	16	13
Turn	9	15	9	12	14	9	11	11
Random coil	30	22	18	21	24	34	24	26

The depletion of the α-helix content of insulin was also reported by Andrade et al. (2015) after lyophilisation. Even though air-drying was used in this study with the advantage of avoiding the potential damaging stress of freezing, it is possible that some insulin molecules may undergo aggregation and irreversible unfolding when dried alone.

Overall, it is well known that the protective mechanism of sugars in a solution state is very different from a dried state, once the surrounded water is partially or completely removed during dehydration (Cicerone, Pikal and Qian 2016; Carpenter and Crowe 1989). Accordingly, the water replacement mechanism is the most accepted theory that tries to explain the mechanism behind the ability of sugars to protect biomolecules in a dried state (Carpenter and Crowe 1989; Haque *et al.* 2015). Therefore, it is suggested that during the dehydration process, sugars may substitute water molecules around the biomolecules of proteins, maintaining its three-dimensional structure by providing sites with hydrogen-bonding species (Carpenter and Crowe 1989; Branca *et al.* 2005; Jain and Roy 2009).

Considering that, it is also possible to see that all insulin-sugar films (Figure 4.10 and Table 4.4

Table 4.4) tend to better maintain the α-helix structure of insulin in the dried system when compared to the dried insulin alone. Interestingly though, xylitol presented the most effective protective properties of all sugars, leading to even higher amounts of α-helix content than the native insulin itself. However, the reason for that remains unclear and further studies are needed.

4.3.8.2 Raman Results

In this study, the spectrum of the native of insulin (Figure 4.11) shows a strong peak of amide I band at 1661 cm^{-1} and a shoulder near 1682 cm^{-1} assigning the α-helix structure and the random coil form, respectively. Amide III bands are noted at 1241 cm^{-1} and 1274 cm^{-1}, being in accordance with Yu et al. (1972).

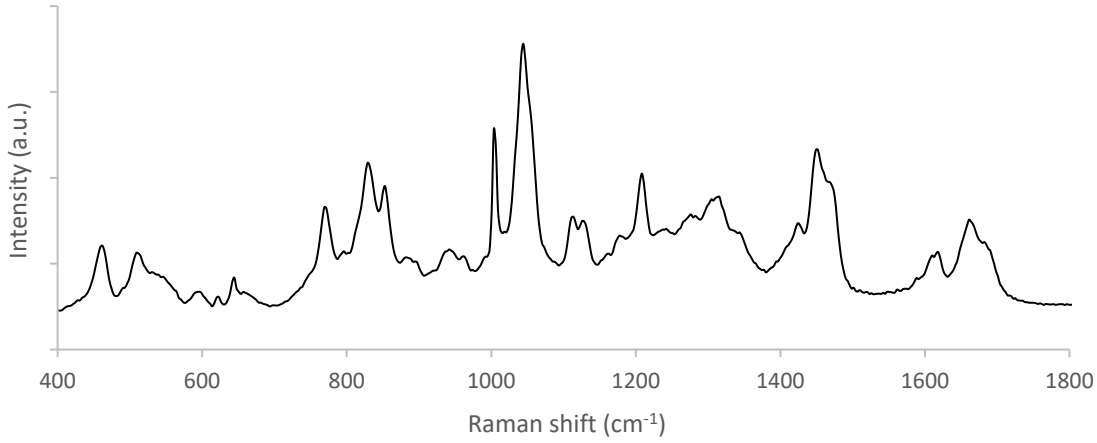

Figure 4.11. Raman spectrum of pure insulin film.

All insulin formulations showed similar Raman spectra (Figure 4.12) to the native insulin, and distinctive peaks of sugars were not found in Raman spectra mainly due to the fact that insulin was more concentrated than the sugars in the films. Furthermore, the amorphous nature of the films (see XRD data) does not afford a strong Raman signal.

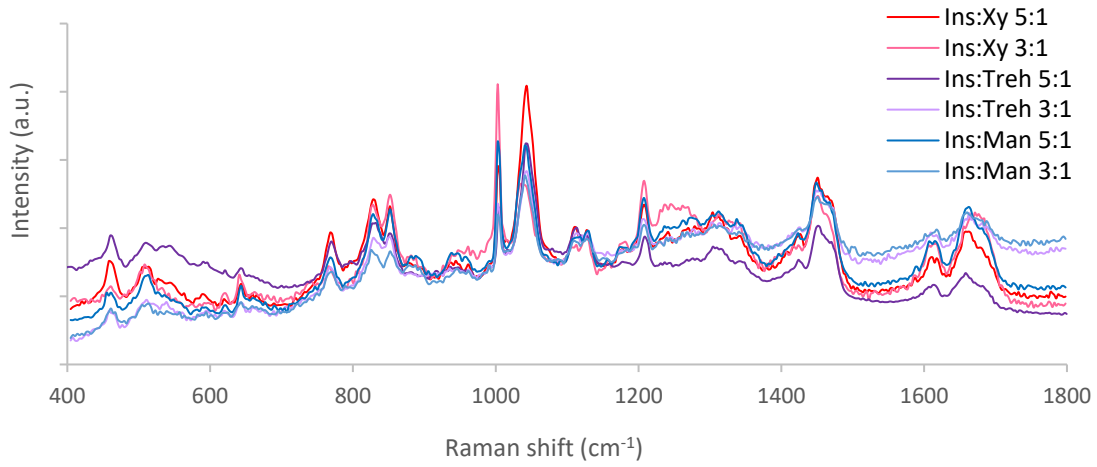

Figure 4.12. Raman spectra of insulin and insulin-sugar formulations.

The spectra show amide I band of insulin-xylitol and Insulin-mannitol 5:1 ratio (w/w) with peaks at about 1662 cm^{-1} whereas insulin-trehalose 5:1 ratio was shifted to 1658 cm^{-1}. Diversely, when the sugar concentration was increased to 3:1 ratio, the amide I band position of insulin-trehalose and insulin-xylitol was shifted to 1663 cm^{-1} and 1665 cm^{-1}, respectively, while insulin-mannitol was shifted to 1660 cm^{-1}. Those changes were also reported by Carpenter and Crowe (1989) and Souillac (2002) and might be due to both the concentration and the different effect of each

sugar on the vibrational spectra of insulin regarding the hydrogen bonding and couplings between the adjacent peptide units.

Amide III is also an important feature for analysing the secondary structure of proteins. From the spectra, it is possible to see that the amide III bands are wider and unresolved compared to the pure insulin spectrum, especially for insulin:xylitol 3:1 sample. Similar results were reported by Zeng et al. (2011) where they have demonstrated that amide III and I bands tend to be unresolved and broadened as the dehydration increases.

The disulphide bonds are very sensitive to conformational changes and so it plays an important role in determining and establishing the folded structure of insulin (Zeng *et al.* 2011). From the spectra, it can be seen that for insulin and insulin formulations, the S-S stretching vibration bands are located close to 510 cm^{-1} suggesting that all disulphide bonds are in the most stable conformation of gauche gauche-gauche with its hydrophobic surfaces buried in its three-dimensional structures as a result of a great water removal.

Raman bands of Tyrosine (Tyr) residues are very sensitive to the environmental changes in proteins, especially in the dehydration process. The Raman spectra show Tyr peaks at about 642, 828, 852, 1174 and 1206 cm^{-1}, with the last being related to both Tyr and Phenylalanine residues. Tyr doublet located at ~830 and ~850 cm^{-1} is the strongest and the most important band of Tyr features for the protein structure determination. Furthermore, the relative intensity ratios of Tyr residues of I_{850}/I_{830} and I_{1174}/I_{206} are sensitive to the environment and the property of the hydrogen bonding (Zeng *et al.* 2011).

In the research, the Tyr doublet appeared at about 828 and 852 $cm^{-1,}$ and the intensity ratios of I_{852}/I_{828} and I_{1174}/I_{1206} obtained varied from 0.91 to 1.05 and 0.73 to 0.90 respectively (Table 4.5). From the table, it is possible to see that the I_{852}/I_{828} values indicate that tyrosine residues tend to be more exposed and establish more hydrogen bonds in the presence of sugars as the intensity ratio increases. Furthermore, most of the films showed an increase in the I_{1174}/I_{1206} ratios indicating further retention of the molecules of water in the films. Interesting though, insulin-xylitol 3:1 showed the lowest I_{1174}/I_{1206} values, suggesting even greater dehydration than pure the insulin film, along with a stronger hydrogen-bonding interaction.

Table 4.5. Relative intensity of Tyr residues of insulin and insulin-polymer films at different ratios (w/w).

	Insulin	Ins:Xy 5:1	Ins:Xy 3:1	Ins:Treh 5:1	Ins:Treh 3:1	Ins:Man 5:1	Ins:Man 3:1
I_{852}/I_{828}	0.91	0.97	1.05	0.92	1.00	1.02	1.00
I_{1174}/I_{1206}	0.77	0.79	0.73	0.81	0.90	0.79	0.89

Overall, the presence of the sugars in the films tends to reduce the number of water molecules that are lost during dehydration and increase the hydrogen-bonds of Tyr residues. Therefore, these results also agree well with many other studies that have demonstrated the formation of hydrogen-bonds between carbohydrates and many dried proteins, supporting the stabilisation theory by the water replacement mechanism (Carpenter and Crowe 1989; Crowe, Reid and Crowe 1996; Prestrelski *et al.* 1993; Jovanović N, Bouchard A, Hofland GW, Witkamp GJ, Crommelin DJ 2006).

4.3.8.3 X-ray diffraction (XRD)

Insulin-sugar films and the films of the pure components were studied by X-ray analysis. The diffractograms were recorded to understand the nature of the films. From Figure 4.13, it is possible to see that insulin exhibited predominant amorphous state with a small peak at 31.79° whereas the sugars' films are prone to crystallise under the same air-drying conditions.

The diffractogram of xylitol showed distinctive peaks at 13.98°, 19.81°, 22.22°, 24.74°, 31.6°, while trehalose displayed singular peaks at 12.70°, 13.75°, 14.64°, 15.38°, 16.62º, 17.01°, 21.21° and 23.94°, both identified in its dehydrated form. Diferently, the main peaks of mannitol are displayed at 9.78°, 17.36°, 20.51°, 22.22° and 24.79°, which are related to the three polymorphs of mannitol.

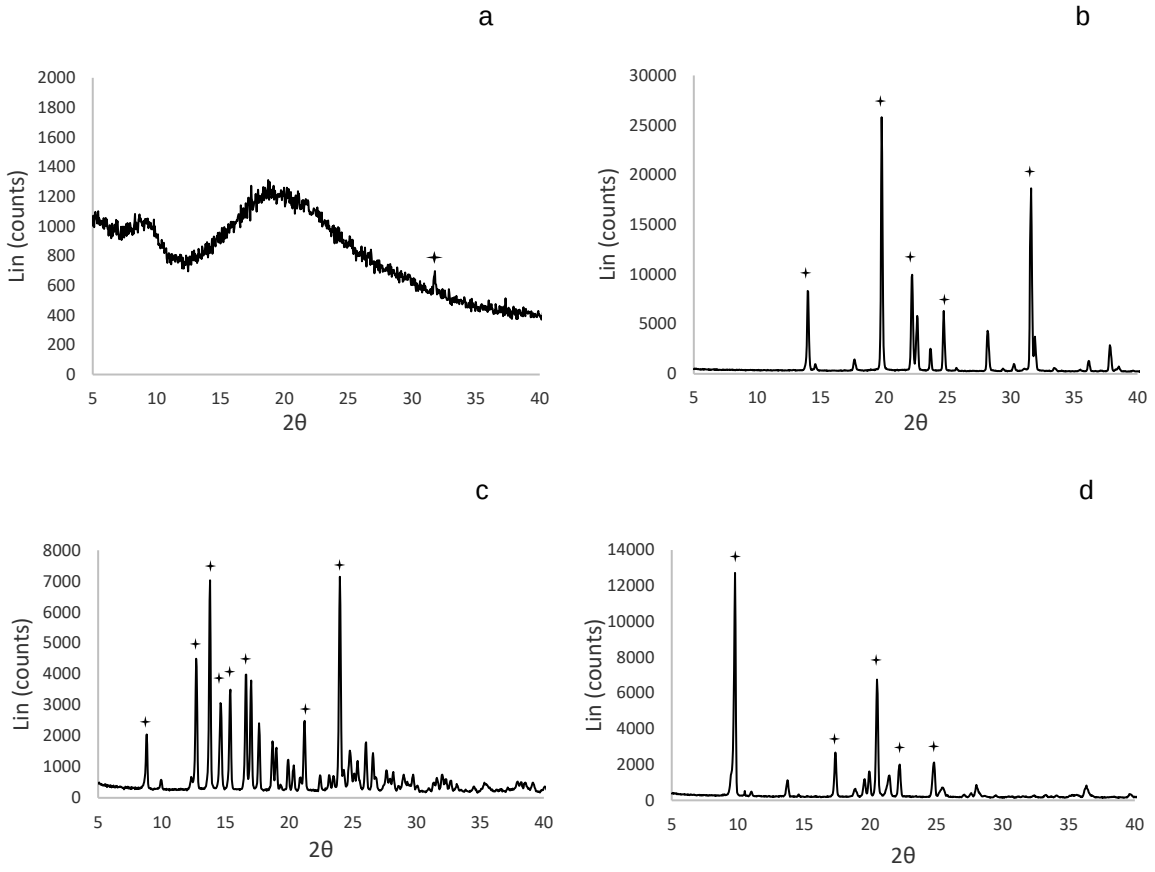

Figure 4.13. Diffractograms of the films of the formulation's components: (a) insulin, (b) xylitol, (c) trehalose and (d) mannitol.

Figure 4.14 shows the diffractograms of insulin-sugar films. Overall, all the films are predominantly amorphous. Ins:Xy did not show any sign of crystallisation. Ins:Man 3:1 displays a peak at 31.71º possible due to insulin contribution while Ins:Treh 5:1 present some crystalline regions with peaks at 9.08°, 29.42° and 31.62°.

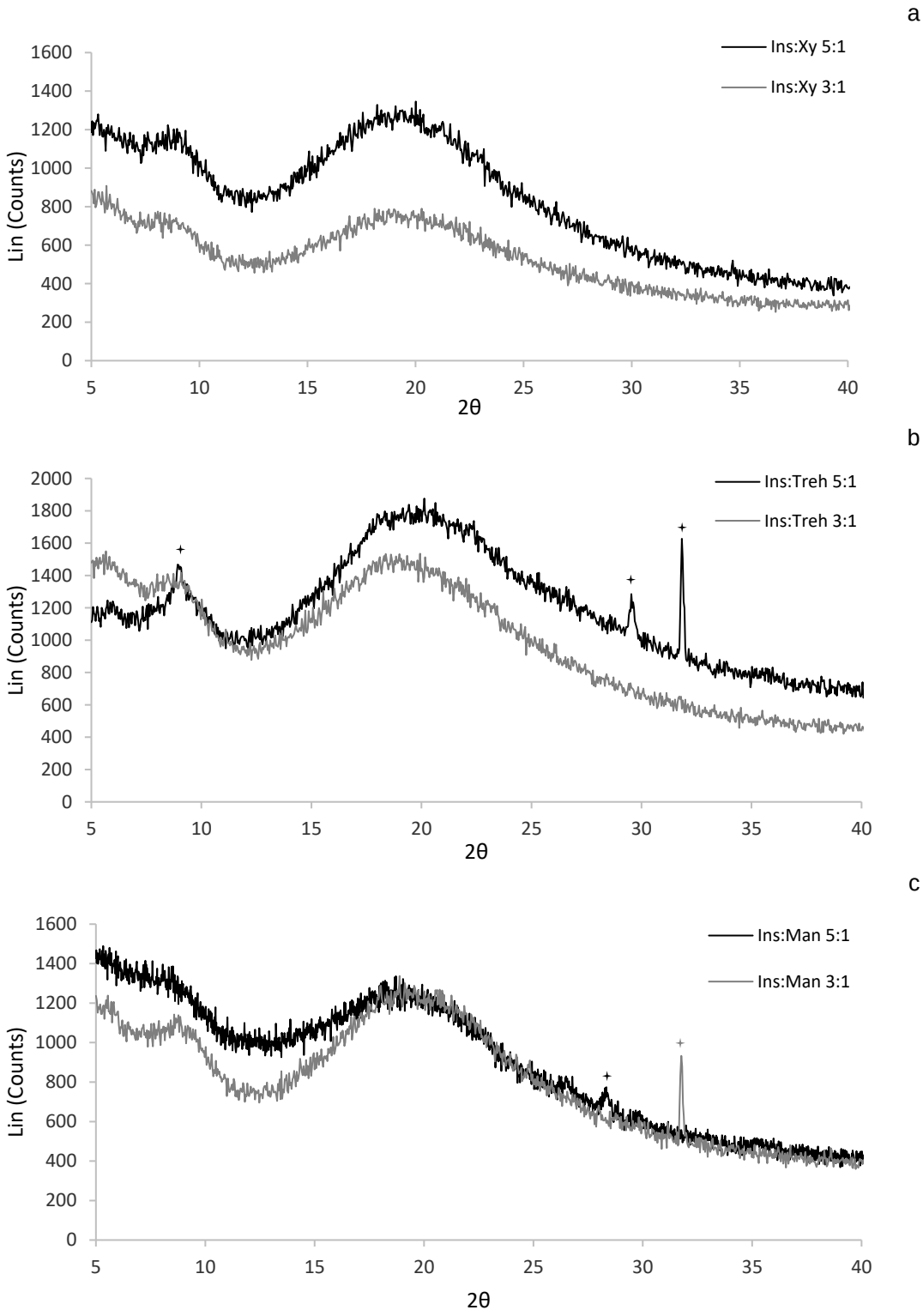

Figure 4.14. Diffractograms of the insulin-polymer films at different ratios (w/w). (a) insulin:xylitol, (b) insulin:trehalose and (c) insulin:mannitol

It is interesting to note that even though the studied sugars show a highly tendency for crystallisation when air-dried alone, in the presence of insulin, xylitol, trehalose and mannitol are prone to form amorphous films. Similar behaviour was

reported in the literature for many different sugars and proteins (Pierre O. Souillac, Middaugh and Rytting 2002; Pierre O Souillac, Middaugh and Rytting 2002; Górska *et al.* 2017).

Izutsu et al. (1994) have studied the stability of different proteins by amorphous and crystallised mannitol. They found that amorphous mannitol preserved L-lactate dehydrogenase and other proteins under freeze-drying conditions while its crystalline form had no protective effect on them (Izutsu, Ken-ichi; Yoshioka, Sumie; Terao 1994). Similar protein protection was also found for amorphous matrixes of trehalose (Imamura *et al.* 2003; Pierre O. Souillac, Middaugh and Rytting 2002; Górska *et al.* 2017). Although xylitol has not been greatly explored for protein stabilisation yet, in this study, amorphous xylitol presented good stabilisation of insulin during drying and even promoted the assembly of its α-helix structure.

The advantage of amorphous systems on the stabilisation of proteins has been reported in several studies. (Faghihi *et al.* 2016; Pierre O. Souillac, Middaugh and Rytting 2002). In fact, the formation of an amorphous matrix during dehydration showed to be crucial for many protein stabilisations such as LDH, Escherichia coli, B-galactosidase and L-asparaginase, rh-DNase (Izutsu, Ken-ichi; Yoshioka, Sumie; Terao 1994; Pierre O Souillac, Middaugh and Rytting 2002).

Overall, the insulin-sugars formulations investigated in this research originated predominantly amorphous films, which is known to be more stable for insulin than the crystalline ones (Pikal, M. J.; Rigsbee 1997).

4.3.9 Insulin stability

The stability of insulin and insulin-sugar films were studied by Circular Dichroism and X-ray diffraction using the same parameters as before. The samples were analysed at time zero (T0) and after thirty days (T30) kept in the fridge at 4^{o}C±1.

Figure 4.15 compares the CD spectrum of insulin at T0 and T30. Both samples showed double minima around 210 and 222 nm at both times, which are

related to α-helix and β–sheet content structures of the native insulin. Furthermore, the estimation of the secondary structure of insulin is summarised in Table 4.6.

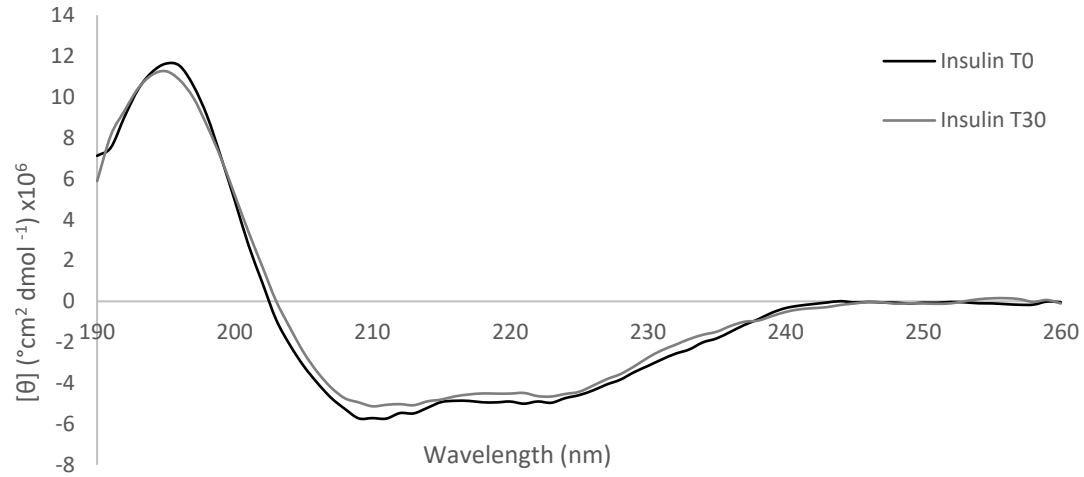

Figure 4.15. CD spectra of insulin film at time zero and after 30 days.

Table 4.6. Percentage of the secondary structure of insulin solution, insulin film and insulin-sugar films at different ratios (w/w) at 1.0mg/mL in PBS 7.4.

	Insulin (%)		Ins:Xy T0 (%)		Ins:Xy T30 (%)		Ins:Treh T0 (%)		Ins:Treh T30 (%)		Ins:Man T0 (%)		Ins:Man T30 (%)	
	T0	T30	5:1	3:1	5:1	3:1	5:1	3:1	5:1	3:1	5:1	3:1	5:1	3:1
α-helix	47	45	52	54	54	52	48	49	49	49	48	49	47	47
β-sheet	15	21	20	12	10	14	14	8	10	9	16	13	22	21
Turn	15	12	9	12	9	9	14	9	12	9	11	11	12	13
Random coil	22	23	18	21	27	25	24	34	29	34	24	26	20	19

From the insulin spectra, it is possible to see a small change in the spectra with a decrease in the Molar ellipticity intensity of insulin during the time, signalling a decrease in alpha-helix content. Exploring further, according to the secondary structure estimation, the data indicate that insulin loses some of its α-helix structure during the time while some β-sheets structures are formed.

Figure 4.16 compares the CD spectra of the insulin-sugar formulations at T0 and T30 with the CD spectrum of insulin at T30 without any sugar protection. Overall, all the samples at both times also showed double minima around 210 and 222 nm, characteristic of helix and β–sheet structures, which agrees with the literature (Sarmento *et al.* 2007). Furthermore, the percentage of insulin content was also estimated by CDSSTR and summarised in Table 4.6.

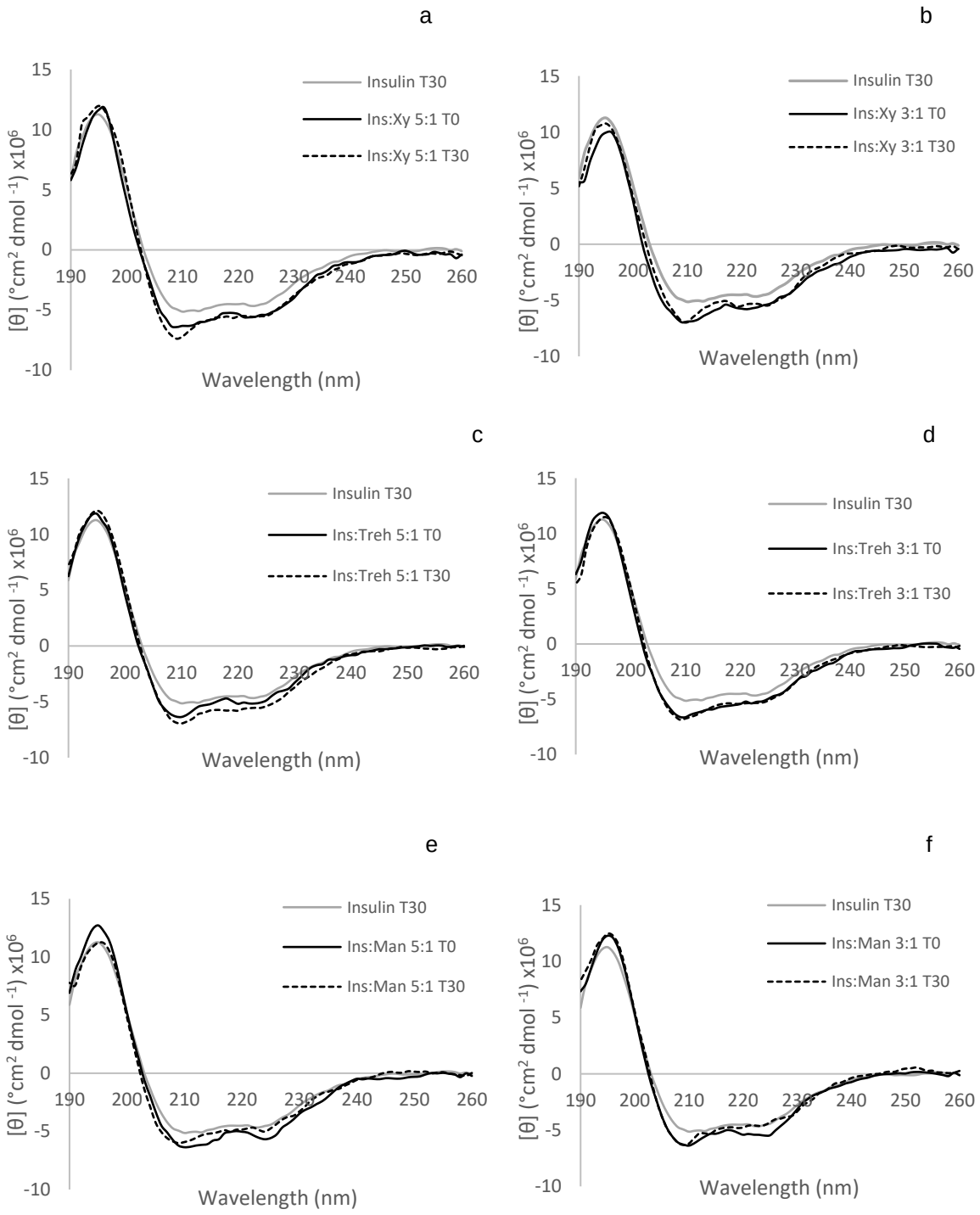

Figure 4.16. CD spectra of insulin and insulin-sugar formulations at 1.0 mg/mL in PBS 7.4 at T0 and T30.

All sugars tested in this study showed a good capability to protect insulin from denaturation during the time kept in the fridge at 4 °C. From the spectra and the estimation of the secondary structure of insulin in the films (Figure 4.16 (a) and (b) and Table 4.6), it is possible to see that Ins:Xy 5:1 ratio had its percentage of α-helix

content increased slightly during the time from 52% to 54% followed by a decrease in β-sheet structures whereas Ins:Xy 3:1 ratio showed the opposite behaviour.

The CD spectra of Ins:Treh films showed almost the same amount of α-helix content at both times, T0 and T30. After thirty days, the 5:1 sample presented a decrease in the β-sheet structures whereas an increase of the random coil forms was noticed for the 3:1 film. Furthermore, Ins:Man films presented a tendency for losing α-helix content and increasing β-sheets structures during the time.

Overall, CD results show that all the studied sugars provided good insulin protection with xylitol showing the best results followed by trehalose and mannitol. However, neither the concentration nor the peculiar role of each sugar on the secondary structure of insulin can be explained based on what it is known until now once the mechanisms involved on sugar-protein protection are not entirely understood as previously discussed.

As mentioned earlier, the stability of the samples was also analysed by X-ray diffraction, and the results and discussion are shown below.

The diffractograms of insulin films at T0 and T30 (Figure 4.17) revealed the predominant amorphous nature of insulin during the time. From it, it is possible to see that insulin T0 shows a small peak at 2θ = 31.79° whose intensity increases and shifts during the time to 31.66° (insulin T30). Furthermore, it is also possible to see the formation of a small peak at 28.33° for the insulin T30, which might indicate the growth of the small crystalline regions of insulin during the time.

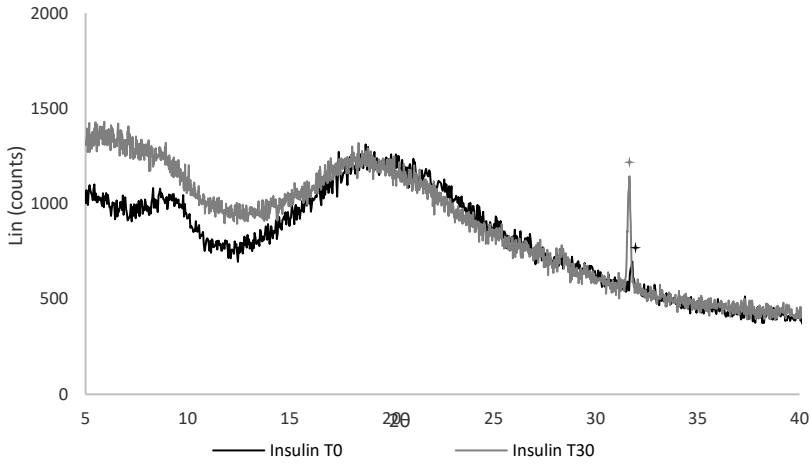

Figure 4.17. Diffractograms of insulin films at T0 and T30.

Figure 4.18 shows the diffractograms of insulin-sugar formulations at T0 and T30. Both ratios of Ins:Xy films showed no crystalline peaks at T0, indicating an amorphous nature of the system. After 30 days, Ins:Xy 5:1 showed a peak at 28.39° while Ins:Xy 3:1 displayed a small peak at 28.33°. Once those peaks are characteristic of insulin, they may indicate crystallisation sites of insulin inside of the amorphous matrix during the time.

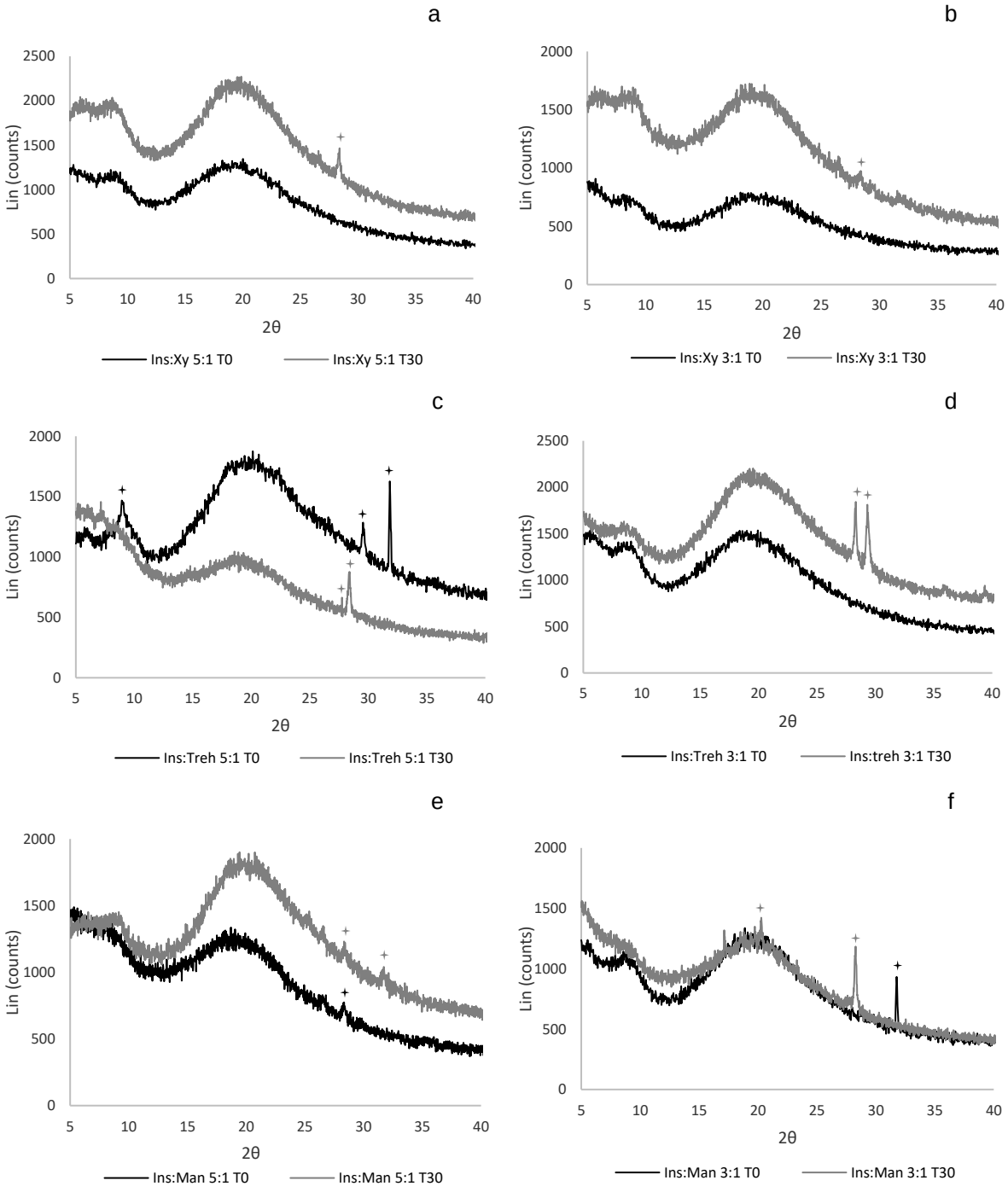

Figure 4.18. Diffractograms of insulin and insulin-sugar films at T0 and T30.

The diffractogram of Ins:Theh 5:1 T0 showed a predominance of amorphous nature with 3 peaks at 8.92°; 29.54° and 31.83°, which resolved into two peaks at 27.75° and 28.39° after thirty days. Likewise, Ins:Treh 3:1 appears to have the same tendency to form crystalline regions on the film matrix during the time. In this sense, Ins:Treh 3:1 changes from a typical amorphous phase with no crystalline peaks at T0 to a predominant amorphous phase with some sites of crystallinity with peaks at 28.31° and 29.30°.

The XRD patterns of Ins:Man films also showed a typical predominance of amorphous phase with formation of some crystalline sites during the time. At 5:1 ratio T0, the Ins:Man diffractogram displays a small peak at 28.33° which increases after 30 days. Additionally, a new small peak is formed at 31.71° for Ins:Man 5:1 T30. In the same way, Ins:Man 3:1 T0 showed a peak at 31.71° while the analysis after thirty days showed the formation of two peaks at 20.26° and 28.27°.

As well pointed by Abdul-fattah et al. (2007), once the thermodynamic equilibrium of the freshly prepared amorphous systems is not reached, there is a tendency for many amorphous solids to either crystallise or at least slowly ‘‘relax,’’ in order to restore the system to equilibrium. In this sense, it is possible that the obtained insulin-sugar films were not in equilibrium at T0 which could explain the changes on the diffractograms during the time. Ultimately, all insulin-sugar formulations presented predominant amorphous matrix even after 30 days which is known to be essential for protein stabilisation as discussed before (Abdul-fattah *et al.* 2007).

From the stability studies, all the insulin-sugar formulations studied provided good insulin protection with xylitol showing the best protective properties followed by trehalose and mannitol. Thereby, once the 5:1 insulin-sugars ratio presented the best stability performance, they were selected as coating formulations for the 3D printed microneedles and further studies were done.

4.3.10 Insulin permeation studies

The *in vitro* permeation profile of insulin from the three different formulations (Ins:Xy, Ins:Treh and Ins:Man at 5:1 ratio) and the three different MNs designs (pyramid, cone and spear) were studied using porcine skin and Franz diffusion cells.

The 3D-printed MNs were coated with 10 IU of insulin and the collected sample fractions quantified by HPLC method.

Figure 4.19 shows the cumulative permeation profile of insulin from the coated MNs (n=6). From the graphs, it is possible to see that pyramid MNs (a) showed insulin permeation variation rates from 63 to 69% in the first two minutes while cone (b) and spear (c) designs showed variations about 57 to 64% and 62 to 70%, respectively. Despite of that, approximately 85 to 95% of insulin permeated from all coated MNs in 30 min and no statistical difference was noted among the carriers nor the MNs (ANOVA, $p>0.05$).

The used carriers not only preserved insulin in its native form but also provided fast permeation rates which is attributed to the hydrophilic nature of the sugars as well as the thin coating layers onto the MNs (10-15µm) as shown from the µ-CT analysis.

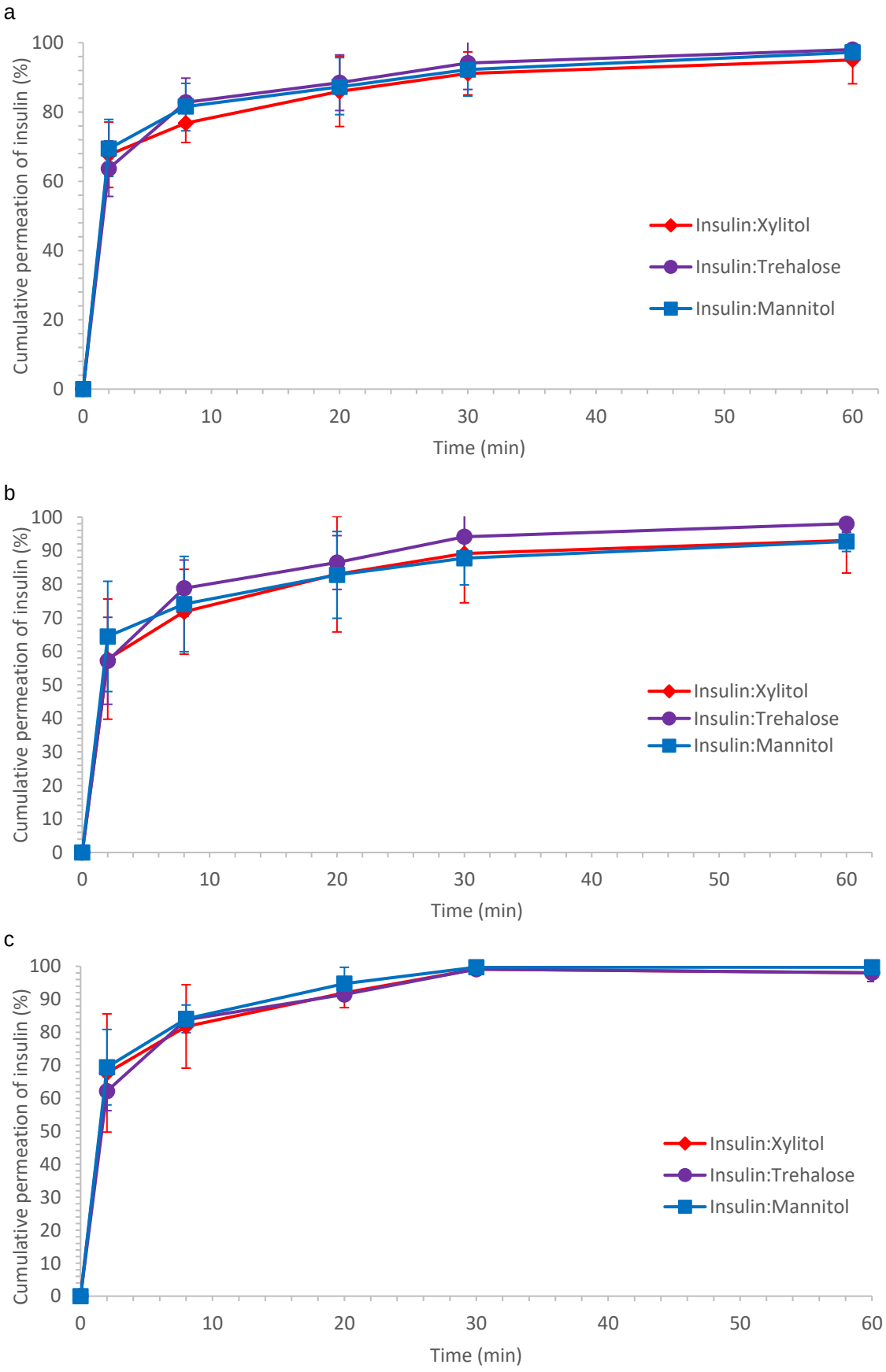

Figure 4.19. *In vitro* permeation profile of insulin from 3D printed MNs designs (a) pyramid MNs, (b) cone MNs and (c) spear MNs (n=6).

4.3.11 Insulin transdermal delivery in diabetic mice

After 7 days from streptozotocin administration, the animals presented hyperglycaemia levels of 340 ± 10 mg/dl, confirming a successful diabetes induction.

The 3D printed microneedles coated with 0.2 IU of insulin (1.206 μmolar) were applied on the shaved skin of the mice and additionally secured with adhesive tape. To compare the delivery efficiency of the microneedles, 3D printed MNs coated with 0.2 IU of insulin per array were applied on the back of the animals whereas 0.2 IU of insulin was subcutaneously injected into mice as positive control. Untreated mice were used as the negative control. Figure 4.20 shows the application process of the 3D printed MN arrays on the animals.

Figure 4.20. Experimental mice during application of the 3D printed MN array for insulin delivery.

To avoid hypoglycemia in mice for 4h, a 0.2 IU dose was selected and the comparative plasma glucose levels and insulin concentration vs time for the three different delivery strategies are shown as follows.

As expected, a quick reduction in plasma glucose level within one hour can be seen after insulin subcutaneous injection (Figure 4.21 and Table 4.7). Interesting though, 3D printed MNs arrays loaded with insulin also showed a similar initial profile, presenting a maximum decrease in glucose levels after one hour of being administered. The minimum glucose level (C_{min}) for both treatments was about 30% of its initial level, and they did not show any statistical difference. This rapid decrease in glucose level for the experimental group indicates the high efficiency of the 3D printed MNs coated with insulin which is consistent with the *in vitro* transdermal profile previously discussed.

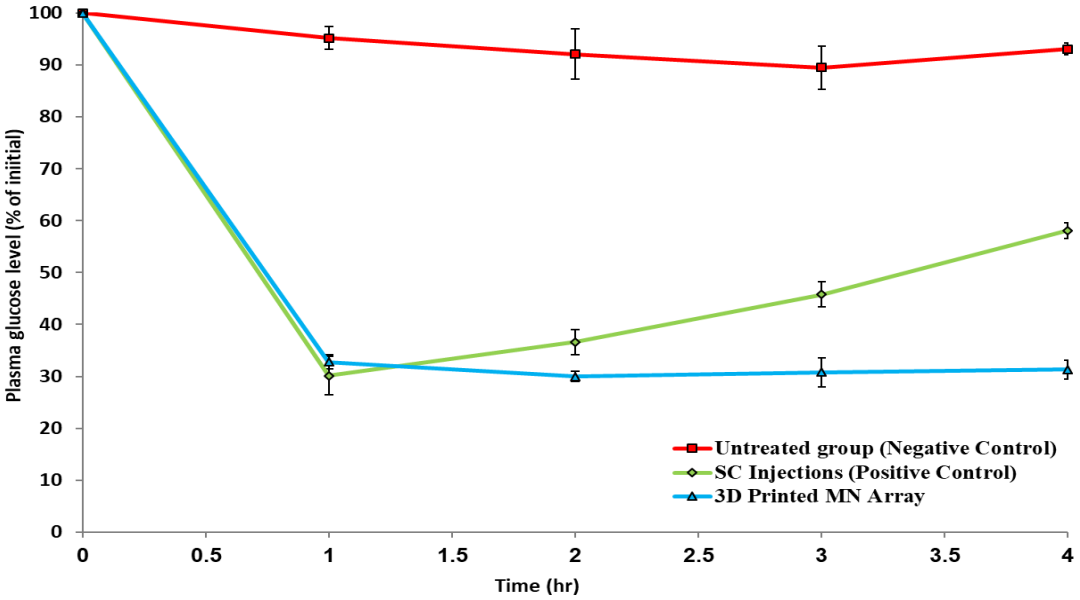

Figure 4.21. Comparative plasma glucose level for untreated group, subcutaneous (SC) injection and 3D printed MNs coated with insulin in international units (IU) (n=3).

Table 4.7.Pharmacodynamic parameters for plasma glucose levels of diabetic mice for untreated groups, subcutaneous (SC) injection (insulin dose: 0.2 IU) and 3D Printed MN array (insulin dose: 0.2 IU) (n=3).

Group	$C_{min\ (\%)}$	$T_{min\ (h)}$	AAC_{0-4}(%h)	RPA(%)
No treatment	89.5	3	26.65	0
Insulin SC	32.8	1	208.45	100
Insulin loaded 3D printed MNs	30.1	1	240.75	122

C_{min}, minimum glucose level; T_{min}, time point of minimum glucose level; $AAC_{0\ to\ 4}$, area above the plasma glucose concentration vs. time curve; RPA, relative pharmacological availability compared to subcutaneous injection.

Previous studies with MNs also have attained similar blood glucose level profiles in the first hour (Ito *et al.* 2006; Qiu *et al.* 2012; Yu, Jiang, Liu, *et al.* 2017). In this study though, after a C_{min} had been reached, a steady state plasma glucose level continued to be maintained at a low level for 3 h after administration of the 3D printed MNs. These findings suggest that insulin is being released from the MNs to the mice bloodstream via passive diffusion. Furthermore, the blood glucose level for the untreated group is kept stable and maintained around 340±10 mg/dL. No hypoglycemia effect were observed for any group for the same period.

Figure 4.22 and Table 5.8 show the pharmacokinetic parameters of the plasma insulin levels for the three groups. As shown, the peak value of insulin

concentration for SC injection is reached in a short period of time (1h). A similar initial profile was also noticed for the 3D printed coated MNs group with the same amount of insulin. Even though the C_{max} of the SC injection group presented to be slightly higher than the 3D printed MNs group, statistical analysis did not show any difference between the groups at time 1h. The control group did not show any detectable insulin in the plasma.

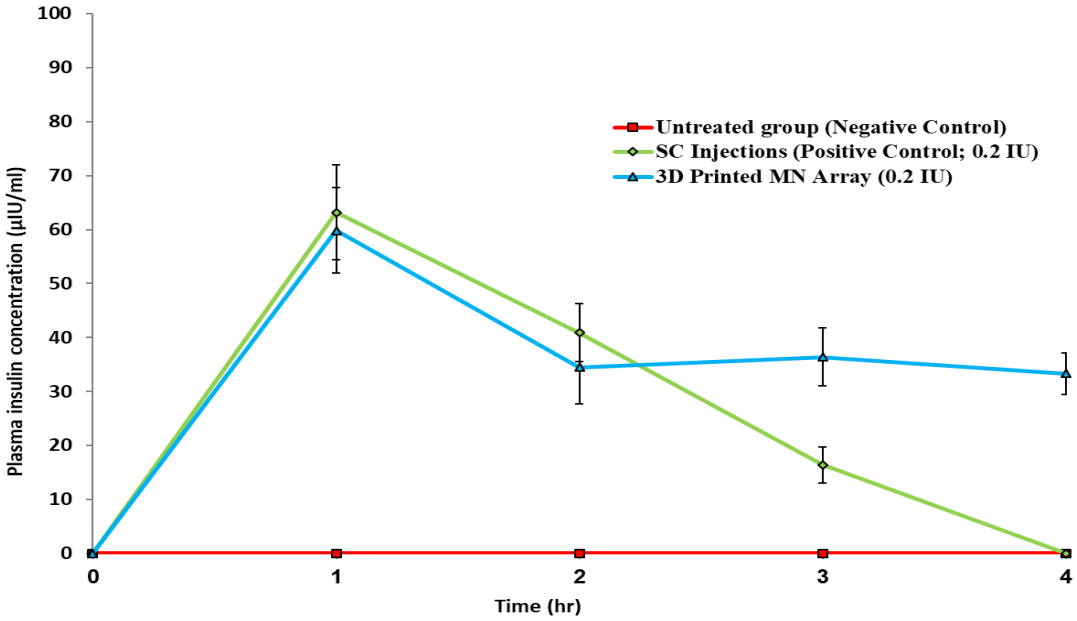

Figure 4.22. Comparative plasma insulin concentration for untreated group, subcutaneous (SC) injection and 3D printed MNs coated with insulin in international units (IU) (n=3).

Table 4.8. Pharmacokinetic parameters for plasma insulin concentrations of diabetic mice for untreated groups, subcutaneous (SC) insulin injection (0.2 IU) and 3D Printed MN array coated with insulin (0.2 IU) (n=3).

Group	$C_{máx}$ ($\mu IU.mL^{-1}$)	$T_{máx}$ (h)	AUC_{0-4} ($\mu IU.mL^{-1}.h$)	RBA(%)
No treatment	0	0	0	0
Insulin SC	63.2	1	120.5	100
Insulin loaded 3D printed MNs	59.9	1	147.41	115

C_{max}, maximum plasma insulin concentration; T_{max}, time point of maximum plasma insulin concentration; $AUC_{0\ to\ 4}$, area under the plasma insulin concentration vs. time curve; RBA, relative bioavailability compared with subcutaneous injection.

Comparatively, Zhang and co-workers (2018) studied the pharmacokinetic parameters of SC injection of insulin (10 IU) and 3 different insulin concentrations using a dissolvable alginate/maltose composite MNs (5, 10 and 20 IU). They found that all loaded biodegradable MNs were quickly dissolved after administration and

reached the peak of insulin concentration in one hour, altogether with the SC injection. Furthermore, their results showed that the level of serum insulin is dose-dependent and even the C_{max} for dissolvable MNs loaded with 5 or 10 IU are lower than the SC injection which suggests that insulin from the dissolvable MNs requires more time for permeation and diffusion to the bloodstream.

Similar pharmacokinetic behaviour was also reported for different biodegradable MNs by Liu et al. 2012, Yu et al. 2017 and Lee et al. 2017 whereas, for other dissolvable MNs, the maximum plasma insulin concentration was attained in 2 hours or more (M. Ling and Chen 2013; Yu, Jiang, Zhang, *et al.* 2017). These results suggest that the formulation of the MNs plays an important role in the release of the drug as well as in the passive diffusion to the blood capillarity and therefore in the insulin bioavailability.

Differently from previous studies though, the concentration of insulin is maintained at a steady rate about 50% of its maximal concentration for the 3D printed MNs coated with insulin. This event supports the hypothesis that after the insertion of the MNs, the insulin is absorbed to the blood capillarity by passive diffusion.

Finally, our research also showed that the relative pharmacological availability (RPA) and the relative bioavailability compared with subcutaneous injection (RBA) for insulin loaded on the 3D printed MNs group were about and 122 and 115 %, respectively, compared with SC injection. These results indicate that insulin released from 3D printed MNs was almost completely absorbed from the skin into the systemic circulation, and the pharmacological activity of the released insulin remained intact after the delivery with the 3D printed MNs.

4.4 Conclusions

The desktop 3D printer stereolithography, Form 2, used in this research is a low-budget printer that demonstrated an exceptional ability for rapid and versatile fabrication of reproducible microneedle arrays with high quality for all proposed designs, pyramid, cone and spear. Although the mechanical properties of the biocompatible MNs need to be further explored, the preliminary studies with the

piercing properties indicate that the biocompatible resin has good mechanical properties and the 3D printed MNs requires low forces to penetrate the skin.

The insulin-sugar formulations presented in this study demonstrated that xylitol, trehalose and mannitol can provide good insulin protection for coated MNs with xylitol showing the best insulin stabilisation performance. The coating method used to coat the 3D printed MNs demonstrated that inkjet printing was successfully used for the application of insulin-sugar formulations on the surface of the microneedles. The results showed that this technology delivered highly uniform, reproducible and accurate coatings on the microneedles.

In vitro studies revealed that all the carriers showed rapid insulin release rates within 30 min. Further studies with diabetic mice confirmed the fast insulin release from the microneedles with a rapid decrease to the plasma glucose levels within one hour like SC injection group. However, differently from the SC injection group, after insulin had reached its peak, the plasma insulin concentration is maintained at a steady state rate at about 50% of its maximal concentration for three hours, probably due to the passive diffusion event.

Overall, the fast fabrication of biocompatible MNs through stereolithography combined with an accurate coating method using inkjet printing and the use of highly dissolvable and stable coatings have been demonstrated to be an exciting strategy for rapid release of insulin.

4.5 References

Abdul-fattah, A.M., Dellerman, K.M., Bogner, R.H., Pikal, M.J. (2007). The Effect of Annealing on the Stability of Amorphous Solids: Chemical Stability of Freeze-Dried Moxalactam. *Journal of Pharmaceutical Sciences*, 96(5), 1237–1250.

Ameri, M., Kadkhodayan, M., Nguyen, J., Bravo, J. A., Su, R., Chan, K., Daddona, P.E. (2014). Human growth hormone delivery with a microneedle transdermal system: Preclinical formulation, stability, delivery and PK of therapeutically relevant doses. *Pharmaceutics*, 6(2), 220–234.

Andrade, F., Fonte, P., Oliva, M., Videira, M., Ferreira, D., Sarmento, B. (2015). Solid state formulations composed by amphiphilic polymers for delivery of proteins:

characterization and stability. *International Journal of Pharmaceutics*, 486(1–2), 195–206.

Baek, S.H., Shin, J.H. and Kim, Y.C. (2017). Drug-coated microneedles for rapid and painless local anesthesia. *Biomedical Microdevices*, 19(1).

Bariya, S.H., Gohel, M. C., Mehta, T.A., Sharma, O.P. (2012). Microneedles: an emerging transdermal drug delivery system. *Journal of Pharmacy and Pharmacology*, 64(1), 11–29.

Boehm, R.D., Miller, P.R., Hayes, S.L., Monteiro-Riviere, N.A., Narayan, R.J. (2011). Modification of microneedles using inkjet printing. *AIP Advances*, 1(2), 1–13.

Boehm, R.D., Miller, P.R., Schell, W.A., Perfect, J.R., Narayan, R.J. (2013). Inkjet printing of amphotericin B onto biodegradable microneedles using piezoelectric inkjet printing. *Jom*, 65(4), 525–533.

Boehm, R.D., Miller, P. R., Singh, R., Shah, A., Stafslien, S., Daniels, J., Narayan, R. J. (2012). Indirect rapid prototyping of antibacterial acid anhydride copolymer microneedles. *Biofabrication*, 4(1).

Boehm, R.D, Daniels, J., Stafslien, S., Nasir, A., Lefebvre, J., Narayan, R.J., Lefebvre, J. (2015). Polyglycolic acid microneedles modified with inkjet-deposited antifungal coatings. *Biointerphases*, 10(1).

Boehm, R.D, Miller, P.R., Daniels, J., Stafslien, S., Narayan, R.J. (2014). Inkjet printing for pharmaceutical applications. *Biochemical Pharmacology*, 17(5), 247–252.

Branca, C., MacCarrone, S., Magazu, S., Maisano, G., Bennington, S.M., Taylor, J. (2005). Tetrahedral order in homologous disaccharide-water mixtures. *Journal of Chemical Physics*, 122(17), 174513–174516.

Carpenter, J.F. and Crowe, J.H. (1989). An infrared spectroscopic study of the interactions of carbohydrates with dried proteins. *Biochemistry*, 28(9), 3916–3922.

Castro, P. M., Fonte, P., Sousa, F., Raquel, A., Sarmento, B., Pintado, M.E. (2015). Oral films as breakthrough tools for oral delivery of proteins/peptides. *Journal of Controlled Release*, 211, 63–73.

Chimate, C. and Koc, B. (2014). Pressure assisted multi-syringe single nozzle deposition system for manufacturing of heterogeneous tissue scaffolds. *International Journal of Advanced Manufacturing Technology*, 75(1–4), 317–330.

Cicerone, M. T., Pikal, M. J., and Qian, K. K. (2016). Stabilization of Proteins in Solid Form. *Advanced Drug Delivery Reviews*, 93, 14–24.

Cormier, M., Johnson, B., Ameri, M., Nyam, K., Libiran, L., Zhang, D.D., Daddona, P. (2004). Transdermal delivery of desmopressin using a coated microneedle array patch system. *Journal of Controlled Release*, 97(3), 503–511.

Correia, M., Neves-Petersen, M.T., Jeppesen, P.B., Gregersen, S., Petersen, S.B. (2012). UV-Light Exposure of Insulin: Pharmaceutical Implications upon Covalent Insulin Dityrosine Dimerization and Disulphide Bond Photolysis. *PLoS ONE*, 7(12).

Crowe, L.M., Reid, D.S. and Crowe, J.H. (1996). Is Trehalose Special for Preserving Dry Biomaterials?. *Biophysical Journal*, 71(October), 2087–2093.

Davis, S.P., Landis, B.J., Adams, Z.H., Allen, M.G., Prausnitz, M.R. (2004). Insertion of microneedles into skin: Measurement and prediction of insertion force and needle fracture force. *Journal of Biomechanics*, 37(8), 1155–1163.

Donnelly, R.F., Singh, T.R.R., Garland, M.J., Migalska, K., Majithiya, R., McCrudden, C.M., Woolfson, A. D. (2012). Hydrogel-forming microneedle arrays for enhanced transdermal drug delivery. *Advanced Functional Materials*, 22(23), 4879–4890.

Doraiswamy, A., Jin, C., Narayan, R.J., Mageswaran, P., Mente, P., Modi, R., Chichkov, B. (2006). Two photon induced polymerization of organic-inorganic hybrid biomaterials for microstructured medical devices. *Acta Biomaterialia*, 2(3), 267–275.

Economidou, S.N., Lamprou, D.A. and Douroumis, D. (2018). 3D printing applications for transdermal drug delivery. *International Journal of Pharmaceutics*, 544(2), 415–424.

Ettinger, M.J. and Timasheff, S.N. (1971). Optical activity of insulin. II. Effect of nonaqueous solvents. *Biochemistry*, 10(5), 831–840.

Ettinger, M.J. and Timasheff, S.N. (1971). Optical Activity of Insulin. I. On the Nature of the Circular Dichroism Bands. *Biochemistry*, 10(5), 824–831.

Faghihi, H., Merrikhihaghi, S., Ruholamini Najafabadi, A., Ramezani, V., Sardari, S., Vatanara, A. (2016). A Comparative Study to Evaluate the Effect of Different Carbohydrates on the Stability of Immunoglobulin G during Lyophilization and Following Storage. *Pharmaceutical Sciences*, 22(4), 251–259.

Gill, H.S. and Prausnitz, M.R. (2007). Coated microneedles for transdermal delivery. *Journal of Controlled Release*, 117(2), 227–237.

Gittard, S.D., Miller, P. R., Jin, C., Martin, T.N., Boehm, R.D., Chisholm, B.J., Narayan, R.J. (2011). Deposition of antimicrobial coatings on microstereolithography-fabricated microneedles. *Jom*, 63(6), 59–68.

Górska, A., Szulc, K., Ostrowska-Ligęza, E., Bryś, J., Wirkowska-Wojdyła, M. (2017). Effect of composition and drying method on glass transition temperature, water sorption characteristics and surface morphology of newly designed β-lactoglobulin/retinyl palmitate/disaccharides systems. *Journal of Thermal Analysis and Calorimetry*, 130(1), 177–185.

Goyanes, A., Buanz, A.B.M., Basit, A.W., Gaisford, S. (2014). Fused- fi lament 3D printing (3DP) for fabrication of tablets. *International Journal of Pharmaceutics*, 476(1–2), 88–92.

Goyanes, A., Buanz, A.B.M., Hatton, G.B., Gaisford, S., Basit, A.W. (2015). 3D printing of modified-release aminosalicylate (4-ASA and 5-ASA) tablets. European *Journal of Pharmaceutics and Biopharmaceutics*, 89, 157–162.

Haj-Ahmad, R., Khan, H., Arshad, M.S., Rasekh, M., Hussain, A., Walsh, S., Ahmad, Z. (2015). Microneedle coating techniques for transdermal drug delivery. *Pharmaceutics*, 7(4), 486–502.

Haque, M.A., Chen, J., Aldred, P., Adhikari, B. (2015). Drying and denaturation characteristics of whey protein isolate in the presence of lactose and trehalose. *Food Chemistry*, 177, 8–16.

Herwadkar, A. and Banga, A.K. (2012). Peptide and protein transdermal drug delivery. *Drug Discovery Today: Technologies*, 9(2), e147–e154.

Imamura, K., Ogawa, T., Sakiyama, T., Nakanishi, K. (2003). Effects of Types of Sugar on the Stabilization of Protein in the Dried State. *Journal of Pharmaceutical Sciences*, 92(2), 266–274.

Ito, Y., Hagiwara, E., Saeki, A., Sugioka, N., Takada, K. (2006). Feasibility of microneedles for percutaneous absorption of insulin. *European Journal of Pharmaceutical Sciences*, 29(1), 82–88.

Izutsu, K., Yoshioka, S. and Terao, T. (1994). Effect of Mannitol Crystallinity on the Stabilization of Enzymes during Freeze-Drying. *Chemical and Pharmaceutical Bulletin*, 42(1), 5–8.

Jain, N.K. and Roy, I. (2009). Effect of trehalose on protein structure. *Protein Science*, 18(1), 24–36.

Jamróz, W., Kurek, M., Ewelina, L., Szafraniec, J., Knapik-kowalczuk, J., Syrek, K., Jachowicz, R. (2017). 3D printed orodispersible films with Aripiprazole. *International Journal of Pharmaceutics*, 533, 413–420.

Jamróz, W., Szafraniec, J., Kurek, M., Jachowicz, R. (2018). 3D Printing in Pharmaceutical and Medical Applications - Recent Achievements and Challenges. *Pharmaceutical Research*, 35(9).

Jovanović, N., Bouchard, A., Hofland, G.W., Witkamp, G.J., Crommelin, D.J. A, Jiskoot, W. (2006). Distinct effects of sucrose and trehalose on protein stability

during supercritical fluid drying and freeze-drying Jovanovi. *European Journal of Pharmaceutical Sciences* 2, 27, 336–345.

Kelly, S.M., Jess, T.J. and Price, N.C. (2005). How to study proteins by circular dichroism. *Biochimica et Biophysica Acta*, 1751(2), 119–139.

Kim, Y.C., Park, J.H. and Prausnitz, M. R. (2012). Microneedles for drug and vaccine delivery. *Advanced Drug Delivery Reviews*, 64(14), 1547–1568.

Larraneta, E., Lutton, R. E. M., Woolfson, A. D., Donnelly, R. F. (2016). Microneedle arrays as transdermal and intradermal drug delivery systems: Materials science, manufacture and commercial development. *Materials Science and Engineering R: Reports*, 104, 1–32.

Lerbret, A., Bordat, P., Affouard, F., Guinet, Y., Hédoux, A., Paccou, L., Descamps, M. (2005). Influence of homologous disaccharides on the hydrogen-bond network of water: Complementary Raman scattering experiments and molecular dynamics simulations. *Carbohydrate Research*, 340(5), 881–887.

Ling, M. and Chen, M. (2013). Dissolving polymer microneedle patches for rapid and efficient transdermal delivery of insulin to diabetic rats. *Acta Biomaterialia*, 9(11), 8952–8961.

Luzuriaga, M.A., Berry, D. R., Reagan, J.C., Smaldone, R.A., Gassensmith, J.J. (2018). Biodegradable 3D printed polymer microneedles for transdermal drug delivery. *Lab on a Chip*, 18(8), 1223–1230.

McCrudden, M.T.C., Alkilani, A.Z., McCrudden, C.M., McAlister, E., McCarthy, H.O., Woolfson, D., Donnelly, R.F. (2014). Design and physicochemical characterisation of novel dissolving polymeric microneedle arrays for transdermal delivery of high dose, low molecular weight drugs. *Journal of Controlled Release*, 180(1), 71–80.

Ohtake, S., Kita, Y. and Arakawa, T. (2011). Interactions of formulation excipients with proteins in solution and in the dried state. *Advanced Drug Delivery Reviews*, 63(13), 1053–1073.

Ovsianikov, A., Chichkov, B., Mente, P., Monteiro-Riviere, N., Doraiswamy, A., Narayan, R. J. (2007). Two Photon Polymerization of Polymer – Ceramic Hybrid Materials for Transdermal Drug Delivery. *International Journal of Applied Ceramic Technology*, 4(1), 22–29.

Park, B.J., Choi, H.J., Moon, S.J., Kim, S.J., Bajracharya, R., Min, J.Y., Han, H.K. (2018). Pharmaceutical applications of 3D printing technology: current understanding and future perspectives. *Journal of Pharmaceutical Investigation*, 1–11.

Park, J.H., Allen, M. G. and Prausnitz, M.R. (2005). Biodegradable polymer microneedles: Fabrication, mechanics and transdermal drug delivery. *Journal of Controlled Release*, 104(1), 51–66.

Pere, C.P.P., Economidou, S.N., Lall, G., Ziraud, C., Boateng, J.S., Alexander, B. D., Douroumis, D. (2018). 3D printed microneedles for insulin skin delivery. *International Journal of Pharmaceutics*, 544(2), 425–432.

Pikal, M.J. and Rigsbee, D.R. (1997). The stability of Insulin in Crystalline and Amorphous Solids: Observation of Greater Stability for the Amorphous Form. *Pharmaceutical Research*, 14(10), 1379–1387.

Prestrelski, S.J., Tedeschi, N., Arakawa, T., Carpenter, J.F. (1993). Dehydration-induced conformational transitions in proteins and their inhibition by stabilizers. *Biophysical Journal*, 65(2), 661–671.

Qiu, Y., Qin, G., Zhang, S., Wu, Y., Xu, B., Gao, Y. (2012). Novel lyophilized hydrogel patches for convenient and effective administration of microneedle-mediated insulin delivery. *International Journal of Pharmaceutics*, 437(1–2), 51–56.

Ross, S., Scoutaris, N., Lamprou, D., Mallinson, D., Douroumis, D. (2015). Inkjet printing of insulin microneedles for transdermal delivery. *Drug Delivery and Translational Research*, 5(4), 451–461.

Sarmento, B., Ferreira, D.C., Jorgensen, L., Van de Weert, M. (2007). Probing insulin's secondary structure after entrapment into alginate/chitosan nanoparticles. *European Journal of Pharmaceutics and Biopharmaceutics*, 65(1), 10–17.

Singh, M., Haverinen, H.M., Dhagat, P., Jabbour, G.E. (2010). Inkjet printing-process and its applications. *Advanced Materials*, 22(6), 673–685.

Souillac, P.O., Middaugh, C.R. and Rytting, J.H. (2002a). Investigation of protein/carbohydrate interactions in the dried state. 1. Calorimetric Studies. *International Journal of Pharmaceutics*, (1–2), 206–216.

Souillac, P.O., Middaugh, C.R. and Rytting, J.H. (2002b). Investigation of protein / carbohydrate interactions in the dried state. 2 . Diffuse reflectance FTIR studies. *International Journal of Pharmaceutics*, 235, 207–218.

Sreerama, N, Venyaminov, S.Y. and Woody, R.W. (1999). Estimation of the number of alpha-helical and beta-strand segments in proteins using circular dichroism spectroscopy. *Protein Science*, 8(2), 370–380.

Sreerama, Narasimha and Woody, R.W. (2000). Estimation of protein secondary structure from circular dichroism spectra: Comparison of CONTIN, SELCON, and CDSSTR methods with an expanded reference set. *Analytical Biochemistry*, 287(2), 252–260.

Tuan-Mahmood, T.M., McCrudden, M.T.C., Torrisi, B.M., McAlister, E., Garland, M.J., Singh, T.R.R., Donnelly, R. F. (2013). Microneedles for intradermal and transdermal drug delivery. *European Journal of Pharmaceutical Sciences*, 50(5), 623–637.

Uddin, M.J., Scoutaris, N., Klepetsanis, P., Chowdhry, B., Prausnitz, M.R., Douroumis, D. (2015). Inkjet printing of transdermal microneedles for the delivery of anticancer agents. *International Journal of Pharmaceutics*, 494(2), 593–602.

Whitmore, L. and Wallace, B.A. (2004). DICHROWEB, an online server for protein secondary structure analyses from circular dichroism spectroscopic data. *Nucleic Acids Research*, 32, 668–673.

Whitmore, L. and Wallace, B.A. (2008). Protein secondary structure analyses from circular dichroism spectroscopy: Methods and reference databases. *Biopolymers*, 89(5), 392–400.

Wu, C.C. and Yang, J.T. (1981). Conformation of Insulin and its fragments in surfactant solutions. *Biochimica et Biophysica Acta*, 667, 285–293.

Yu, W., Jiang, G., Liu, D., Li, L., Chen, H., Liu, Y., Tong, Z. (2017). Fabrication of biodegradable composite microneedles based on calcium sulfate and gelatin for transdermal delivery of insulin. *Materials Science & Engineering C*, 71, 725–734.

Yu, W., Jiang, G., Zhang, Y., Liu, D., Xu, B., Zhou, J. (2017). Polymer microneedles fabricated from alginate and hyaluronate for transdermal delivery of insulin. *Materials Science and Engineering C*, 80, 187–196.

Zeng, G., Shou, J.J., Li, K.K., Zhang, Y.H. (2011). *In-situ* confocal Raman observation of structural changes of insulin crystals in sequential dehydration process. *Biochimica et Biophysica Acta*, 1814(12), 1631–1640.

Zhang, Y., Siebenaler, K., Brown, K., Dohmeier, D., Hansen, K. (2012). Adjuvants to prolong the local anesthetic effects of coated microneedle products. *International Journal of Pharmaceutics*, 439(1–2), 187–192.

5 CHAPTER

ANIMAL STUDIES

5.1 Introduction

Since it was discovered in the 1920s, exogenous insulin therapy has helped to improve the quality of life of many people as well as save many people's lives. The first insulins available for commercial use were extracted from bovine and porcine pancreas. However, a strong immune response was very common due to their impurity and therefore other alternatives started to be studied.

Due to the advance in the field of genetic engineering, in the 1980s the human proinsulin gene was inserted into a bacterium's gene by recombinant DNA technique and started to be produced by cultures of bacteria (Saccharomyces cerevisiae and by a non-pathogenic strain of Escherichia coli). Since then, many modifications in the human insulin structure have been proposed and many insulin analogs are now available on the market.

Once insulin therapy aims to mimic the physiologic pattern of insulin secretion, short-insulin analogs were designed for bolus insulin therapy to control postprandial hypoglycemia whereas intermediate and long-acting insulin analogs were proposed to simulate the basal insulin secretion. While it is not possible yet to achieve both patterns with only one insulin analog, the combination of short with intermediate or long-acting insulin is very common.

Despite the advances in the genetic engineering and drug delivery fields, the administration of insulin through oral route is still a challenge and the subcutaneous injections remains the most common alternative.

The promising results described in the previous chapter have suggested that the 3D printed microneedles coated with bovine insulin-xylitol showed good insulin stability and the same effectiveness as the subcutaneous injection in reducing blood-glucose levels. Therefore, in this study, a short and long-acting insulin therapy were evaluated in mice by coated 3D printed microneedles.

5.2 Materials and methods

5.2.1 Materials

Insulin aspart (Novolog) and insulin glargine (Lantus) were commercially available. Xylitol powder (Xylisorb® 90) was donated by Roquette Freres (France). The streptozocin and citric acid were both purchased from Merck Chemical Co. (Darmstadt, Germany). Phosphate buffer PBS 7.4 was purchased from Sigma-Aldrich. The resin used to fabricate the MNs was the biocompatible Class I resin, Dental SG, purchased from Formlabs. All the solvents used were of analytical grades.

5.2.2 Coating formulations

Xylitol was weighted and added to either the insulin aspart or glycine solution at 5:1 ratio (w/w). The solution was left it stirring until complete dissolution.

5.2.3 Coating microneedles through inkjet printing

The 3D printed microneedles with pyramid design containing 48 needles/array was selected for this study. The printing and the coating process follow the same procedure described in chapter 4. For each coating array, two droplets of 10 spots of the coating formulation were dispensed on each needle's surface. A total of 7 and 18 layers were dispensed on the 0.2 and 0. 5 IU MN arrays, respectively. The coated MNs were left at room temperature for 24h to allow the evaporation of the water and formation of uniform films.

5.2.4 Animal studies

The protocol for the animal experiments were submitted and approved by the Research Ethics Committee (reference number 0008/18, Department of Pharmacy, Southern University Bangladesh) and conducted according to the Southern University Bangladesh policy for the protection of Vertebrate Animals used for

Experimental and Other Scientific Purposes, with implementation of the principle of the 3Rs (replacement, reduction, refinement).

5.2.4.1 Diabetic mice model

Swiss albino female mice (130 ± 10 g) were allowed to free access to food and water for 3 days prior to diabetes therapy. To generate the diabetic animal model, Streptozotocin (70 mg/kg) in citric acid buffer (pH 4.5) was subcutaneously injected on the flank of the animals and the blood glucose levels were daily monitored at specific times using a one-touch glucometer (ACCU-CheckVR Active, Roche, Germany). After 7 days of streptozotocin administration, mice with blood glucose exceeding 300 mg/dl were considered as diabetic.

5.2.4.2 Insulin transdermal delivery in diabetic mice

Twenty-four hours before the experiment, the animals were anesthetized with pentobarbital and carefully shaved using an electric razor (Panasonic, USA). Followed that, the animals were left for fasting for 12 hours prior to the beginning of the experiment.

For each insulin analog (aspart or glargine), the diabetic mice were randomly divided into five groups (n = 5 for each group): (1) negative control: uncoated MNs; (2) Positive control 1: subcutaneous injection of insulin with 0.2 IU/animal; (3) Positive control 2: subcutaneous injection of insulin with 0.5 IU/animal; (4) Coated MNs with 0.2 IU/animal of insulin:xylitol 5:1 (w/w) and (5) Coated MNs with 0.5 IU/animal of insulin:xylitol 5:1 (w/w).

For the positive control groups, the animals received subcutaneous injection of insulin onto the dorsal skin using hypodermic needles. For the negative control and the experimental groups, the respective uncoated and coated microneedles were applied onto the dorsal skin of the animals and secured with an adhesive tape to prevent dislodgement. After two hours, the MNs arrays were removed from the skin of the mice.

For all groups, the blood samples were collected from the jugular vein at 0, 1, 2, 3, 4 and 5 hours after the administration for the insulin aspart group while for

the insulin glargine group the samples were collected at time 2, 4, 6, 8, 10, 12, 14, 16, 18, 20, 22 and 24 hours after the treatment. The samples were centrifuged at 3000 r.p.m. for 5 min to immediately separate the plasma. Plasma glucose levels were measured with a glucometer (ACCU-CheckVR Active, Roche, Germany) whereas insulin plasma concentrations were determined using insulin ELISA kit.

The pharmacokinetics and the pharmacodynamic parameters were calculated as described in session 4.1.4.3.

5.3 Results and Discussion.

5.3.1 Insulin transdermal delivery in diabetic mice

The animals were successfully induced to diabetes after 7 days of streptozotocin treatment showing more than 300 mg/dl of glucose levels. Figure 5.1 shows the animals before and after the MNs treatment.

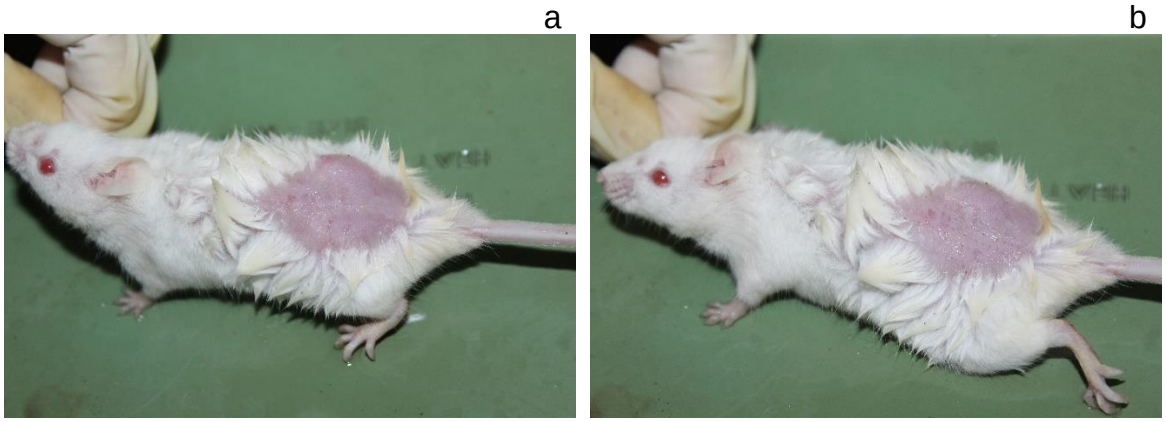

Figure 5.1. Experimental mice: (a) before the MNs treatment and (b) after the MNs treatment.

A 0.2 and 0.5 IU of insulin dose (1.206 and 3.017 μM, respectively) were selected in order to avoid hypoglycemia in the animals. The results of both fast and long-acting insulin treatments are individually described below.

5.3.1.3 Fast-acting insulin treatment

Insulin Aspart is a short-acting insulin analog with an onset of action between 5 to15 minutes, peak action between 1 to 2 hours and a duration of action between

3 to 4 hours (Østerberg *et al.* 2003). From Figure 5.2 and Table 5.1 it is possible to see that except for the negative control group (uncoated MNs), all the animals presented a rapid decrease in the plasma glucose level within one hour.

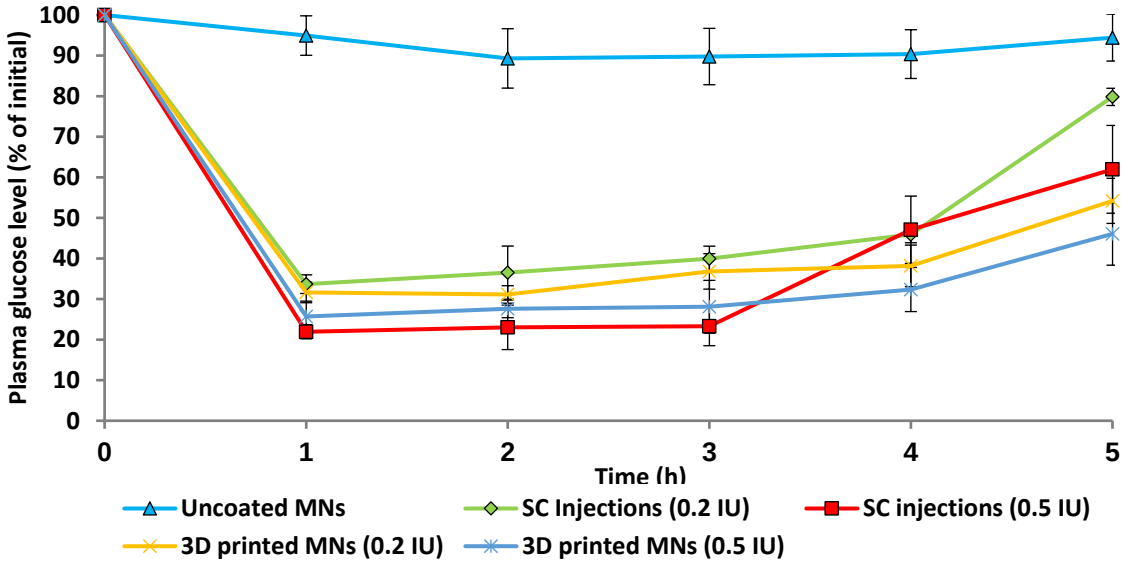

Figure 5.2. Comparative plasma glucose level vs time profiles in diabetic mice after uncoated MNs, subcutaneous injections and coated MNs treatments in international units (IU) (n=5).

Table 5.1.Pharmacodynamic parameters for plasma glucose levels in diabetic mice after uncoated MNs, subcutaneous injections and coated MNs treatments (n=5).

Group	C_{min} (%)	$T_{min\ (h)}$	$AAC_{0\text{-}5}$ (%h)	RPA(%)
Uncoated MNs	94.9	2	38.42	0
SC injections (0.2 IU)	33.7	1	254.08	100
SC injections (0.5 IU)	21.9	1	303.70	100
3D printed MNs (0.2 IU)	31.1	2	285.18	112
3D printed MNs (0.5 IU)	25.7	1	313.27	103

C_{min}, minimum glucose level; T_{min}, time point of minimum glucose level; $AAC_{0\ to\ 4}$, area above the plasma glucose concentration vs. time curve; RPA, relative pharmacological availability compared to subcutaneous injection.

For the 0.2 IU dose treatment groups, the C_{min} was reduced to about 32% of its initial value and no statistical difference was noted between the SC injection group and the MNs group ($p<0.05$). As expected, when the insulin dose was increased to 0.5 IU, a further reduction in the glucose levels was noted, reaching about 23% of its initial value. The rapid decrease in the glucose levels for the MNs treatments indicates that insulin is being absorbed very quickly; being as effective as the subcutaneous injection treatment.

After the first hour, the plasma glucose levels of SC injection and MNs groups with 0.2 IU were maintained at low levels with a slightly increase for four hours with no difference between them ($p>0.05$). After that, the plasma glucose levels start to rise more considerably; being more pronounced for the SC injection group.

Interestingly though, the treatments with 0.5 IU dose shows that the SC injection and the MNs treatment show similar sustained low levels of glucose for 3 hours ($p>0.05$). After this period, the plasma glucose level for the MNs treatment starts to gradually increase whereas for SC injection group, the plasma glucose level rises suddenly.

The pharmacokinetic parameters were also studied, and the results are shown in Figure 5.3 and Table 5.2. As shown, insulin levels are quickly raised within one hour in all treatments.

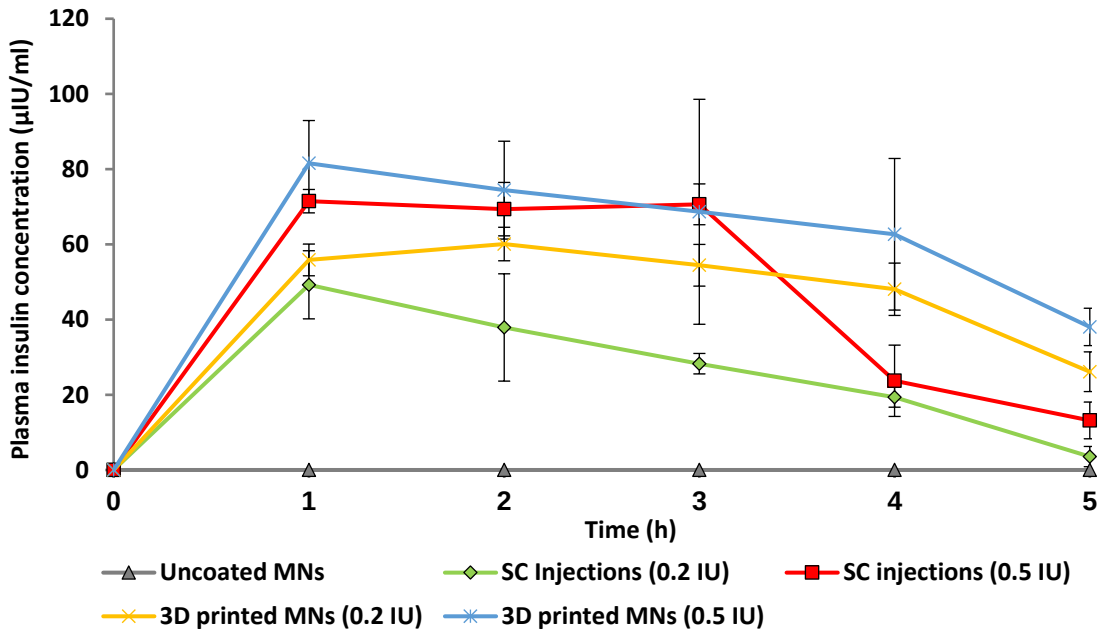

Figure 5.3. Comparative plasma insulin levels in diabetic mice after uncoated MNs, subcutaneous injections and coated MNs treatments in international units (IU) (n=5).

Table 5.2. Pharmacokinetic parameters for plasma insulin levels in diabetic mice after uncoated MNs, subcutaneous injections and coated MNs treatments (n=5).

Group	$C_{máx}$ (μIU.mL^{-1})	$T_{máx\ (h)}$	AUC_{0-5} (μIU.mL^{-1}.h)	RBA(%)
Uncoated MNs	0	0	0.00	0
SC injections (0.2 IU)	49.2	1	125.07	100
SC injections (0.5 IU)	71.5	1	223.34	100
3D printed MNs (0.2 IU)	60.1	2	194.41	155
3D printed MNs (0.5 IU)	81.6	1	223.34	115

C_{max}, maximum plasma insulin concentration; T_{max}, time point of maximum plasma insulin concentration; $AUC_{0\ to\ 4}$, area under the plasma insulin concentration vs. time curve; RBA, relative bioavailability compared with subcutaneous injection

From the graph, one can see that after reached C_{max}, the insulin concentration constantly drops to almost zero within four hours for the SC injection group (0.2 IU). However, when the dose is increased to 0.5 IU, the insulin concentration is maintained at the highest level for 3 hours before a suddenly decline. This event may be due to a possible depot formed into the skin allied to the insulin diffusion into the systemic circulation which may be responsible for the maintenance the high levels of insulin.

Differently though, for both MNs treatment (0.2 and 0.5 IU), the insulin levels were sustained at high levels with a gradual decrease for four hours, after which a more pronounced reduction in the insulin concentration can be seen. Moreover, no difference could be seen between for the 0.5 IU dose of SC injections and MNs for 3 hours ($p>0.05$).

The glucose responses are also consistent with the insulin doses. Similar sustainable insulin levels and hypoglycemic responses were also reported by others using biodegradable MNs loaded with insulin (Zhang *et al.* 2018; Yu, Jiang, Zhang, *et al.* 2017; Liu *et al.* 2012). The observed maintenance of the pharmacological activity can be attributed to both the MNs formulation and to the passive diffusion of the insulin.

5.3.1.4 Long-acting insulin treatment

Insulin glargine is a long-acting insulin analog administered as a solution which precipitates into the subcutaneous tissue and it is slowly released being absorbed at a constant rate. It has an onset of action between 2 to 4 hours and a

duration of action between 20 to 24 hours (Barnett 2006). Figure 5.4 and Table 5.3 shows the pharmacodynamic of insulin upon the treatments.

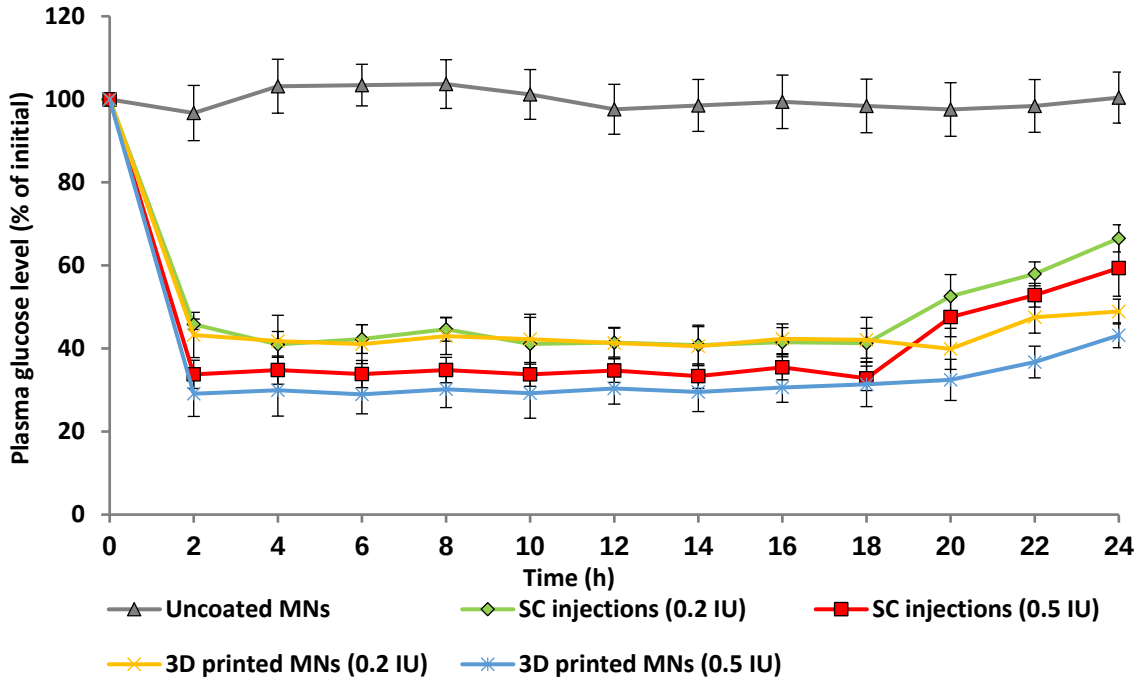

Figure 5.4. Comparative plasma glucose level vs time profiles in diabetic mice after uncoated MNs, subcutaneous injections and coated MNs treatments in international units (IU) (n=5).

Table 5.3. Pharmacodynamic parameters for plasma glucose levels in diabetic mice after uncoated MNs, subcutaneous injections and coated MNs treatments (n=5).

Group	C_{min} (%)	$T_{min\ (h)}$	$AAC_{0\text{-}24}$ (%h)	RPA(%)
Uncoated MNs	97.6	20	3.44	0
SC injections (0.2 IU)	40.8	14	1252.70	100
SC injections (0.5 IU)	32.8	18	1425.31	100
3D printed MNs (0.2 IU)	39.9	20	1320.98	105
3D printed MNs (0.5 IU)	29.2	10	1579.93	111

C_{min}, minimum glucose level; T_{min}, time point of minimum glucose level; $AAC_{0\ to\ 4}$, area above the plasma glucose concentration vs. time curve; RPA, relative pharmacological availability compared to subcutaneous injection.

From the graph, it is possible to see that both MNs and SC injection groups presented similar behaviour up to 18 hours. A rapid decrease in the glucose levels followed by a sustained minimum glucose level up to 18hs can be seen for all insulin treatments. No difference could be seen between the SC and MNs for the 0.2 IU ($p>0.05$) or 0.5 IU ($p>0.05$) treatments. After the 18 hs, both SC injection treatments

(0.2 and 0.5 IU) showed a faster increase in the glucose levels whereas for the MNs group, they tended to increase more slowly.

Figure 5.5 and Table 5.4 shows the pharmacokinetic parameters of the plasma insulin levels of all treatment groups.

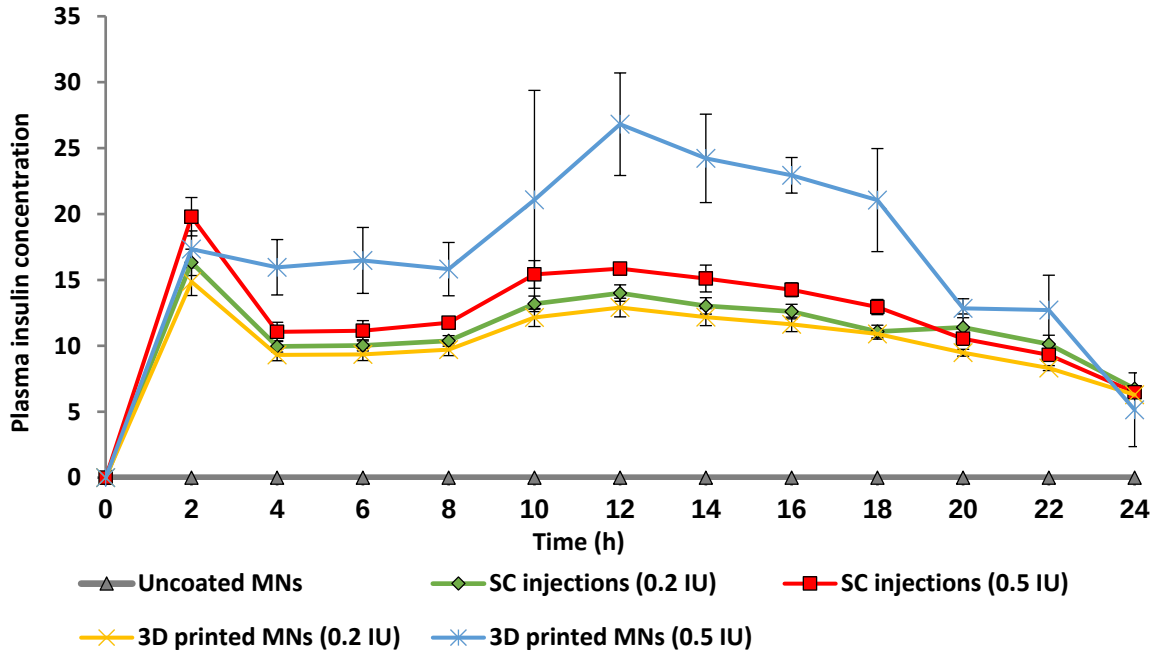

Figure 5.5. Comparative plasma insulin levels in diabetic mice after uncoated MNs, subcutaneous injections and coated MNs treatments in international units (n=5).

Table 5.4. Pharmacokinetic parameters for plasma insulin levels in diabetic mice after uncoated MNs, subcutaneous injections and coated MNs treatments (n=5).

Group	$C_{máx}$ (μIU.mL^{-1})	$T_{máx\ (h)}$	AUC_{0-24} (μIU.mL^{-1}.h)	RBA(%)
Uncoated MNs	0	0	0.00	0
SC injections (0.2 IU)	14.0	12	271.03	100
SC injections (0.5 IU)	15.9	12	300.85	100
3D printed MNs (0.2 IU)	12.9	12	247.88	91
3D printed MNs (0.5 IU)	26.8	12	419.71	140

C_{max}, maximum plasma insulin concentration; T_{max}, time point of maximum plasma insulin concentration; $AUC_{0\ to\ 4}$, area under the plasma insulin concentration vs. time curve; RBA, relative bioavailability compared with subcutaneous injection

Except for the treatment with the MNs loaded with 0.5 IU, all insulin treatments showed an initial peak of insulin plasma concentration at 2 hours which is decreased in about 50% in the next 2 hours. At this point, insulin levels are sustained for 4 hours. Interestingly though, the levels of insulin in the plasma start to rise again at 8h, reaching another peak at 12 h which slowly decreases until the

24 hours experiment. This behaviour might be due to changes in the equilibrium of the dissolution of the precipitated insulin.

Even though the microneedles containing the 0.5 IU of insulin presented a significant superior release behaviour than the SC injection with the same dose ($p<0.05$) no statistical difference was noted on the level of glucose response for 18 hours.

5.4 Conclusions

The animal studies revealed that insulin retained its pharmacological activity on the microneedles. Overall, the MNs provided a fast and efficient delivery of insulin for all treatments, producing a significant hypoglycemic response with a sustained effect. Moreover, the MNs treatment also presented higher relative bioavailability and pharmacological availability than the subcutaneous injections.

Moreover, once insulin therapy aims to mimic the normal physiological insulin response, the sustained release of insulin glargine is desired for a basal insulin therapy, however it is not suitable for a bolus therapy (insulin aspart). In this case, insulin levels should return to the basal levels between 2-3 hours.

5.5 References

Barnett, A.H. (2006). Insulin glargine in the treatment of type 1 and type 2 diabetes. *Vascular Health and Risk Management*, 2(1), 59–67.

Ito, Y., Hagiwara, E., Saeki, A., Sugioka, N., akada, K. (2006). Feasibility of microneedles for percutaneous absorption of insulin. *European Journal of Pharmaceutical Sciences*, 29(1), 82–88.

Ito, Y., Nakahigashi, T., Yoshimoto, N., Ueda, Y., Hamasaki, N., Takada, K. (2012). Transdermal Insulin Application System with Dissolving Microneedles. *Diabetes Technology and Therapeutics*, 14(10), 891–899.

Lahiji, S.F., Dangol, M., and Jung, H. (2015). A patchless dissolving microneedle delivery system enabling rapid and efficient transdermal drug delivery. *Scientific Reports*, 5, 1–7.

Lee, I. C., Lin, W.M., Shu, J.C., Tsai, S.W., Chen, C.H., Tsai, M.T. (2017). Formulation of two-layer dissolving polymeric microneedle patches for insulin transdermal delivery in diabetic mice. *Journal of Biomedical Materials Research Part A*, 105(1), 84–93.

Ling, M. and Chen, M. (2013). Dissolving polymer microneedle patches for rapid and efficient transdermal delivery of insulin to diabetic rats. *Acta Biomaterialia*, 9(11), 8952–8961.

Liu, S., Jin, M., Quan, Y., Kamiyama, F., Katsumi, H., Sakane, T., Yamamoto, A. (2012). The development and characteristics of novel microneedle arrays fabricated from hyaluronic acid, and their application in the transdermal delivery of insulin. *Journal of Controlled Release*, 161(3), 933–941.

Liu, Y., Lee, J., Mans, K.M., Ko, J.H., Sallam, S., Wesdemiotis, C., Maynard, H. D. (2017). Trehalose Glycopolymer Enhances Both Solution Stability and Pharmacokinetics of a Therapeutic Protein. *Bioconconjugate Chemistry*, 28(3), 836–845.

Martanto, W., Davis, S. P., Holiday, N.R., Wang, J., Gill, H.S., Prausnitz, M. R. (2004). Transdermal Delivery of Insulin Using Microneedles *in Vivo. Pharmaceutical Research*, 21(6), 947–952.

Østerberg, O., Erichsen, L., Ingwersen, S. H., Plum, A., Poulsen, H. E., Vicini, P. (2003). Pharmacokinetic and pharmacodynamic properties of insulin aspart and human insulin. *Journal of Pharmacokinetics and Pharmacodynamics*, 30(3), 221–235.

Pettis, R.J., Ginsberg, B., Hirsch, L., Sutter, D., Keith, S., McVey, E., Heinemann, L. (2011). Intradermal Microneedle Delivery of Insulin Lispro Achieves Faster Insulin Absorption and Insulin Action than Subcutaneous Injection. *Diabetes Technology and Therapeutics*, 13(4), 435–442.

Qiu, Y., Qin, G., Zhang, S., Wu, Y., Xu, B., Gao, Y. (2012). Novel lyophilized hydrogel patches for convenient and effective administration of microneedle-mediated insulin delivery. *International Journal of Pharmaceutics*, 437(1–2), 51–56.

Wang, P. M., Cornwell, M., Hill, J., Prausnitz, M.R. (2006). Precise Microinjection into Skin Using Hollow Microneedles. *Journal of Investigative Dermatology*, 126(5), 1080–1087.

Yu, W., Jiang, G., Zhang, Y., Liu, D., Xu, B., Zhou, J. (2017). Polymer microneedles fabricated from alginate and hyaluronate for transdermal delivery of insulin. *Materials Science and Engineering C*, 80, 187–196.

Zhang, Y., Jiang, G., Yu, W., Liu, D., Xu, B. (2018). Microneedles fabricated from alginate and maltose for transdermal delivery of insulin on diabetic rats. *Materials Science and Engineering C*, 85, 18–26.

6 CHAPTER

CONCLUSIONS AND FUTURE WORK

Diabetes is considered a global epidemic disease that affects more than 425 million people worldwide. In many cases, the administration of exogenous insulin is necessary for the treatment, however, the patient compliancy can be very low due to the anxiety and fear of needles. In this sense, transdermal microneedle arrays can provide a safe and painless alternative for insulin treatment.

In this study we developed coated microneedles for rapid transdermal delivery of insulin using metallic and polymeric microneedles. All different designs of polymeric microneedles were successfully fabricated by a biocompatible resin class I using stereolithography. Furthermore, the 3D printed microneedles offered a larger area for drug deposition and superior penetration capacity compared to the metallic microneedle's ones. Our results also showed that the inkjet printing technique was successfully used for depositing uniform and accurate coatings on the surface of the microneedles, overcoming the drawbacks imposed by other coating methods.

Among all the carriers studied for the coating formulations, the sugars, specially xylitol, demonstrated the best insulin stability performance. Overall, the release studies showed rapid release rates within 30 min. The animal studies revealed that the insulin treatments with the 3D printed microneedles provided fast and efficient delivery of insulin producing a significant hypoglycemic response with a sustained effect.

Further investigations about the mechanical strength of the microneedles are needed to provide a better understanding of the developed 3D printed MNs. The study of the long-term stability of the coated formulations, the transepidermal water loss and human models would also be interesting.